School of Chemical Technology
Degree Programme of Chemical Technology

Dominik Wowczyk

Effect of the solute on the micellization process by molecular dynamics simulations

Final Project (30 cr) submitted for inspection, Espoo, 27th February, 2014.

Supervisor **Professor Kari Laasonen**

Instructor **Dr. Maria Sammalkorpi**

Aalto University
School of Chemical
Technology

Aalto University, P.O. BOX 11000, 00076 AALTO
www.aalto.fi

Abstract of Final Project

Author Dominik Wowczyk

Title of final project
Effect of the solute on the micellization process by molecular dynamics simulations

Department of Chemistry

Professorship Chemistry **Code of professorship** Kem-31

Thesis supervisor Prof. Kari Laasonen

Thesis advisor(s) / Thesis examiner(s) Dr. Maria Sammalkorpi

Date 25.02.2014 **Number of pages** 67 + 11 **Language** English

Abstract

Alcohol molecules are known to change micelle features during the CTAB micellization process. For instance, the presence of ethanol brings about an increase of the critical micelle concentration (cmc) of CTAB and a decrease of the aggregation number. These two effects become larger raising the ethanol concentration. Longer chain alchols like octanol or nonanol are known to decrease the cmc and to raise the aggregation number. However, it is not yet experimentally possible to investigate the influences of alcohols on the micelle structure and the behavior of the alcohols itself on an atomistic level. That is why in this work molecular dynamics simulations of CTAB with the three alcohols ethanol, 1-hexanol and 3-hexanol in aqueous solution are carried out with regard to the influences of the alcohols on the micelle structure of a pre-formed CTAB micelle and to the behavior of the alcohols itself. This is done, to my knowledge, for the first time. While all three alcohols in their small concentration do not affect the micelle structure, the high ethanol concentration brings about a small swelling of the micelle and higher fluctuations of its structure due to penetration of ethanol into the micelle. However, 1- and 3-ethanol in their high concentrations behave similarly, but compared to ethanol differently. Both medium chain alcohols, which like to reside between the surfactant molecules, tend to form comicelles with CTAB (act as cosurfactants), although a few alcohol molecules also leave the micelles for a certain time. On the contrary, ethanol acts as a cosolvent, enhancing the solubility of the CTAB molecules in water. The simulations indicate that the alcohol concentration should be further raised and the simulation times extended, in order to obtain clearer results, since the changes are still rather small and the equilibration time might not be reached yet

(200 ns). This is supported by an additional simulation of a CTAB micelle in pure ethanol, which shows clearer results: the micelle already breaks down after a short time.

Keywords CTAB, ethanol, 1-hexanol, 3-hexanol, molecular dynamics simulations

Acknowledgements

First I would like to thank Dr. Maria Sammalkorpi and Prof. Dr.-Ing. Irina Smirnova for giving me the opportunity to combine my stay abroad in Finland and the Final Project or the Master's Thesis, respectively. Furthermore, I would like to thank Dr. Maria Sammalkorpi, M.Sc. Jukka Määttä and M.Sc. Eric Ritter for patiently introducing me into the world of molecular dynamics simulations along with many great discussions, which could sometimes go on till the late evening. Additionally, I would like to thank the CSC in Espoo for letting me use their supercomputers, which decreased the duration of my simulations significantly and simply made life easier for me. Finally I want to thank my family and my friends for the financial and mental support during the Thesis.

Table of Contents

Table of Symbols

Symbol	Meaning	Unit (in this thesis)
a	Interval border for Simpson numerical integration rule	-
a_i	Acceleration of particle i	nm/ps²
a_k	Principal axis (of molecule)	-
b	Interval border for Simpson numerical integration rule	-
b_k	Principal axis (of molecule)	-
c	constant	-
c_k	Principal axis (of molecule)	-
d/d^2	First and second differential	-
D_i	Diffusion coefficient	m²/s
f	function	-
F_k	Force on particle k (in GROMACS)	kJ/(mol·nm)
$\vec{g}(x_k)$	Gradient of potential energy at x_k	-
H	Matrix of simulation box vectors (in the Parrinello-Rahman algorithm)	-
h_k	Maximum displacement (in GROMACS)	nm
I_i/I_{ii}	Moment of inertia (components)	a.m.u·nm²
I_{tot}	Total moment of inertia	a.m.u·nm²
K_b	Stretching constant for bonds in force-field	-
K_γ	Constant for the angle potential in force-field	-
K_φ	Constant for the dihedral potential in force-field	-
L	Largest box matrix element (in the Parrinello-Rahman algorithm)	-
$logP^{OW}$	octanol-water partition coefficient	-
l_P	Persistence length	nm
m	Number of data points for numerical integration rule	-
$max\|F_k\|$	Maximum of all forces in the system (GROMACS)	kJ/(mol·nm)
m_i	Mass of particle i	a.m.u
n	Multiplicity for the dihedral potential in force-field	-

N_{agg}	Aggregation number of micelles	-
N_i	Number of particles of type i	-
num	Number of observations for linear regression analysis	-
P	Pressure	kJ/(mol·nm³)
P_{ref}	Reference pressure	kJ/(mol·nm³)
Q	Coupling strength parameter for Nosé-Hoover thermostat	-
q	Charge	e
r	Bond length distance (bond-length in force-field)	nm
r_0	Reference bond length in force-field	nm
R_g	Radius of gyration	nm
$\vec{r}_i$	Position of particle i	nm
$R_{min,ij}$	Minimum energy distance between particles i and j	nm
t	Time	ps
T	Temperature	K
T_{ref}	Reference Temperature	K
V	Potential	kJ/mol
V	Volume of the simulation box	nm³
v_i	Velocity of particle i	nm/ps
W	Mass parameter matrix (in the Parrinello-Rahman algorithm)	-
x_i	Observed independent variable for linear regression	ps
$\bar{x}$	Mean of the independent variable for linear regression	ps
x_k	Starting point for steepest descent method with running index k	-
x_{k+1}	Next point for steepest descent method	-
y_i	Observed dependent variable for linear regression	nm²
$\hat{y}_i$	Predicted values of the dependent variable for linear regression	nm²
α	Angle	°
α_{i-j}	CTAB dihedral angle between atoms i and j	°
$\beta_{i,j}$	Isothermal compressibility	(mol·nm³)/kJ
β_{i-j}	1-hexanol dihedral angle between atoms i and j	°

γ	Torsion angle	°
Δ	Difference	-
δ	Shift for the dihedral potential in the force-field	-
ε_D	Dielectric constant	-
$\varepsilon_{i.j}$	Potential energy minimum between particles i and j for the Lennard-Jones potential	kJ/mol
Θ_{i-j}	3-hexanol dihedral angle between atoms i and j	°
λ_K	Step size for the steepest descent method	-
ξ	Friction parameter for the Nosé-Hoover thermostat	-
ρ_i	Particles density of particle i	nm^{-3}
τ_P	Time constant for the Parrinello-Rahman barostat	ps
τ_T	Time constant for the Nosé-Hoover thermostat	ps
φ	Angle for the angle potential in the force-field	°
φ_0	Reference angle for the angle potential in the force-field	°

Abbreviations

a.m.u	Atomic mass unit ($1.6605 \cdot 10^{-27}$kg)
CHARMM	Chemistry at Harvard Molecular Mechanics
cmc	Critical micelle concentration
COM	Center of Mass
CTAB	Cetrimonium bromide
ESR	Electronic spin resonance spectroscopy
LINCS	Linear constraint solver (bonds length constraining algorithm)
MD	Molecular dynamics
mM	Millimolar (10^{-3} mol/l)
MSD	Mean square deviation
NPT	Canonical ensemble of constant number of particles, constant pressure and constant temperature
NVT	Canonical ensemble of constant number of particles, constant

	volume and constant temperature
PBC	Periodic boundary conditions
QENS	Incoherent quasielastic neutron scattering
RDF	Radial distribution function
SDS	Sodium dodecyl sulfate
SPC	Simple point charge water model
TIPS3P	Transferable intermolecular potentials-three point water model
VMD	Visual Molecular Dynamics (visualization software)

1. Introduction

Surfactants are amphiphilic molecules, which start to aggregate in a solution as soon as a certain surfactant concentration, the critical micellar concentration (cmc), is reached. In these aggregates, the micelles, the hydrophobic or hydrophilic part of the molecule is screened off the hydrophilic or hydrophobic solvent molecules, respectively. Over the last decades both surfactants and micelles have been gaining growing attention because of their versatile application possibilities. As an alternative to usual liquid-liquid-extraction processes for instance, micellar extraction processes (Cloud Point Extractions) are characterized by their "mild" working conditions like ambient pressure and temperature, low costs and low toxicities as well as high extraction efficiencies and selectivities.[1-3] Additionally surfactants are commercially employed as detergents,[4-6] emulsifiers,[7-8] drug carriers, in pharmaceutical and biomedical applications,[4-7, 9-11] in phase transfer catalysis,[5-6] as wetting agents,[4, 7] solubilizers,[7] in foods and in cosmetics/health care products.[4-7] Moreover they are used for the removal of grease/oil or dirt/stain from fabrics,[7] for tertiary oil recovery,[4, 9] remediation of soils and waste sites[4, 9, 12] or for the synthesis of materials, nanostructured materials as well as for nanolithography.[4-6, 13-14]

Alcohols are known to change certain micelle behaviors during the micellization process due to experimental results. For example, an increase of ethanol concentration brings about an increase of the cmc and a decrease of the aggregation number, N_{agg}, of CTAB. Furthermore an increase of the concentration of longer chain alcohols, like octanol, decreases the cmc and increases the aggregation number of CTAB. However, it is still not experimentally possible to investigate the influences of the alcohols on the micelle structure and the behavior of the alcohols itself on an atomistic level. At this point computer simulations can be used, which additionally save time and costs compared to experiments. Therefore, in this work, the influence of three short-to-medium chain alcohols, in particular ethanol, 1-hexanol and 3-hexanol on the behavior of a micelle of the cationic surfactant cetrimonium bromide (CTAB) in aqueous surrounding and the behavior of the alcohol molecules itself shall be investigated and compared using molecular dynamics simulations with the software package of GROMACS.[45] Namely the changes in the micelle structure, like elongating effects, size

fluctuations and changes in angles/dihedrals or positioning and bending of the alcohol molecules shall be analyzed. Alcohols are the most common cosurfactants added to the surfactant/oil-system, with which certain behavior or features of the surfactants can be adjusted.[5] To my knowledge, that is the first time this is investigated. On the other hand this topic is of major importance, because CTAB belongs to the most commonly utilized surfactants in the world.[5] Among other things it is applied in hair products, in the extraction of DNA of plants or bacteria and as a template for the creation of nanostructures such as gold-nanoparticles.[5-6, 15-17]

2. Background

2.1. Surfactant Systems

Surfactants are amphiphilic molecules which consist of a polar headgroup and a nonpolar tail, which makes them soluble in water and oil phases. The surfactant molecules will first concentrate at the interphase of the solvent phase and the adjacent phase, before, at concentrations exceeding the critical micellization concentration, surfactant molecules start to aggregate and build micelles. In these micelles, the polar headgroups of the surfactants are oriented towards the hydrophilic solvent phase, whereas the nonpolar tails point in the opposite direction. The general micellization process is depicted in Figure 2.1. If other molecules are present in the solution, they can be either solubilized in the solvent phase or on/inside the micelles. Here they can concentrate on the surface, between the headgroups, between the headgroups and the first carbon atoms of the nonpolar tail and more deeply within the same region (palisade layer) or inside the core.[5]

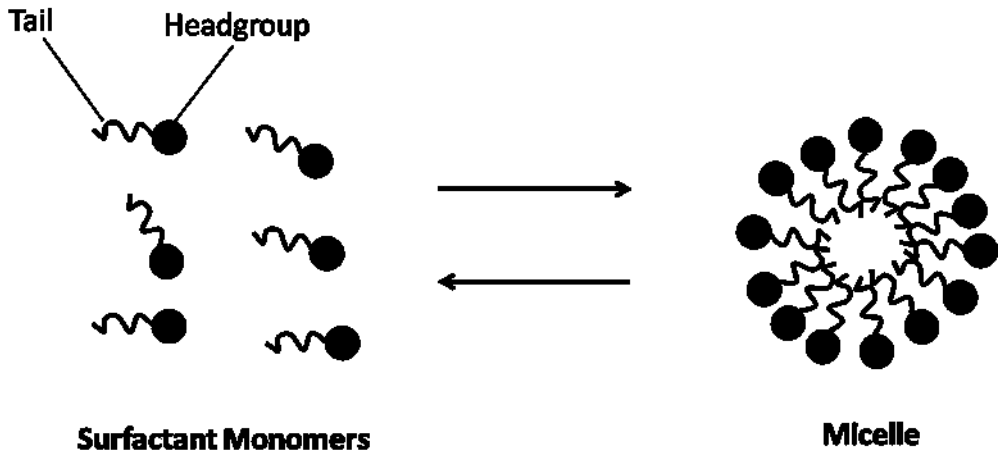

Figure 2.1: Thermodynamic equilibrium of the micellization process in surrounding water phase. In the micelle, polar headgroups point towards polar water phase and nonpolar tails towards the micelle core.

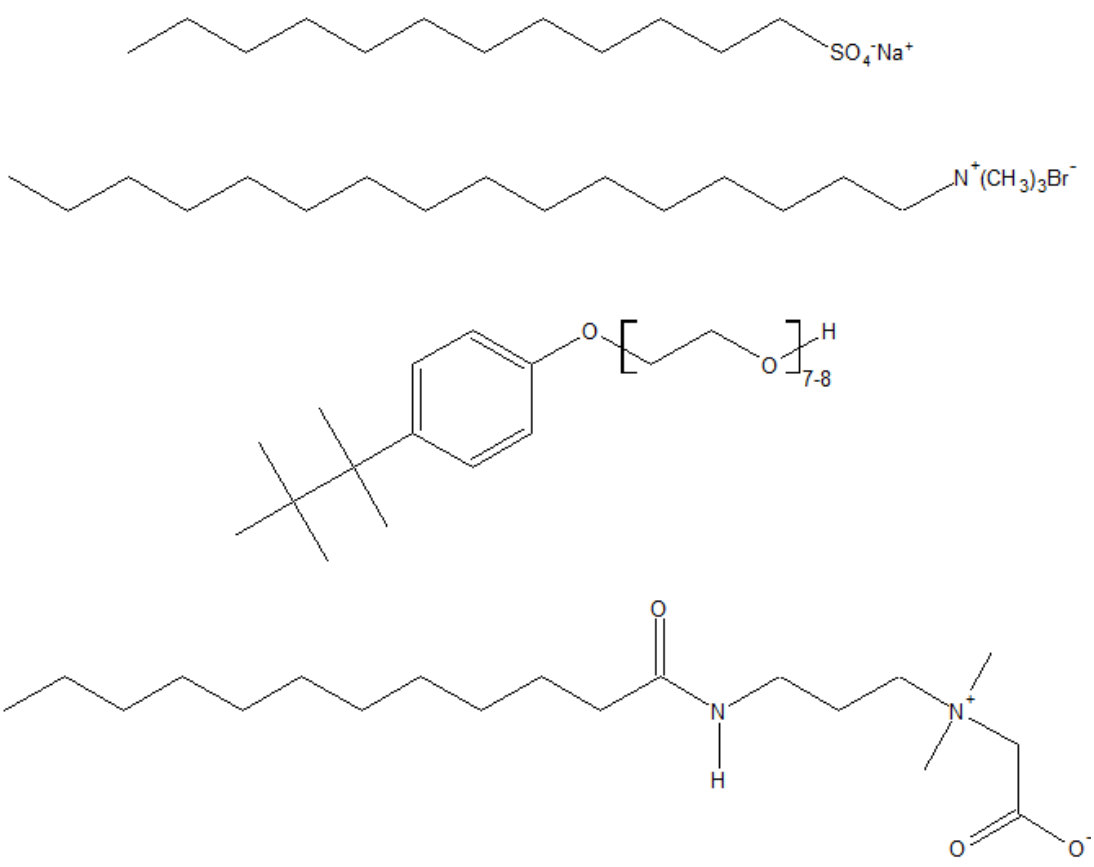

Figure 2.2: Four examples of surfactant molecules. From top to bottom: anionic SDS, cationic CTAB, nonionic Triton X-114 and zwitterionic cocamidopropyl betaine.

Furthermore surfactants can be categorized into cationic, anionic, nonionic or zwitterionic based on positive, negative, neutral or both negative and positive charge of the headgroup, respectively. Figure 2.2 shows four examples of these four kinds of surfactants.

2.2. CTAB Micelles

During the last decades a lot of research in the surfactant field due to its enormous possibilities has been carried out regarding their applications as well as their structures, dynamics and behavior. For CTAB this also involves both experimental work and theoretical investigations with computer simulations gaining growing attention.

2.2.1. Experimental Research

For pure CTAB surfactant molecules in aqueous solutions, the critical micellar concentration (cmc) is one of the most determined properties. For example Bahri et al.[25] used the electron spin resonance spectroscopy (ESR) to measure the cmc by observing the microviscosity at various concentrations. They obtained a cmc of 0.4 mM at ambient temperature. Density, viscosity, conductivity and light scattering measurements of Zdziennicka et al.[28] at 293 K revealed cmc values of 0.915 mM, 0.765 mM, 0.933 mM and 0.977 mM, which are quite different compared to the one determined by Bahri et al.[25] In addition to that, Zdziennicka et al.[28] calculated the aggregation number, N_{agg}, by means of light scattering measurements. At 293 K and a surfactant concentration of 1 mM they obtained values of 128 ± 3, 125 ± 3 and 97 ± 1 calculated on the basis of the apparent molar volume, the partial molar volume and the surfactant molecule length, respectively. The aggregation number was also determined by Anachkov et al.[30], who applied stratifying foam film experiments at 298.15 K. From the height and step of the final foam thickness, they achieved values of 95, 119, 137, 136 and 135 for CTAB concentrations of 10, 20, 30, 40 and 50 mM, respectively. Furthermore, Anachkov et al.[30] obtained the micelle ionization degree, α, from their experiments. Values of 0.2, 0.23, 0.26, 0.26 and 0.29 could be shown for CTAB concentrations of 10, 20, 30, 40

and 50 mM, respectively. These results reveal that micelles with a higher aggregation number have a lower degree of ionization and thus less counterion binding. Moreover the local dynamics of C_nTAB micelles were analyzed by Sharma et al.[32-33] by means of quasi-neutron scattering technique and incoherent quasielastic neutron scattering (QENS). According to them the dynamics can be split into two parts: the global Fickian diffusion of the micelles and faster internal segmental motions and torsions. These motions are hindered with longer chain length.

Besides experiments of pure CTAB, experiments with CTAB surfactants in the presence of cosurfactants like alcohols have also been carried out. The cmc for CTAB in the presence of methanol, ethanol and 1-propanol was investigated by Bielewska et al.[29] based on surface tension, density, viscosity, conductivity and dynamic light scattering measurements at 293 K. Depending on the experimental technique, the cmc of pure CTAB is between 8 and 11 mM. They found out that methanol first strongly raises the cmc to 40 mM at a molar fraction of 19%, then raises it slowly to 44 mM at 64%, before a decrease to 35 mM at 100% methanol content can be observed. For ethanol first a decrease to 6 mM at a molar fraction of approximately 1.5% can be seen, before the value strongly goes up to 52 mM at 18%, but falls down to 30 mM at 100% afterwards. An initial increase to 140 mM at a molar fraction of 10% and a following decrease to 25 mM at 100% can eventually be noticed for 1-propanol. The cmc for CTAB in the presence of ethanol was also determined by Li et al.[21, 31], who observed polarity changes from steady-state fluorescence measurements at 298 K. However, they show a constant increase of the cmc to 240 mM at a volume fraction of 100% for ethanol. Furthermore, they obtained the aggregation number in dependence on the ethanol volume fraction. A decrease from initial 60 molecules per micelle for the pure micelle to 10 at a volume fraction of 0.8 for ethanol can be seen. Moreover, the ionization degree of the micelle was determined for CTAB in the presence of methanol, ethanol and 1-propanol by Bielewska et al.[29] by means of surface tension, density, viscosity, conductivity and dynamic light scattering measurements at 293 K. From an initial α-value of 0.24 for a pure micelle, methanol first reduces the ionization degree to 0.12 (15 mol-%), before it raises it to 0.75 (80 mol-%). For ethanol and 1-propanol a different behavior can be observed. While ethanol and 1-propanol first increase the value to 0.92 and 0.84 (22 mol-%), respectively, they decrease it to 0.6 and 0.41 (100 mol-%) afterwards. The cmc, the aggregation number as well as the ionization degree for CTAB in the presence of the longer chain alcohols 1-octanol and

1-nonanol were determined by Dubey[24], who carried out density, speed of sound, electric conductivity measurements as well as a fluorescence method at 298.15 K. Raising the 1-octanol concentration from 0 to 30 mM, the cmc decreases from 0.97 mM ± 0.04 mM to 0.90 mM ± 0.04 mM, whereas the α-value increases from 0.31 ± 0.02 to 0.44 ± 0.02. Raising the 1-octanol concentration from 0 to 19.4 mM brings about an increase of the aggregation number from initial 73 ± 3 to 83 ± 8 for a CTAB concentration of 50 mM. Raising the 1-nonanol concentration from 0 to 27.5 mM leads to a decrease in the cmc value to 0.89 mM ± 0.06 mM and an increase in the ionization degree to 0.44 ± 0.02. Raising the 1-nonanol concentration from 0 to 23 mM the aggregation number increases to 88 ± 6 for a CTAB concentration of 50 mM. The results indicate that large comicelles are formed by the alcohol and CTAB, since the cmc was lowered and N_{agg} as well as α were raised. Furthermore, Oelschlaeger et al.[26] investigated the behavior of $C_{(16)}$TAB-C_nTAB wormlike mixed micelles by means of high frequency rheometry experiments. They showed that upon increasing the concentration of C_nTAB, the persistence length, l_P, of the elongated comicelles diminishes exponentially. For example raising the C_{12}TAB concentration in a solution with CTAB from 0 to 4 wt-% reveals a reduction of the l_P-value from 35 nm to 20.17 nm. Thus the micelle gets more flexible. In addition, Francisco et al.[27] utilized cryo-transmission electron miscroscopy and small angle neutron scattering to examine the effect of several cosurfactants like ethanol on the rheological properties of wormlike CTAB micelles. The results show that hydrophilic compounds like ethanol do not have any influence up to a concentration of 20 mM at all, whereas hydrophobic ones can alter the rheological properties considerably at smaller concentrations (5 mM). As an example adding 5 mM PPO 2000 to a solution of CTAB and NaSal (both 100 mM) brings about a decrease of the relaxation time, τ_R, from 4.6 to 0.4 s and a decrease of the plateau modulus, G_0, from 55 to 52 Pa. However adding ethanol up to 20 mM does not show striking differences.

Generally the influences of alcohols on micelles can be summarized in the following way: when adding alcohols to the solution, in order to evoke certain behavior or features of the micelles and solutes with these cosurfactants/cosolvents, they preferably solubilize near the palisade layer.[18] The longer the hydrophobic chain length or the higher the ionic strength of the alcohol molecule, the more of them will accumulate inside the micelles.[18] This incorporation causes changes in the micellar shape, micellar swelling and changes in the transport properties.[19-20] These changes strongly depend on both the surfactant and alcohol

concentration.[18] Furthermore added alcohol molecules modify the bulk phase, which in turn effects the interactions between the solvent and the surfactant molecules.

The increasing of the ethanol concentration in an aqueous CTAB system for example, brings about an increase of the cmc and a decrease of the number of surfactants per micelle, N_{agg}.[18, 21-22, 31] The greater amount of surfactant needed to form micelles is caused by the water structure breaking process of ethanol, which lowers the hydrophobic effect of the surfactant tails.[21, 23] Additionally the dielectric constant of the system decreases upon adding ethanol, which augments the repulsive interactions of the headgroups and consequently leads to a reduction of the surfactant number per micelle.[18]

A different behavior is observed for CTAB aqueous solutions with long chain alcohols like hexanol, octanol or nonanol. Although the repulsions of the headgroups are at first increased due to a decrease in polarity, some surfactant molecules move out of the micelle, which are then partially replaced by alcohol molecules. This in turn reduces the electrostatic repulsions of the headgroups and thus leads to a decrease of the cmc.[19] Moreover the ionization degree, α, is reduced, due to the increasing distance of the headgroups, which raises the micelle surface charge density. This effect becomes larger with increasing alcohol chain length and alcohol concentration. This process also increases the number of molecules per micelle N_{agg}, whereas mixed micelles are formed which tend to be less spherical.[24]

2.2.2. Computational and Theoretical Research

Besides experimental research, computational investigations can also be found in literature. Yuan et al.[34] and Phan et al.[35] carried out computer simulations of the adsorption of CTAB at the air-water interface for instance. Pérez-Sánchez et al.[36] modelled the aggregation of CTAB-silica-structures (synthesis of nanoporous solids) by molecular dynamics simulations. Here the formation of long, rodlike micelles can be observed, whereas CTAB micelles in pure water stay in a spherical form. Wang et al.[37] investigated the micelle shape transition of rodlike CTAB-micelles upon the addition of NaCl and NaSal salts by using atomistic molecular dynamics simulations. For the former salt a change from rod to sphere like micelles is observed for small concentrations, however, the micelles stay stable from a certain

concentration on. This can be explained by the ions screening off the electrostatic repulsions. On the other hand the salicylate ions interact strongly with the headgroups, hence leading to denser packing and increased ordering of the headgroups, thereby a threadlike structure is favored.

Additionally, there is literature dealing with the self-assembly of CTAB surfactant molecules in aqueous solution. For example Stephenson et al.[38] carried out molecular dynamics simulations of a CTAB-monomer-water system. Ingram et al.[39] investigated the same, but further used the built micelles for calculating free energy profiles (partitioning) for numerous solutes by means of the program COSMO-RS. Finally a series of several pre-formed/equilibrated CTAB micelles in aqueous solution, each containing a different number of monomers, were simulated for 10 ns by Catá et al.[40], in order to analyze the behavior of the micelles. The results indicate that two or three spherical micelle layers form during the simulation. Each layer inside the micelle is confined by the headgroups of surfactant molecules.

Some theoretical calculations including methods have also been published. For instance Sprunger et al.[9] developed a prediction method/equation for the partitioning of solutes between CTAB and water, which shows up to be a very good mathematical description. The results reveal a standard deviation of 0.175 log units. Li et al.[22] proposed a thermodynamic model to predict the aggregation behavior, meaning cmc and N_{agg}, of CTAB in water-ethanol mixtures, which is consistent with experimental data.

3. Modelling of Surfactant Systems

In comparison to experimental/laboratory experiments, computer simulations may have the advantage of saving time, material and especially costs. In addition, they allow more detailed analysis of results like the atomistic resolution one would not be able to obtain using laboratory equipment. The basic idea behind the molecular simulations is to approach the mean values of thermodynamic functions by mean values of a huge number of intermediate microstates, thus giving the trajectory of the system in space. One possible way is

represented by Molecular dynamics (MD) simulations, which consider the motions of atoms over time, while interactions of those are described by so called force fields. Nowadays there are two kinds of molecular dynamics simulations available: the classical and the quantum simulations. The first implements classical mechanical treatments of atoms completely neglecting the motions and behavior of electrons, whereas the latter one includes "quantum nature of chemical bonds" using the Schroedinger equation for its description.[41] Therefore the quantum molecular dynamics simulations provide more realistic and exact results, however requiring far more computational time and power. This especially comes into effect when dealing with a huge number of atoms. That is, why most of the simulations are still carried out by classical molecular mechanical simulations, which will also be applied in this work. A more detailed overview of the classical MD simulations features is given in the following subchapters.

3.1. Classical Molecular Dynamics Simulations

3.1.1. Molecular Dynamics Algorithm

In order to produce the time development of a molecular system from its initial state, forces between the molecules and atoms have to be determined. This can be achieved by calculating the negative gradient of the potential energy, which represents the forces (force field). Based on these forces, the accelerations of the molecules can be calculated, which in turn give the changes in velocities. By means of the velocity changes, the new positions of atoms and molecules can finally be computed. In classical molecular dynamics, the atom's positions and movements as a function of time can be obtained applying Newton's equation of motion for positions r_i and accelerations a_i in all three dimensions:

$$F_i = m_i \frac{d^2 r_i}{dt^2} = m_i \cdot a_i \qquad 3.1$$

To obtain the time development, the Newtonian equations have to be integrated, which gives the time trajectories (positions and velocities functions of time) of all atoms. In this work, the Leapfrog algorithm[42, 43] is used. This is a development of the Verlet algorithm.[43-44] The latter one uses positions and accelerations at time t and $t - \Delta t$ to predict the positions at $t + \Delta t$ (Δt = integration step):

$$r_i(t + \Delta t) = 2 \cdot r_i(t) - r_i(t - \Delta t) \cdot v(t) + \Delta t^2 \cdot a(t) \qquad 3.2$$

However, to obtain higher accuracy, the Leapfrog integration uses velocities v_i at half integration steps:

$$r_i(t + \Delta t) = r_i(t) + \Delta t \cdot v\left(t + \frac{1}{2}\Delta t\right) \qquad 3.3$$

$$v_i\left(t + \frac{1}{2}\Delta t\right) = v\left(t - \frac{1}{2}\Delta t\right) + \Delta t \cdot a(t) \qquad 3.4$$

At first, the velocities at $t + \frac{1}{2}\Delta t$ are calculated from the velocities at $t - \frac{1}{2}\Delta t$ and the accelerations at time t, before the positions at $t + \Delta t$ and t are determined. Thereafter the velocities at time t can be obtained:

$$v_i(t) = \frac{1}{2} \cdot \left[v_i\left(t + \frac{1}{2}\Delta t\right) + v\left(t - \frac{1}{2}\Delta t\right)\right] \qquad 3.5$$

Especially for large systems the Leapfrog algorithm stands out with its low computational costs and storage capacity.[59] The basic flow chart of the creation of the trajectories is given hereafter in Figure 3.1. The initial velocities could be computed from a Maxwell-Boltzmann-distribution for example.[43]

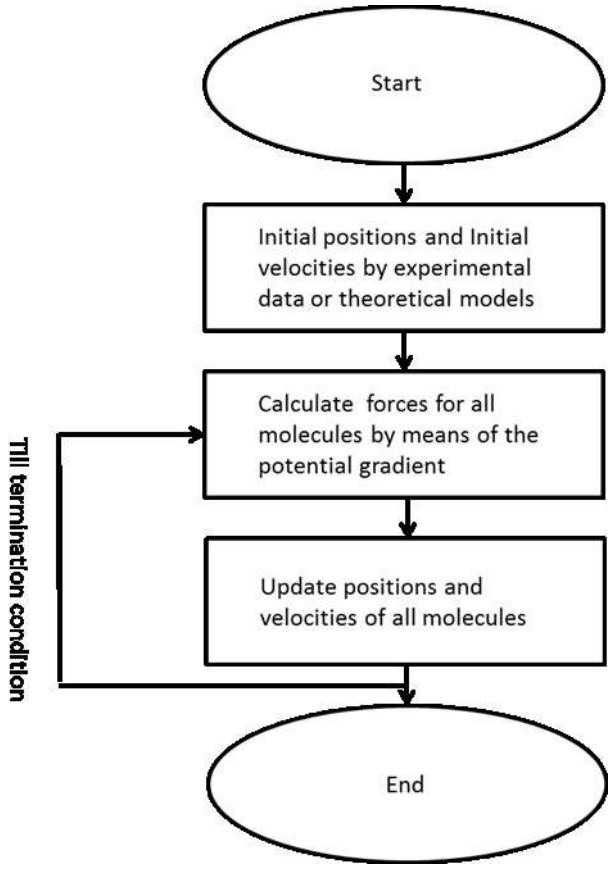

Figure 3.1: Flow scheme for the determination of the trajectories for molecular dynamics algorithm.

3.1.2. Force Fields

The interactions in a molecular system are described by a force field based on an analytical expression. Force Fields methods "freeze" the electronic motions and calculate the energy of the system in dependence on the nuclei's movements only. Despite its simple form, very accurate results can be obtained for many biological and chemical systems within a relative short simulation time. One widely used functional form of a force field, separating the total potential, V_{tot}, into four different contributions, V_i, is shown in the following equation:[43,45]

$$V_{tot} = V_{bonds} + V_{angles} + V_{torsions} + V_{non-bonded} \quad 3.6$$

Here, the first three terms on the right side of the equation reflect bonded interactions and the last term stands for non-bonded interactions of and within molecules. However, there

are many different parameters and different forms used for the single terms in the energy function. In this work, the CHARMM 36-force field is solely used,[46-47] for which the single terms are discussed in the following. The bond stretching for covalently bound atoms at distance r from each other can simply be approximated by a harmonic potential:

$$V_{bonds}(r) = \sum_{bonds} K_b \cdot (r - r_0)^2 \qquad 3.7$$

with the stretching constant for each bond, K_b, and the reference bond length, r_0.

The angle potential term (for valence angles φ between three molecules) is approached with a similar harmonic function:

$$V_{angles}(\varphi) = \sum_{angles} K_\varphi \cdot (\varphi - \varphi_0)^2 \qquad 3.8$$

where K_φ denotes a constant and φ_0 the reference angle.

The torsion or dihedral term is most often described by a cosine series expansion as a function of the torsion angle, γ. One example is shown hereafter:

$$V_{torsions}(\gamma) = \sum_{dihedrals} \left[\sum_j K_{\gamma,j} \cdot \left(1 + \cos\left(n_j \cdot \gamma - \delta_j\right)\right) \right] \qquad 3.9$$

where K_γ is a constant, n a multiplicity and δ a shift.

The relations between non-bonded atoms or atoms of a molecule, that are at least three bonds apart from each other, encompass electrostatic and van der Waals interactions, which are pair-additive and symmetric to the center.[45] The electrostatic interactions for two charged particles with charges q_i and q_j and distance r_{ij} can be approached by a Coulombic term with ε_D as the dielectric constant, which is 1 in explicit solvent simulations:

$$V_C(r_{ij}) = \sum_{\substack{non-bonded \\ pairs\ i,j}} \frac{q_i \cdot q_j}{\varepsilon_D \cdot r_{ij}} \qquad 3.10$$

To determine van der Waals pair potential a Lennard-Jones function is applied:

$$V_{LJ}(r) = \sum_{\substack{non-bonded \\ pairs\ i,j}} \varepsilon_{ij} \cdot \left[\left(\frac{R_{min,ij}}{r_{ij}} \right)^{12} - 2 \cdot \left(\frac{R_{min,ij}}{r_{ij}} \right)^{6} \right] \qquad 3.11$$

with the potential energy minimum, ε_{ij}, of two particles with the distance r_{ij} and $R_{min,ij}$ as the position of the minimum. The $(1/r)^{12}$- and the $(1/r)^{6}$ -term in Equation 3.11 describe the repulsive and the attractive part, respectively.

3.1.3. Periodic Boundary Conditions

Whenever finite systems are investigated, it is useful to avoid boundary effects at the edges of the system. Therefore the Periodic Boundary Conditions (PBC) are utilized: the system to be analyzed (the atoms) is composed in a space-filling box and whenever an atom leaves the system on one side, it is then mirrored to the opposite side of the box. Thus the number of particles of the system is kept constant. As a mental aid, one can imagine the PBC as copies of the system, which surround the original box. For a two-dimensional system eight copies are thus used (see Figure 3.2), for a three dimensional system this amounts to 26 periodic images. The coordinates of the particles in the copied boxes can be simply obtained by adding or subtracting multiples of the box edge vectors. Additionally in GROMACS, the so called minimum image convention is used parallelly, which makes the system only take into account the nearest image of each particle for the short-range non-bonded interactions.

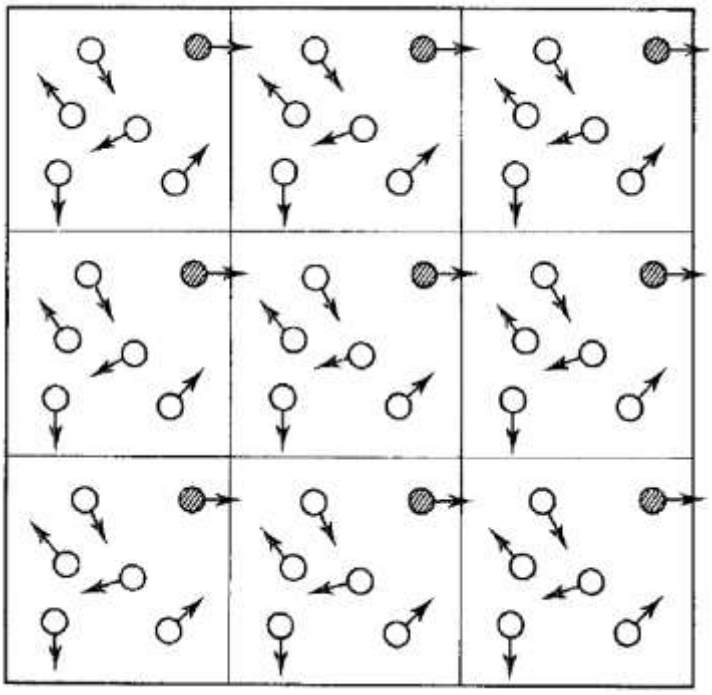

Figure 3.2: Periodic boundary conditions of a two-dimensional system (taken from Ref. 43).

3.1.4. Constant Pressure and Temperature Simulations

In order to be comparable to experimental results, in most cases it is necessary for the simulated system to remain at constant pressure as well as constant temperature. One option to control the pressure in the simulation is provided by the Parrinello-Rahman barostat,[48] which works best for an already equilibrated system. To keep the system pressure at a desired value, the size and shape of the simulation box can vary over time. The box vectors (e.g. x,y,z), which are represented by a matrix H:

$$H = \{x, y, z\} \qquad 3.12$$

are altered according to the matrix equation of motion:

$$\frac{dH^2}{dt^2} = V \cdot W^{-1} \cdot H^{'-1} \cdot \left(P - P_{ref}\right) \tag{3.13}$$

where t is the time, V is the volume of the box, $H^{'}$ is the transposed matrix of H, P and P_{ref} are the tensors of the current and reference pressure. The inverse mass parameter matrix W^{-1}:

$$(W^{-1})_{i,j} = \frac{4\pi^2 \cdot \beta_{i,j}}{3\tau_p^2 \cdot L} \tag{3.14}$$

sets the strength of the pressure coupling. Here, L corresponds to the largest box matrix element, $\beta_{i,j}$ to the isothermal compressibility and τ_p to the pressure time constant. The two latter quantities have to be inserted into the input files of GROMACS.

Additionally the particles equations of motion are also modified, which is presented in the following:

$$\frac{d^2 r_i}{dt^2} = \frac{F_i}{m_i} - M \cdot \frac{dr_i}{dt} \tag{3.15}$$

with

$$M = H^{-1}\left[H \cdot \frac{dH'}{dt} + H' \cdot \frac{dH}{dt}\right] \cdot H'^{-1} \tag{3.16}$$

Here r_i, F_i and m_i denote the radius of particle i from origin, the forces on particle i and the mass of particle i, respectively.

In order to obtain comparable results, a constant temperature in addition to constant pressure of the system is also needed. For this purpose Nosé and later Hoover developed the temperature coupling-algorithm for canonical ensemble simulations,[49-50] which works fine for equilibrated compositions. The Nosé-Hoover thermostat represents a heat bath, which is an integral part of the system. The system then oscillatory advances a desired value. The

equations of motion of the particles are extended by a "thermal reservoir" and friction term ξ, which has its own equation of motion and is multiplied by the particle's velocity:

$$\frac{d^2 r_i}{dt^2} = \frac{F_i}{m_i} - \xi \cdot \frac{dr_i}{dt} \qquad 3.17$$

$$\frac{d\xi}{dt} = \frac{1}{Q} \cdot \left(T - T_{ref}\right) \qquad 3.18$$

with T as the instantaneous temperature and T_{ref} as the reference temperature. Q represents the coupling strength parameter, which implies the period of oscillation of the kinetic energy between the system and the thermostat, τ_T:

$$Q = \frac{\tau_T^2 \cdot T_{ref}}{4\pi^2} \qquad 3.19$$

τ_T has to be specified in the input files.

3.1.5. Energy Minimization

If the starting configuration of the system is too far away from equilibrium, the forces might attain considerable high values that could make the simulation fail. Moreover all the kinetic energies should be removed, in order to lower the thermal noise of the system.[45]

Therefore an energy minimization should first be implemented, which moves the system to the nearest local minima of the potential energy function or stable state, respectively. In general the minimization problem can be specified as follows: for a function depending on several variables, those values of the variables have to be found, for which the function has a minimal value. Since such as system has a vast number of minimal values, the energy minimization procedure hardly ever shifts the system to the global minimum. At a minimum point the following conditions for the function f with respect to each of its variables apply:

$$\frac{\delta f}{\delta x_i} = 0 \qquad 3.20$$

$$\frac{\delta^2 f}{\delta {x_i}^2} > 0 \qquad 3.21$$

Several methods and algorithms have been proposed, of which a derivative one, the steepest descent method, is used in this work.[43] This particular method is presented hereafter.

3.1.5.1. Steepest Descent Method

Despite being not the most efficient method, the steepest descent method can easily be implemented and has proven to be robust.[45] The choice of the direction is where the forces decrease most rapidly, which is reflected by the negative gradient of the potential energy $-g(x_k)$. The iteration procedure therefore can be shown by:

$$x_{k+1} = x_k - \lambda_k \cdot g(x_k) \qquad 3.22$$

with x_k as a random starting point, x_{k+1} as the next iteration point and λ_k as the step size. This algorithm continues either applying the line search or the arbitrary step approach until it has reached a certain accuracy.[43] In GROMACS the steepest descent method is performed in the following way: [45]

$$x_{k+1} = x_k + \frac{F_k}{max|F_k|} \cdot h_k \qquad 3.23$$

where F_k denotes the force or the negative potential of the system, $max|F_k|$ the largest of the absolute force values and h_k the maximum displacement. At point x_{k+1} the forces are again calculated for the new positions and it is checked, whether the potential $V_{k+1} < V_k$. If

this is true, h_{k+1} is set $1.2 \cdot h_k$ and the new positions are accepted. Otherwise h_{k+1} is set $0.2 \cdot h_k$ and the integration step is repeated.

4. Studied System and Analysis Methods

In this chapter the employed software, the parametrization and the implementation of the simulation of the studied systems are discussed. Finally a description of the different analysis methods is given.

4.1. Computational Model

For this work the Gromacs 4.6.3 simulation package[45] along with the CHARMM-36 force field[46-47] with the all-atom parametrization for the atomistic MD simulations was used. In order to minimize the energies of the initial systems the steepest descent method was applied like discussed in Chapter 3.1.5.1. After the energy minimization the simulations were carried out in the NPT-ensemble at p = 1 bar and T = 298 K by means of the Parrinello-Rahman Barostat and the Nosé-Hoover Thermostat, respectively (see Chapter 3.1.4). Here the time constants for the pressure and temperature coupling were set to 1 and 2 ps, respectively. The pressures and temperatures for the solvents, the counterions, the surfactant and the alcohol molecules were controlled independently. The LINCS-algorithm[51] was used to constrain the bond lengths with 4 as the highest order in the expansion of the constraint coupling matrix and 2 as the number of iterations in the final step of the algorithm. All simulations were carried out with a time step of 2 fs, whereas the Lennard-Jones interactions were cut off between 0.8 and 1.2 nm and the Particle Mesh Ewald method[52] for the long-range electrostatic interactions was applied with a cut-off of 1.0 nm. The bromide counterions were described according to Horinek et al.[58] For the water molecules, the TIPS3P-model[47] was chosen, which is consistent with the CHARMM 36-force field. All visualizations were created with the Visual Molecular Dynamics (VMD)[53] software.

4.2. Simulated System

In this thesis, the aqueous systems of a pure micelle consisting of 110 CTAB molecules, a pure micelle consisting of 80 CTAB molecules and CTAB micelle with added ethanol/1-hexanol/3-hexanol in a small concentration (five molecules or 11.4 mM) or in a large concentration (30 molecules or 68.3 mM) have been analyzed.

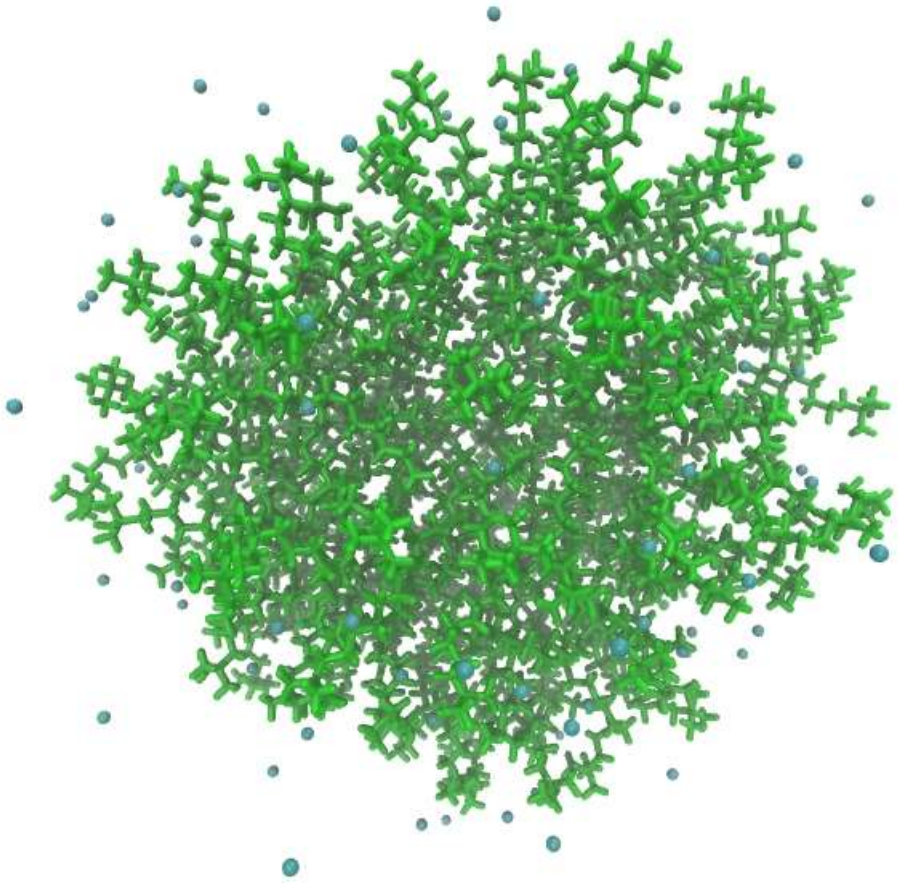

Figure 4.1: CTAB micelle containing 110 surfactant molecules (green) and 110 bromide counterions (blue) (snapshot taken with VMD[53]).

For all analyzed systems the size of the cubic simulation box was fixed to 9 nm in all three dimensions. This ensured the micelle not "seeing" its periodic images and not interacting with itself according to the van-der-Waals long-range interactions cut-off (distance between periodic images should be two times the van-der-Waals cut-off). First, one micelle containing

110 CTAB molecules and bromide counterions near the head region was centered in the box (see Figure 4.1). This micelle was provided by Storm et al.[54] and the reason for taking a pre-formed/equilibrated micelle is to save considerable computational time.[40] In case of the simulations containing ethanol, either five or 30 alcohol molecules were put randomly around the micelle (see Figure 4.2).

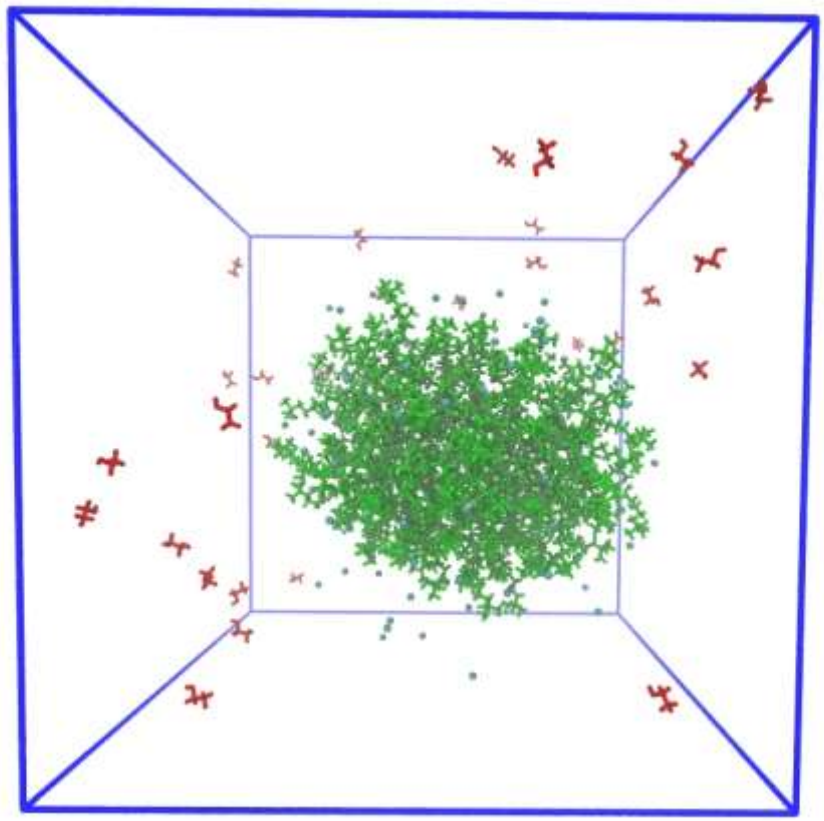

Figure 4.2: CTAB micelle (green) with bromide counterions (blue) and 30 ethanol molecules (red) randomly placed around the surfactants in the simulation box.

For 1-hexanol and 3-hexanol, either five or thirty randomly chosen CTAB surfactant molecules were replaced by the same number of alcohol molecules (see Figure 4.3), because this also saved a lot of computational time and it is known, that the longer chain alcohols are located inside the micelle.[24] The replacement was done by manually changing the molecules in the molecule input-files from the terminal tail-atom onward, regarding the correct angles of the OH-groups. That is why a comparative simulation of a pure micelle containing only 80

CTAB molecules was also done. Next step was to add the appropriate number of water molecules to the simulation box containing the micelle (and alcohol). After that all the water molecules residing inside the micelle were removed by means of a python-script. This step is necessary to avoid long simulation times as well as possible simulation crashes, as water has

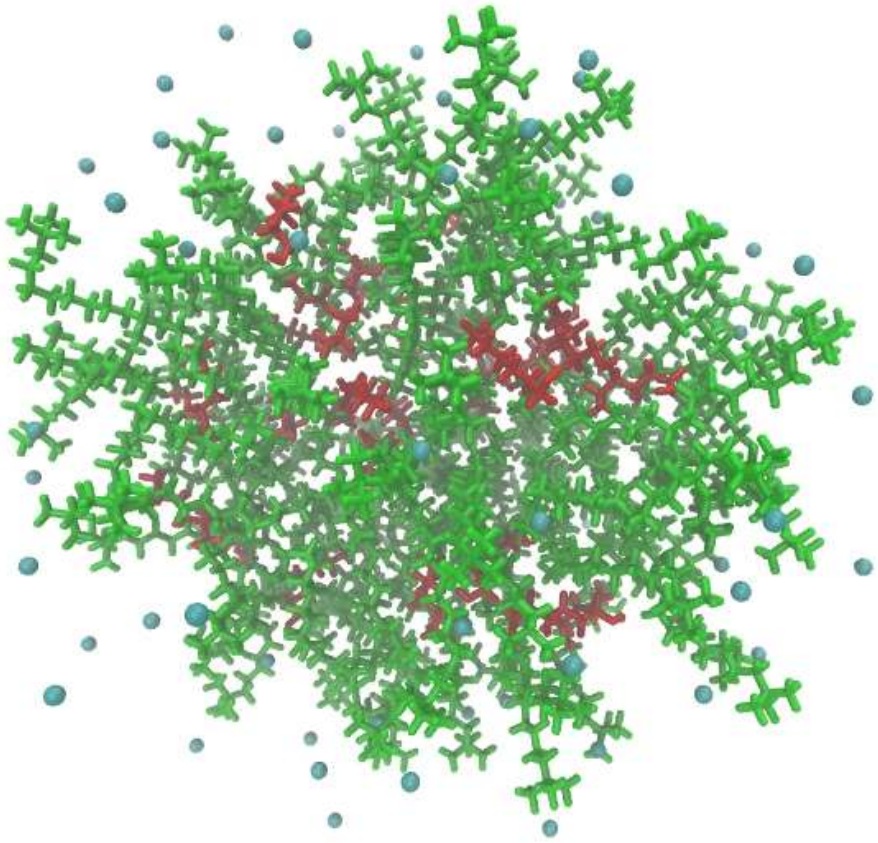

Figure 4.3: CTAB micelle containing 80 surfactant molecules (green) and 80 bromide ions (blue) as well as 30 1-hexanol molecules (red).

to move out of the hydrophobic micelle parts and the forces inside the micelle could reach too huge values. Subsequently the energy minimization by means of the steepest descent method was carried out, before the simulations were run in the NPT-ensemble at a constant temperature of 298 K and a constant pressure of 1 bar for 200 ns each.

Additionally, a simulation of the pre-formed CTAB micelle solvated in 100% ethanol was also carried out. Instead of water, the box was filled with an appropriate number of ethanol molecules. Subsequently the system was submitted to an energy minimization, before it was

simulated for 200 ps in the NVT-ensemble by removing the barostat. Afterwards the simulation was performed in the NPT-ensemble for 20 ns.

4.3. Analysis Methods

In order to highlight the influences of ethanol, 1-hexanol and 3-hexanol on a CTAB micelle and the behavior of the alcohol itself, several quantities and physical values were calculated. Most of these values were calculated from the simulations cutting off the first 25 ns to account for the equilibration time of the system. To determine the influence on the structure and size of the micelle, the moments of inertia, I_{ii}, which are the diagonal elements of the diagonalized inertia tensor, were computed about the principal molecule axes of the CTAB micelle, a_k, b_k, and c_k (axes were chosen such that they pass the micelle center of mass):

$$I_{aa} = \sum_k m_i \cdot \left(b_k^2 + c_k^2\right) \quad 4.1$$

$$I_{bb} = \sum_k m_i \cdot \left(a_k^2 + c_k^2\right) \quad 4.2$$

$$I_{cc} = \sum_k m_i \cdot \left(a_k^2 + b_k^2\right) \quad 4.3$$

The total moment of inertia, I_{tot}, can then be obtained the following way:

$$I_{tot} = \sqrt{{I_{aa}}^2 + {I_{bb}}^2 + {I_{cc}}^2} \quad 4.4$$

Another way to describe the change in form and seize is calculating the radius of gyration, R_g, which gives the rough compactness of the CTAB micelle:[45]

$$R_g = \left(\frac{\sum_i \|r_i\|^2 \cdot m_i}{\sum_i m_i}\right)^{\frac{1}{2}} \qquad 4.5$$

with r_i as the position of the atom i with respect to the micelle center of mass. Furthermore, changes in the micelle structure as well as the places, the alcohol molecules preferably like to be located, i.e. how far away from the micelle center of mass or the headgroups, can be analyzed by means of the radial distribution function (RDF). The RDF characterizes the variation of particle density as a function of distance to a reference particle and is defined for particle A and B as follows:[45]

$$RDF_{AB}(r) = \frac{\langle \rho_B(r) \rangle}{\langle \rho_B \rangle_{local}} = \frac{1}{\langle \rho_B \rangle_{local} \cdot N_A} \cdot \sum_{i \epsilon A}^{N_A} \sum_{j \epsilon B}^{N_B} \frac{\delta(r_{ij} - r)}{4\pi \cdot r^2} \qquad 4.6$$

where $\langle \rho_B(r) \rangle$ denotes the particle density of particle B at distance r around particles. $\langle \rho_B \rangle_{local}$ stands for particle density of particle B averaged over all spheres around particles A with the maximum radius (usually half the box length) and N_A is the number of particles A present in the simulation box. The δ-function in practice is replaced by a histogram of spherical slices (from r to $r + dr$), which is depicted in Figure 4.4 for a general RDF calculation.

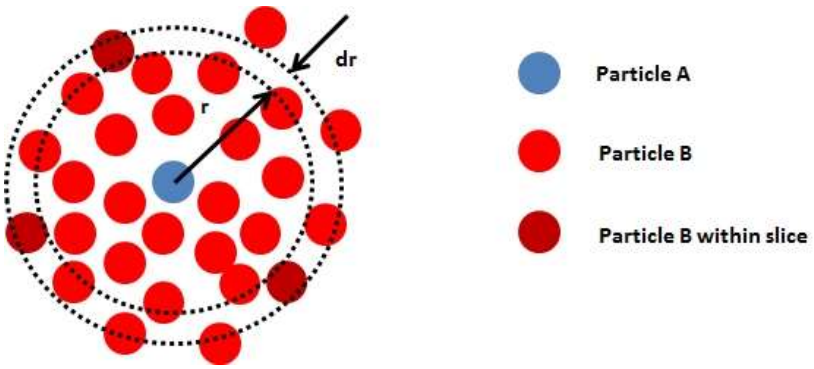

Figure 4.4: General principle of calculating the radial distribution function (RDF) of particles B around particle A. The distribution is based on calculating particles B within spherical slices of dr.

Additionally the mean square displacement (MSD) was computed for CTAB molecules as well as for alcohol molecules (within intervals) to get information about the self-diffusion of those molecules which in turn reveals the dynamics of the micelle and the alcohol molecules. The diffusion constant for particle A, D_A, can be calculated by means of the Einstein-equation:[45]

$$\lim_{t\to\infty}\langle\|r_i(t)-r_i(0)\|^2\rangle_{i\in A}=6\cdot D_A\cdot t \qquad 4.7$$

which is obtained by the slope of the mean square deviation-curve (by least squares method fitting the linear part):

$$MSD(t)=6\cdot D_A\cdot t+c \qquad 4.8$$

where c represents a constant.

The linear regression was done manually until a satisfying value of R^2 (> 0.99) was achieved. The y of the linear regression equation represents MSD(t) and the slope of the linear regression line corresponds to $6\cdot D_A$. The standard error of the slope, SE, can be calculated by the following equation:[62]

$$SE=\frac{\sqrt{\frac{\sum(y_i-\hat{y}_i)^2}{num-2}}}{\sqrt{\sum(x_i-\bar{x})^2}} \qquad 4.9$$

with x_i and y_i as the observed values of the two variables, $\hat{y}_i$ as the predicted values of the variable, $\bar{x}$ as the mean value of the observed variable and num as the number of observations.

In order to detect possible gauche defects, the dihedrals (angles between two planes spanned by two atoms each) within CTAB molecules and within 1-hexanol and 3-hexanol molecules were also analyzed. Dihedrals having an angle between 0 and 120° as well as between 240 and 360° are considered as gauche defects.

5. Results and Discussion

The results of the simulations are presented and discussed in the following subchapters. This chapter is divided into a part dealing with CTAB and ethanol and a part, which shows the results of CTAB in the presence of 1- and 3-hexanol, since the latter ones behave quite similarly. Afterwards the simulations with the short chain and the long chain alcohols are compared. Finally the results of the simulation of the CTAB micelle in pure ethanol are presented.

5.1. Simulation of CTAB with Ethanol

The aqueous CTAB-ethanol-system for both low and high concentrations as well as the pure aqueous CTAB system containing no alcohol for comparison was composed as described in Section 4.2. The simulations were then carried out for 200 ns at p = 1 bar and T = 298 K in the NPT ensemble according to Chapter 4.1. First it has to be clarified, where the ethanol molecules are preferably located, in order to make further conclusions regarding the influence of ethanol on the micelle structure. As the ethanol molecule has an octanol-water partition coefficient $\log P^{OW}$ of -0.3,[55] it is preferably located in the water phase due to its hydrophilic trait. On the other hand the surroundings of the charged headgroups of the CTAB molecules and the palisade layer offer a potential position for ethanol, too. That is why the ethanol molecules flow through the water phase and some of them even enter the palisade layer or regions near or below the CTAB headgroups, which can be seen from the simulation snapshots of a pure CTAB micelle, a CTAB micelle with five ethanol molecules and a CTAB micelle with 30 ethanol molecules after 200 ns Figure 5.1.

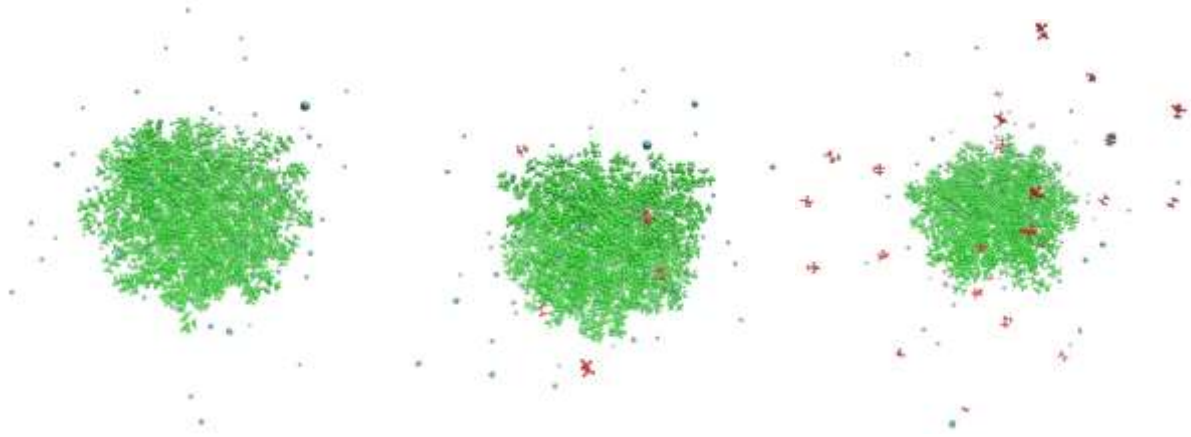

Figure 5.1: Simulation snapshots after 200 ns of a pure CTAB micelle (110 molecules) (left), a CTAB micelle (110 molecules) with five ethanol molecules (middle) and a CTAB micelle (110 molecules) with 30 ethanol molecules (right). (CTAB = green; bromide ions = blue; ethanol = red; water was omitted in the visualization).

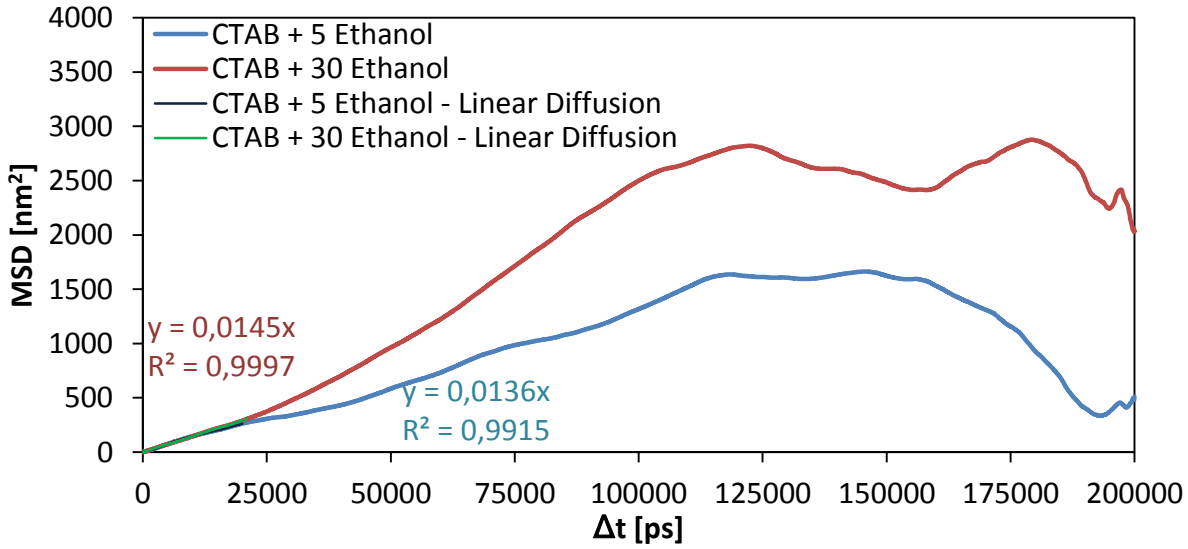

Figure 5.2: Mean square displacement (MSD) with respect to center of mass including linear diffusion part of ethanol molecules for the simulation of CTAB and low ethanol concentration and CTAB and high ethanol concentration. Y represents the MSD as function of time x for the linear part, R^2 the coefficient of determination.

From the mean square displacement (MSD) (see Equation 4.7) of ethanol over the simulation time in Figure 5.2 huge motions of the ethanol molecules throughout the solution can be noticed. The flattening and the decrease of the MSD-values after 100 ns occur due to less available data points for greater time intervals, which cause the noise. Therefore, the data points after 100 ns were disregarded. The difference between the curves of the high and low concentration can simply be explained by the greater number of alcohols, since the probability of some alcohols molecules moving far away from its initial position increases. From the linear parts and the linear regression functions of both curves in Figure 5.2, ethanol self-diffusion coefficients can be calculated using Equation 4.8, which reveal the speed of the ethanol motions in the solution. Thus, a self-diffusion coefficient, $D_{A,}$ for ethanol of $2.27 \cdot 10^{-9} \pm 0.01 \cdot 10^{-9}$ $m^2 \cdot s^{-1}$ for the simulation containing low ethanol concentration and $2.42 \cdot 10^{-9} \pm 0.002 \cdot 10^{-9}$ $m^2 \cdot s^{-1}$ for the simulation containing high ethanol concentration can be obtained. Additionally, the average values of the diffusion coefficients for each separate ethanol molecule calculated by GROMACS with 1 ns intervals (0-1 ns, 1-2 ns, 2-3 ns) are $2.18 \cdot 10^{-9} \pm 0.28 \cdot 10^{-9}$ $m^2 \cdot s^{-1}$ and $2.00 \cdot 10^{-9} \pm 0.51 \cdot 10^{-9}$ $m^2 \cdot s^{-1}$ for the low and the high alcohol concentration, respectively. The relatively large errors can be attributed to the fact that some ethanol molecules diffuse and others are stuck inside the micelle (see Figure 5.1). All these values are larger than the experimental value of $0.84 \cdot 10^{-9}$ $m^2 \cdot s^{-1}$ for ethanol in water at 298.15 K at infinite dilution,[56] but smaller than $3.25 \cdot 10^{-9} \pm 0.4 \cdot 10^{-9}$ $m^2 \cdot s^{-1}$ for a simulation of one ethanol molecule in water (infinite dilution), that was also done for comparison in the NPT-ensemble in this work. Hence, the CHARMM-36 force field, in conjunction with the TIPS3P-water model, seems to be unsuitable for determining reasonable self-diffusion coefficients. However, comparing the self-diffusion of one ethanol molecule in water and the simulations containing the CTAB micelle, a reduced motion for the ethanol molecules in the presence of a CTAB micelle can be noticed. The micelle acts like a barrier for the alcohol molecules, when they move inside the surfactant aggregate. As soon as the ethanol molecules reach the palisade layer, they stop moving deeper into the micelle, reside for a certain time at that position and move out again (see Figure 5.1). This constant flow into and out of the micelle can also be observed from Figure 5.3, where the number of ethanol

molecules present inside the micelle are plotted over the simulation time for the simulations of a CTAB micelle with low and high ethanol concentration. Both simulations show an equilibrium between ethanol molecules entering and exciting the CTAB micelle, since the values fluctuate around the mean value. As an average, approximately 60% of the ethanol molecules are located inside the micelle during the simulation. However, a relatively greater amount of ethanol molecules move into and out of the micelle for the simulation with low

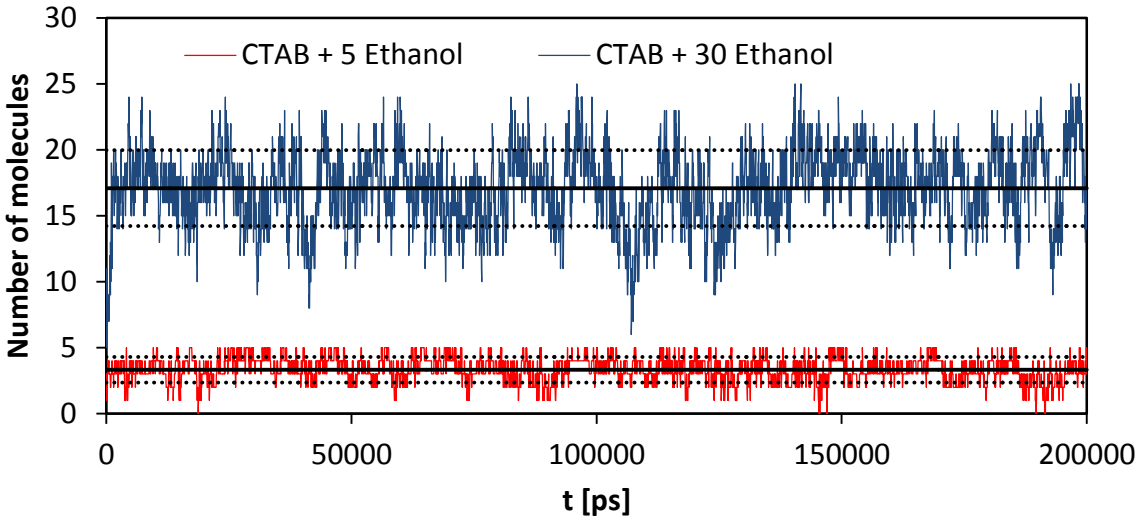

Figure 5.3: Time development of the number of whole ethanol molecules inside the CTAB micelle. The micelle is assumed to have a radius of 2.3 nm (around the micelle center of mass). Black lines represent the mean values, dashed black lines the standard deviations of the respective simulations.

ethanol concentration, which could explain the lower value for the self-diffusion coefficient compared to the simulation with high ethanol content. In order to derive information of the changes in the micelle structure and form, the moments of inertia about the three principal micelle axes, I1 to I3, as well as the total moment of inertia, Itot, were computed for the three systems as shown in Chapter 4.3 (see Equations 4.1 to 4.5). The moments of inertia for the aqueous solutions of a pure CTAB micelle, a CTAB micelle in the presence of low ethanol concentration (5 molecules ≙ 11.4 mM) and a CTAB micelle in the presence of high ethanol concentration (30 molecules ≙ 68.3 mM) are plotted over the simulation time (omitting first

25 ns as equilibration time) in Figure 5.4 and in the Figure 8.1 and Figure 8.2 in the Appendix. The average values of the moments of inertia with their standard deviations for the three simulations are depicted in Table 1 and visualized in Figure 5.5. Additionally the corresponding radii of gyration (see Chapter 4.3) are shown in Figures Figure 8.3 to

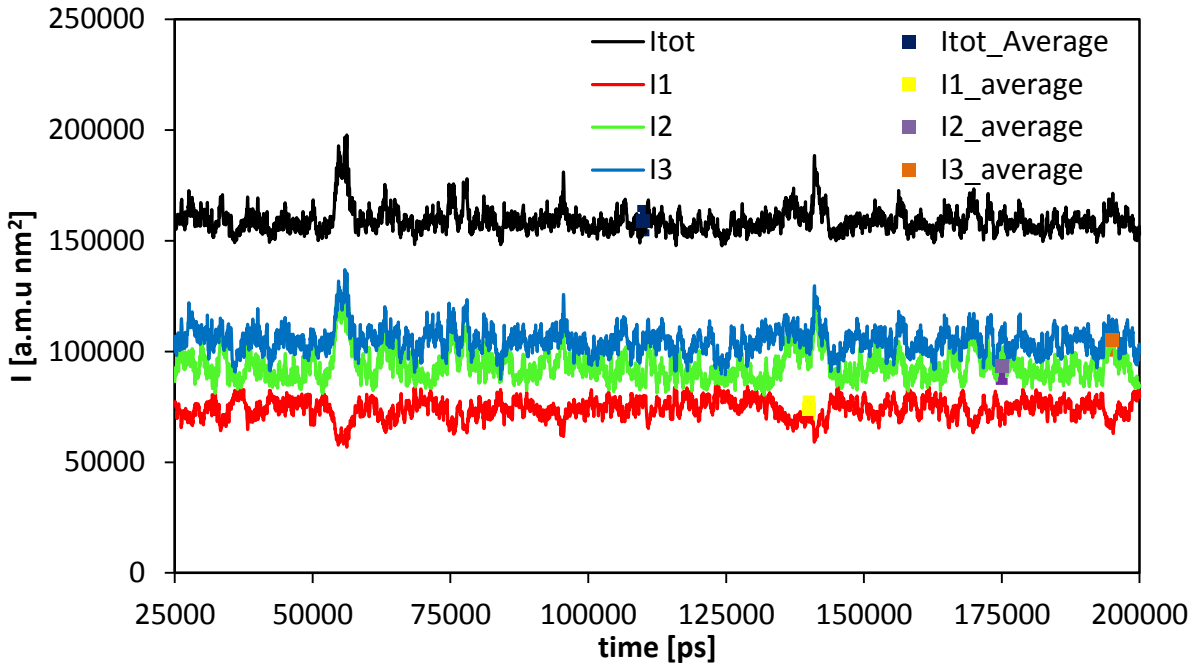

Figure 5.4: Time development of the moments of inertia for all three principal micelle axes and the total moment of inertia for pure CTAB micelle containing 110 surfactant molecules in aqueous solution. The average is calculated over period 25-200 ns and the error bar is calculated as the standard deviation.

Figure 8.5 in the Appendix. Figure 5.4 shows that the pure CTAB micelle solvated in water exhibits an oblate form, since the total radius of gyration is greater than one and the moment of inertia I1 lies beneath I2 and I3, which differ only slightly. Moreover, all the moments of inertia and radii of gyration do not fluctuate significantly, which means that the micelle does not vary much in form over time. Looking at the results of the CTAB micelle simulation with low ethanol content in Table 1 and Figure 5.5 reveals that the micelle behaves similarly in the presence of five ethanol molecules. These five alcohol molecules present do not influence the structure of the micelle at all. The assembled CTAB molecules keep their stable form. Even if not considerably much, the thirty ethanol molecules do seem

to affect the CTAB micelle, as all the moments of inertia fluctuate more than in the two other systems. Also, the micelle is more oblate, which is shown by the change in the mean values of the simulation of CTAB and high ethanol concentration compared to the pure

Table 1: Average values and standard deviations of the moments of inertia for the simulations of the aqueous systems of a pure CTAB micelle containing 110 surfactant molecules, a CTAB micelle (110 molecules) with low and a CTAB micelle (110 molecules) with high ethanol concentration.

[a.m.u nm^2]	CTAB (110 molecules)	CTAB + 5 ethanol molecules	CTAB + 30 ethanol molecules
Itot	159100 ± 5500	159700 ± 4700	161500 ± 6400
I1	74100 ± 4500	73600 ± 4200	72900 ± 4800
I2	93400 ± 6800	94000 ± 6000	95900 ± 7600
I3	105100 ± 5900	106000 ± 5200	107200 ± 6300

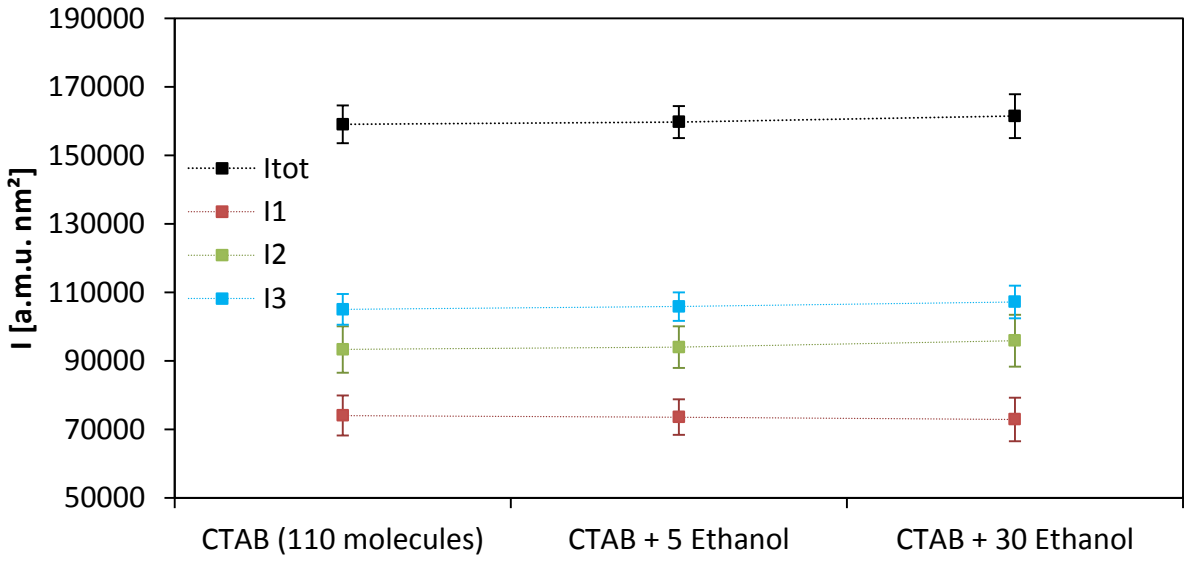

Figure 5.5: Mean values and standard deviations of the moments of inertia for the simulations of a pure CTAB micelle (110 molecules), a CTAB micelle with five ethanol molecules and a CTAB micelle with 30 ethanol molecules.

micelle system. The greater fluctuations and the small changes in the micelle structure compared to the pure CTAB micelle and the micelle with low ethanol concentration can be explained by the sustained flow of ethanol molecules into and out of the micelles, like discussed above (see Figure 5.1 and Figure 5.3). This flow is less strongly pronounced for the small ethanol concentration. Ethanol is known to raise the cmc and to reduce the aggregation number of CTAB, due to a decrease of the dielectric constant of water.[18, 21, 29, 31] At the same time the ionization degree, α, is raised. Both effects lead to an intensification of the repulsions of the headgroups. Furthermore ethanol molecules break the water structure, which causes a weakening of the hydrophobic interaction between the surfactant tails.[18, 21-22, 31] As a result, the micelle fluctuates more in form and is more unstable. Although the differences lie within the error bars, the tendency of the ethanol molecules causing higher fluctuations of the micelle form shown in this work is in good agreement with the experimental data.

The radial distribution functions (RDFs) in Figure 5.6 and Figure 5.7 calculated according to Equation 4.6 shall reveal the place, the ethanol molecules favor. Here, the RDFs between the micelle center of mass (COM), surfactant headgroup atoms and surfactant tail atoms as well as between the ethanol OH-groups, surfactant headgroup atoms and micelle center of mass are depicted for the simulation of the CTAB micelle (110 molecules) with five ethanol molecules and for the simulation of the CTAB micelle (110 molecules) with the high alcohol concentration. The surfactant headgroup consists of the N-atom and the three methyl groups and the rest of the molecule refers to the surfactant tail. The values for the ethanol-RDFs, which are normalized by the number of present alcohol molecules, are multiplied by a factor of five and 30, respectively, in order to make the curves visible in the plot. The RDFs between ethanol and the micelle center of mass and both CTAB-RDFs in Figure 5.6 and Figure 5.7 show that the ethanol molecules are most likely found beneath the headgroups of the CTAB molecules at a distance to the micelle center of mass of approximately 1.98 to 2.1 nm. These values are obtained by picking the highest points of the respective peaks for both simulations. The fact that the ethanol molecules favor a position within the palisade layer of the micelle has been be confirmed experimentally for example by Zana et.al[18] and theoretically by Patra et al.[63] The little difference in the values for the low and high ethanol concentration can be a result of the higher fluctuation of the micelle structure in the

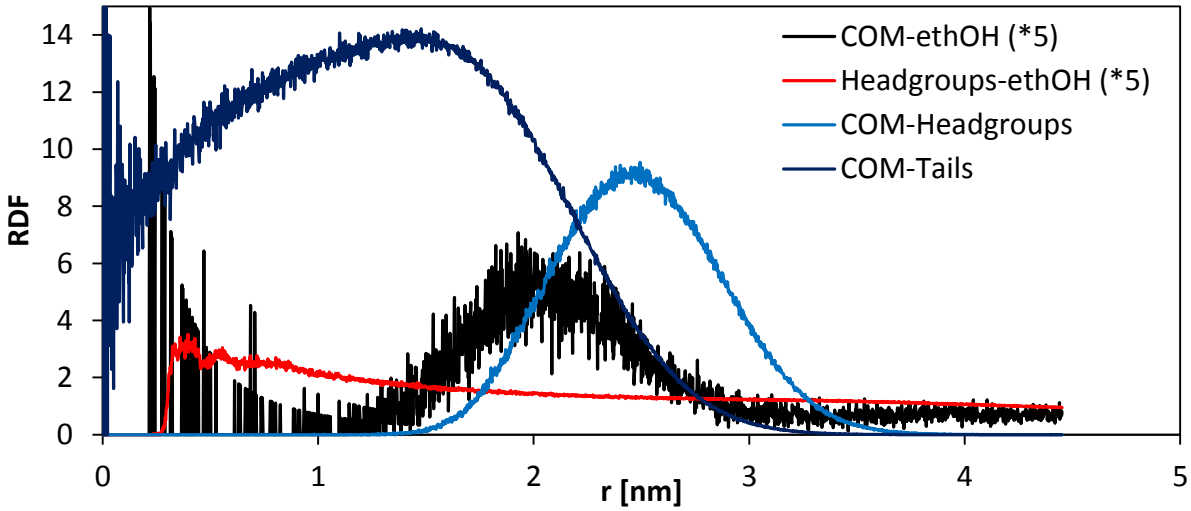

Figure 5.6: Radial distribution functions (RDFs) for the CTAB micelle simulation containing 5 ethanol molecules. The RDFs between the micelle center of mass (COM), headgroup atoms, tail atoms and the ethanol OH-groups as well as between surfactant headgroup atoms and the ethanol OH-groups are shown.

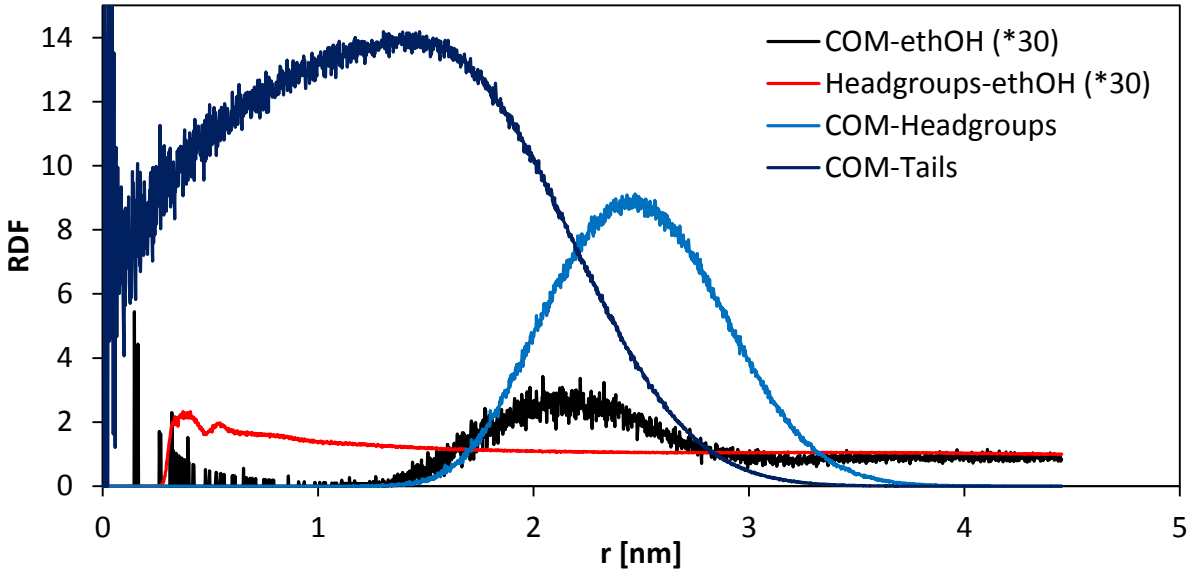

Figure 5.7: Radial distribution functions (RDFs) for the CTAB micelle simulation containing 30 ethanol molecules. The RDFs between the micelle center of mass (COM), headgroup atoms, tail atoms and the ethanol OH-groups as well as between surfactant headgroup atoms and the ethanol OH-groups are shown.

presence of high ethanol content as discussed above (see for example Table 1). Furthermore, both peaks are quite broad, meaning that the ethanol molecules move around much. This can also be concluded from both RDFs between the surfactant headgroup atoms and the ethanol OH-groups, which do not become zero for larger distances. However, two small peaks at a distance of approximately 0.35 and 0.55 nm from the headgroups can be noticed, which show two preferential positions around the headgroups for the ethanol molecules. These two distances agree with the findings of the RDFs between micelle COM and the ethanol OH-groups and between micelle COM and the headgroup atoms and the discussed above. The noise at the beginning of the RDFs between the micelle COM and the surfactant tail atoms and between the micelle COM and the ethanol OH-groups for both alcohol concentrations is expected of the RDF calculation method for small distances: since the volume of the slice around the central point, the micelle center of COM, exhibits very small values for short radii (see Figure 4.4) and surfactant tail atoms and obviously even some ethanol OH-groups are located in the close vicinity of the micelle COM at some points during the simulation, huge values of the RDF can be generated.

Furthermore, in order to compare the CTAB micelle with no added alcohol to both ethanol simulations, the RDFs between the micelle COM, the surfactant tail atoms and surfactant headgroup atoms for the three systems are depicted in Figure 5.8. Looking at the graphs, no considerable differences can be derived. Only the RDF between the micelle center of mass and the headgroup atoms for the simulation with high ethanol concentration lies slightly below and is slightly broader than the other two curves. This means that there is a little more fluctuation in the micelle structure noticeable. Additionally, the distance between the micelle center of mass and the headgroups (radius of micelle) can be obtained by looking at the peak values of the RDF between the micelle center of mass and the surfactant headgroup atoms in Figure 5.8. Thus, a micelle radius of approximately 2.4 nm can be shown by picking the highest value of the peak. For example Cata et al.[40] simulated CTAB micelles in aqueous solution and also computed the outer micelle radius. For a CTAB micelle containing 110 surfactant molecules they obtained 2.69 nm for the distance between the micelle center of mass and the headgroups, by also referring to the maximum of the peak values. Taking into account that they only simulated for 10.5 ns at 300 K in the NVT ensemble with a

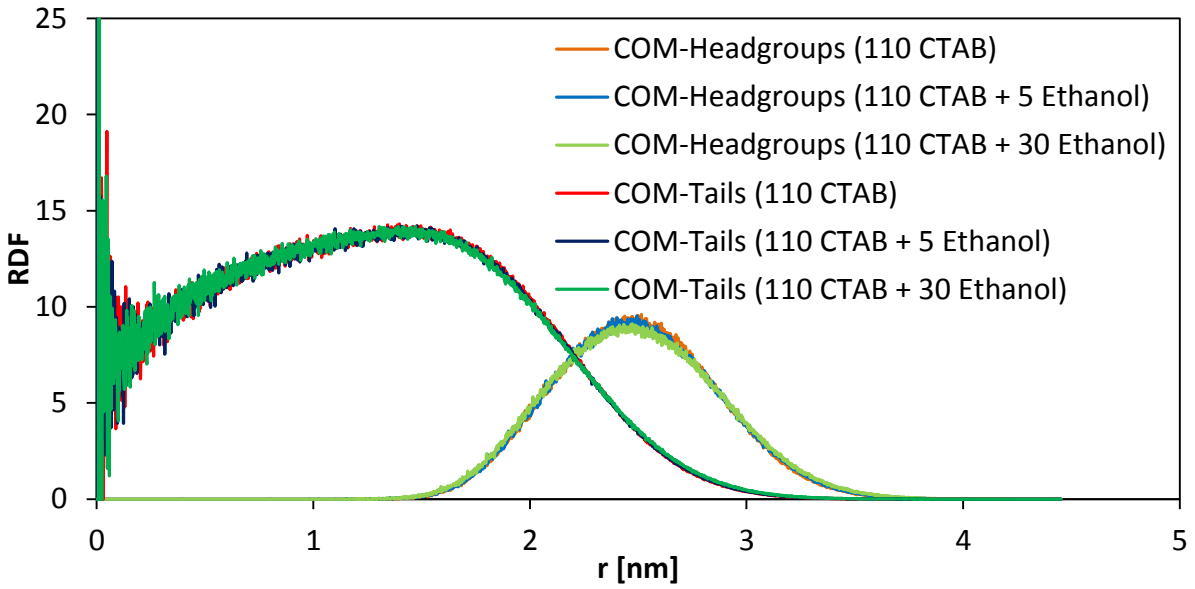

Figure 5.8: Radial distribution functions between the micelle center of mass, the surfactant headgroup atoms and surfactant tail atoms for the simulations of the micelle containing 110 surfactant molecules with no added alcohol, the CTAB simulation with 5 ethanol molecules and from the CTAB simulation with 30 ethanol molecules.

different water model (SPC)[45] in comparison to 200 ns at 298 K in the NPT ensemble, the finding for the radius in this work shows up to be reasonable.

In order to obtain information about the inner structure of the CTAB micelle, the dihedral angle distribution and hence the gauche defect probabilities for the CTAB surfactant tail groups were also calculated. This calculation gives the probabilities for the surfactant tails of having a kink along the chain. The labelling of the dihedral along the CTAB chain is presented in Figure 5.9. The dihedral angle distribution of the surfactant tails for the CTAB simulation (110 molecules) with no added alcohol is presented in the Figure 5.10.

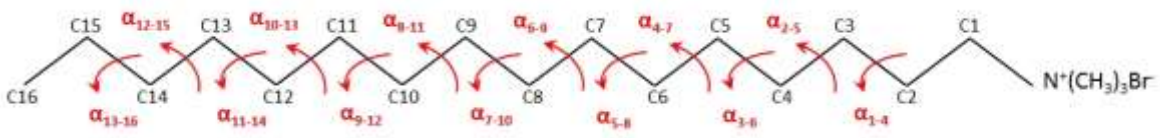

Figure 5.9: CTAB molecule with its dihedrals α_{i-j} along the carbon chain (C_i).

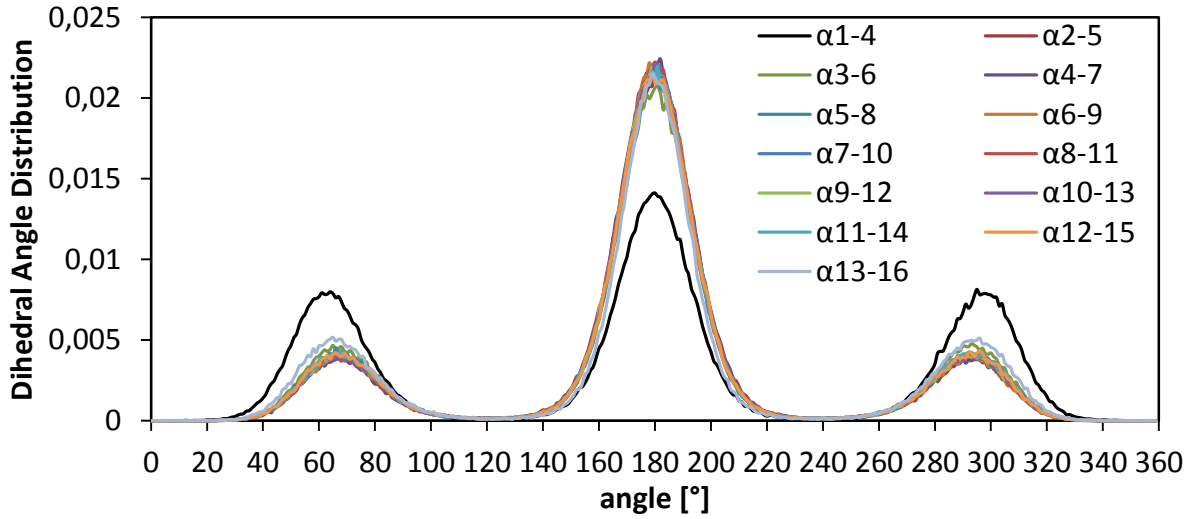

Figure 5.10: Dihedral angle distribution for the CTAB micelle containing 110 surfactant molecules and no added alcohol. Labeling is according to Figure 5.9.

Almost all dihedrals behave equally, meaning that the gauche defects (peaks at 60° and 300°) are distributed equally with little fluctuations. The striking high gauche probability for the first dihedral of the carbon chain below the headgroup is caused by the influence of the polar headgroup and was also reported for the micelles of SDS by Sammalkorpi et al.[57] The dihedral angle distributions for the surfactant tails for the simulations of a CTAB micelle with low and high ethanol concentration, which are shown in Figure 8.6 and Figure 8.7 in the Appendix, basically look alike. The short chain alcohols do not affect the micelle structure to a noticeable degree.

Since it is hard to distinguish between the curves for all the other dihedrals in all three systems, the gauche probabilities were calculated by integrating the areas under the peaks (subtracting the area for the trans dihedral angle with the peak at 180°) by means of the Simpson-rule:

$$I = \frac{b-a}{m} \cdot \frac{1}{3} \cdot \sum_{i=1}^{n-1} [f(x_{i-1}) + 4 \cdot f(x_i) + f(x_{i+1})] \qquad 5.1$$

with a and b as the interval borders, m as the number of data points x_i and $f(x_i)$ as the according function values. The gauche defect probabilities of the surfactant tail dihedrals for

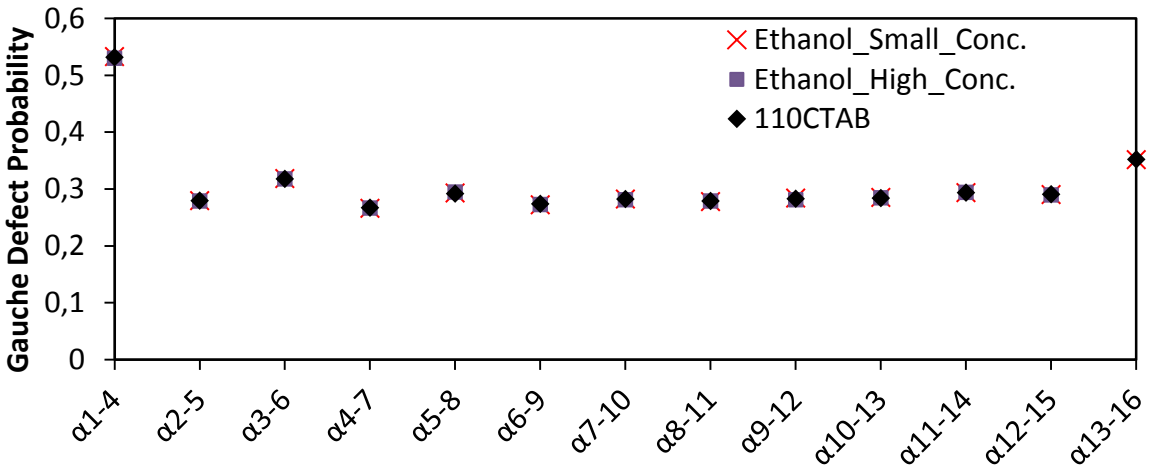

Figure 5.11: Gauche defect probabilities of the surfactant tail group dihedrals for the systems CTAB (110 surfactant molecules), CTAB with 5 ethanol molecules and CTAB with 30 ethanol molecules. Labeling is according to Figure 5.9.

the CTAB micelle with no added alcohol, the CTAB micelle with five added ethanol molecules and the CTAB micelle with 30 added ethanol molecules are depicted in Figure 5.11. Like already seen in the dihedral angle distribution diagrams the probabilities for all three simulations almost completely match. Furthermore, an increase of the gauche probability for the last dihedral can be noticed. The third and fifth dihedrals also exhibit higher values, which can be explained by the influence of the first dihedral. This fact was also found by Sammalkorpi et al.[57] All the other dihedrals show nearly the same gauche probabilities.

5.2. Simulation of CTAB with 1-Hexanol and 3-Hexanol

This chapter deals about the simulations of the aqueous CTAB micelle systems containing 1-hexanol and 3-hexanol in both low and high concentrations (5 and 30 molecules ≙ 11.4 mM and 68.3 mM). As described in Section 4.2, randomly picked CTAB molecules of the micelle with 110 surfactant molecules were first replaced by the same amount of alcohol molecules. After that the systems were composed and simulated at T = 298 K and p = 1 bar in the NPT

ensemble for 200 ns like shown in Chapters 4.1 and 4.2. Additionally to the CTAB micelle containing 110 surfactant molecules and no added alcohol, a CTAB micelle with only 80 surfactant molecules and no added alcohol was also simulated for comparison to the simulations with high alcohol concentration, since 30 surfactant molecules were replaced by 30 alcohol molecules in the 1- and 3-hexanol simulations. First it is shown, how the micelles look after 200 ns of simulation and where the longer chain alcohols like to reside during the simulation. Therefore simulation snapshots after 200 ns for the pure CTAB micelle containing 80 molecules, a CTAB micelle with low and high 1-hexanol concentration and a CTAB micelle with low and high 3-hexanol concentration are depicted in Figure 5.12 and Figure 5.13.

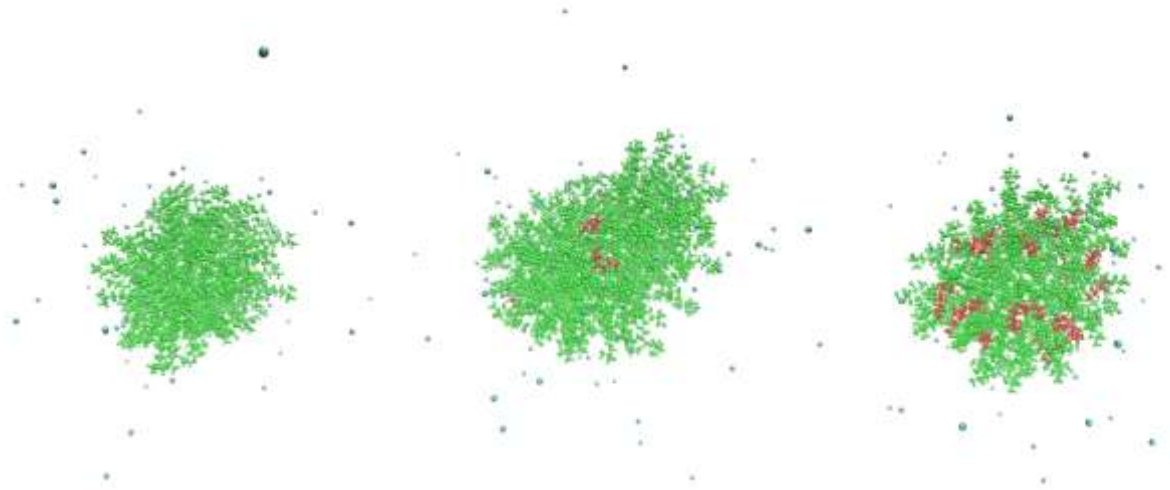

Figure 5.12: Simulation snapshots after 200 ns of a pure CTAB micelle (80 molecules) (left), a CTAB micelle (105 molecules) with five 1-hexanol molecules (middle) and a CTAB micelle (80 molecules) with 30 1-hexanol molecules (right). (CTAB = green; bromide ions = blue; 1-hexanol = red; water was omitted in the visualization).

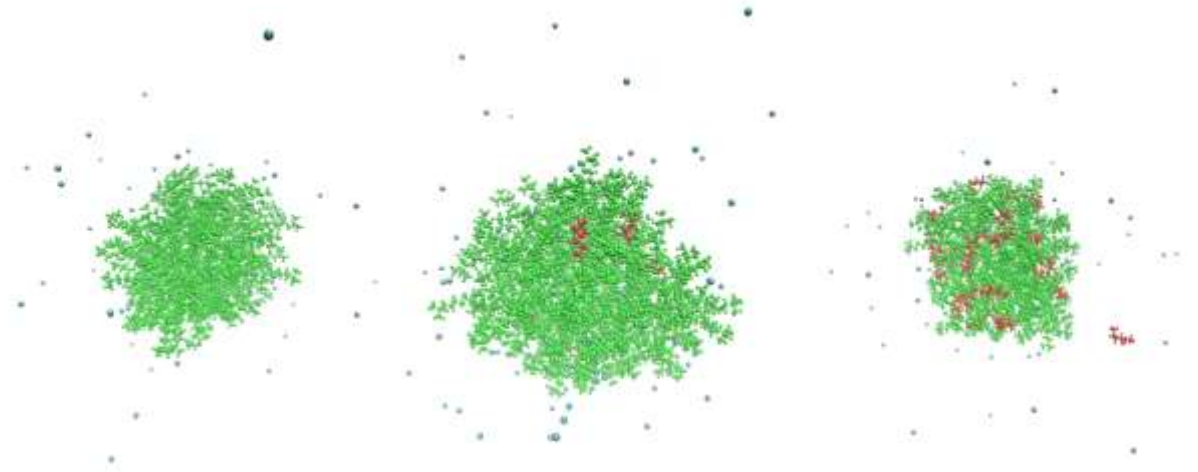

Figure 5.13: Simulation snapshots after 200 ns of a pure CTAB micelle (80 molecules) (left), a CTAB micelle (105 molecules) with five 3-hexanol molecules (middle) and a CTAB micelle (80 molecules) with 30 3-hexanol molecules (right). (CTAB = green; bromide ions = blue; 3-hexanol = red; water was omitted in the visualization).

From these pictures no noticeable visual differences in form and structure between the micelles can be observed. Furthermore these figures show that for both 1- and 3-hexanol in low and high concentration the alcohol molecules stay within the micelles with an exception for the high 3-hexanol concentration in Figure 5.13 (right), where one lose alcohol molecule flows through the water phase. In order to clarify to what extent this flowing out occurs, the number of alcohol molecules outside the micelle during the simulations was calculated. The results for the simulation with low and high 1-hexanol concentration and the results for the simulation with low and high 3-hexanol concentration are shown in Figure 5.14 and Figure 5.15. Both plots reveal that some alcohol molecules move out of the micelle during the simulation, but never more than 16% at the same time (for the high concentrations). This is because they favor a position between the surfactant molecules due to their relatively great hydrophobic parts. In addition to this, the propensity of leaving the micelle is slightly higher for the 3-hexanol molecules, which can be derived from the higher mean value for the high concentration simulation. This could stem from the fact that 3-hexanol, different to 1-hexanol, has its OH-group bonded to the middle of the carbon chain. This could lead to a higher probability of being in “unfavorable” positions between the CTAB micelle, which in

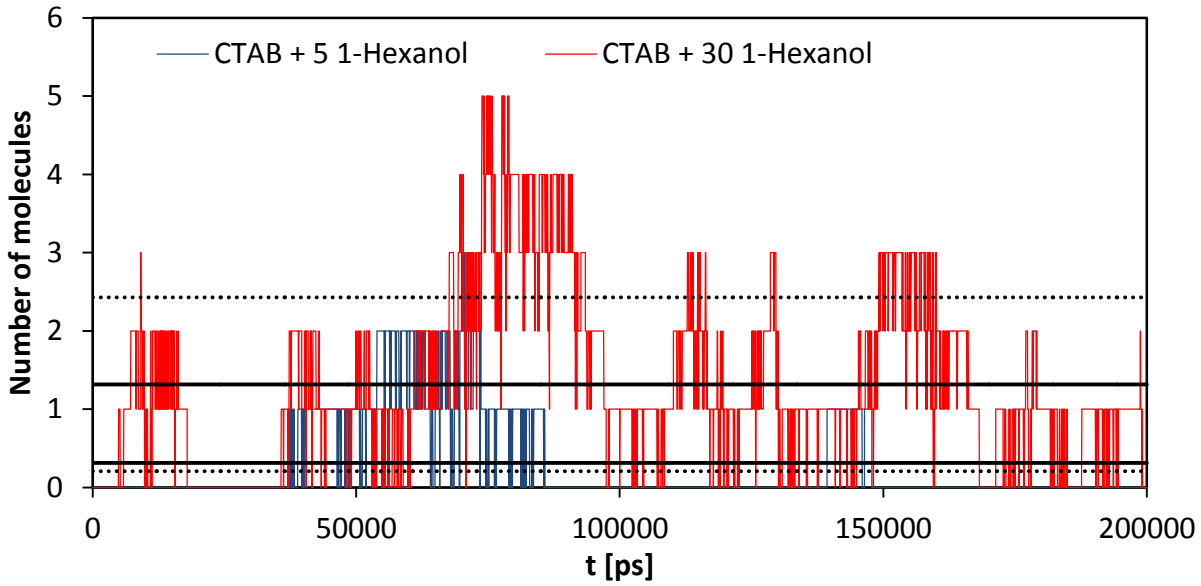

Figure 5.14: Time development of the number of whole 1-hexanol molecules outside the CTAB micelle. The micelle is assumed to have a radius of 2.3 nm (around the micelle center of mass). Black lines represent the mean values, the dashed black lines the standard deviations for the high concentration simulation.

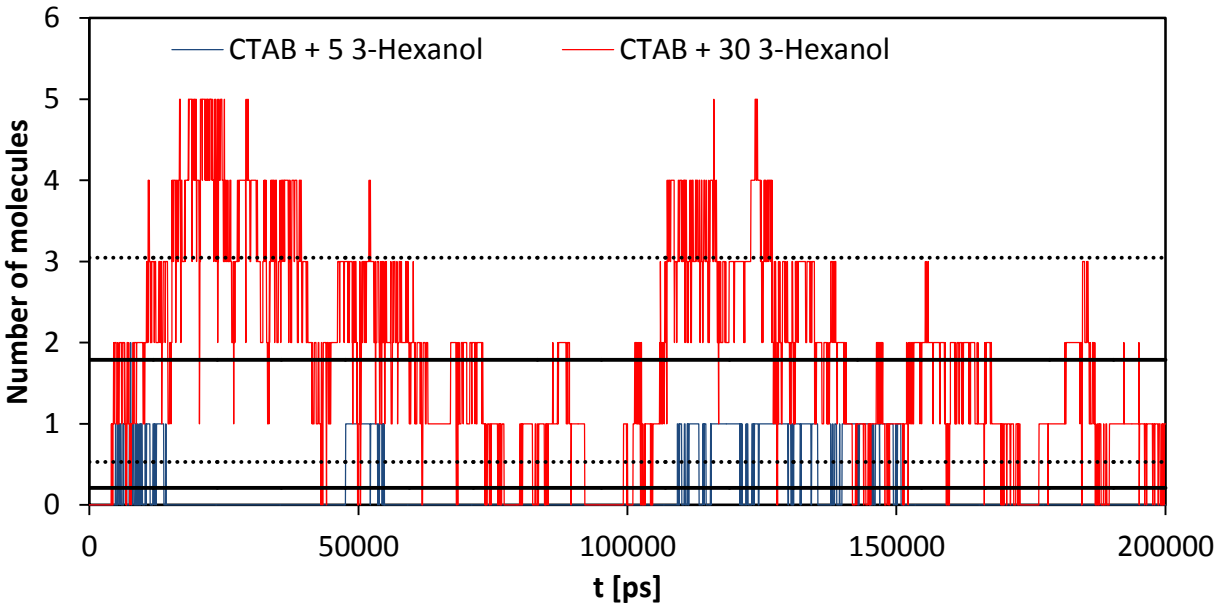

Figure 5.15: Time development of the number of whole 3-hexanol molecules outside the CTAB micelle. The micelle is assumed to have a radius of 2.3 nm (around the micelle center of mass). Black lines represent the mean values, the dashed black lines the standard deviations for the high concentration simulation.

turn could facilitate the 3-hexanol molecules moving out of the micelle. On the contrary, the structure of 1-hexanol resembles the one of the CTAB molecules with the polar group at one end of the molecule. However, in general most of the 1-hexanol and 3-hexanol molecules stay within the micelle, whereas just a small fraction tends to leave it. To further demonstrate the dynamics of the 1-hexanol and 3-hexanol molecules, the mean square displacements (MSDs) for both alcohols, which were calculated for both low and high concentration according to Equation 4.7, are presented in Figure 5.16 and Figure 5.17. From both figures less motion compared to ethanol (see Figure 5.2) can be noticed. This is due the fact that the longer chain alcohols are stuck inside and move along the micelle for most of the time. The flattening and the decrease of the MSD-values at the end parts of the curves occur due to less available data points for greater time intervals, which cause the noises. As the CHARMM-36 force field is not able to predict reasonable self-diffusion coefficients, which was already discussed in Section 5.1, it was not found necessary to calculate these for 1- and 3-hexanol. Nevertheless, motions, which are one order smaller than for ethanol, can be observed for 1- and 3-hexanol, whereas both high concentration curves nearly exhibit the same appearance and maxima. For the small concentrations simulations a different behavior can be noticed. The slope of the 1-hexanol curve, which only differs from the high concentration curve at the end part, is more than twice as high as for the 3-hexanol curve.

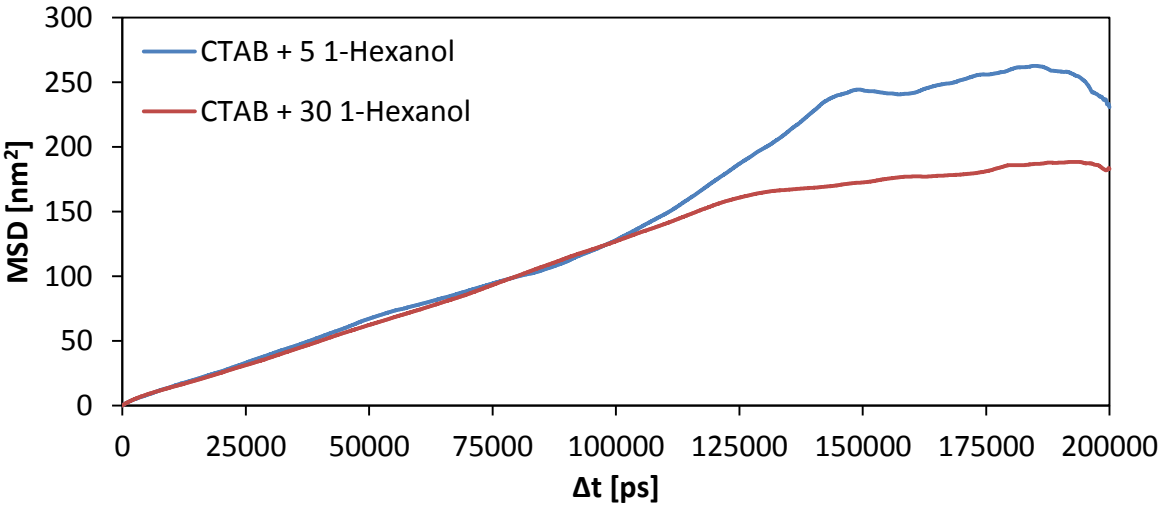

Figure 5.16: Mean square displacement (MSD) with respect to the center of mass of 1-hexanol for the simulation of CTAB and low 1-hexanol concentration and CTAB and high 1-hexanol concentration.

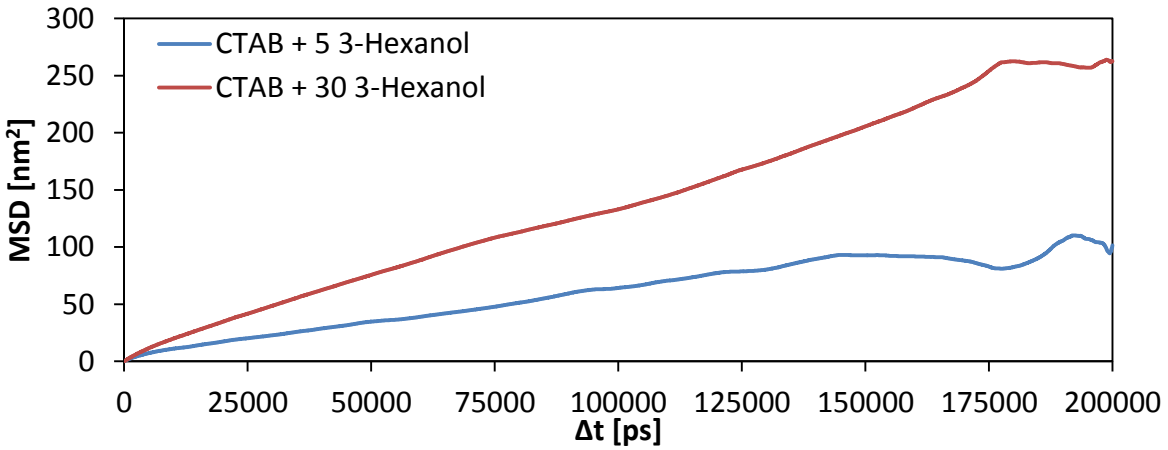

Figure 5.17: Mean square displacement (MSD) with respect to the center of mass of 3-hexanol for the simulation of CTAB and low 3-hexanol concentration and CTAB and high 3-hexanol concentration.

The difference can be elucidated by the fact that one 1-hexanol molecule moves far away from its initial position, whereas more 3-hexanol molecules seem to move out of the micelle (see Figure 5.14 and Figure 5.15). This is visualized in Figure 5.18 and Figure 5.19, where the MSD for all five molecules of each 1-hexanol and 3-hexanol simulation are depicted.

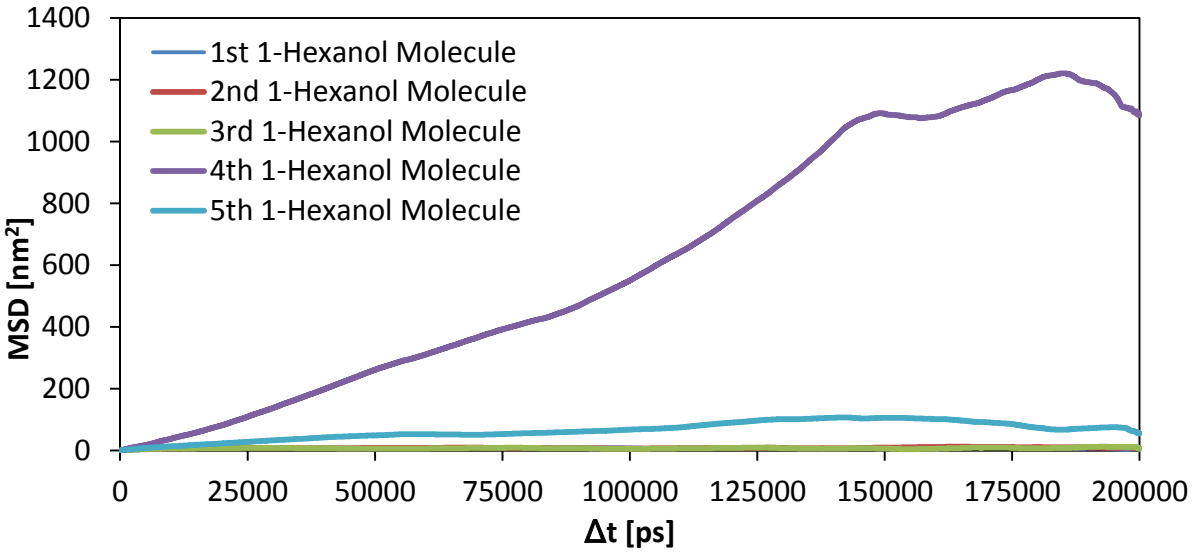

Figure 5.18: Mean square displacement (MSD) with respect to the center of mass for all five 1-hexanol molecules for the simulation of CTAB and low 1-hexanol concentration.

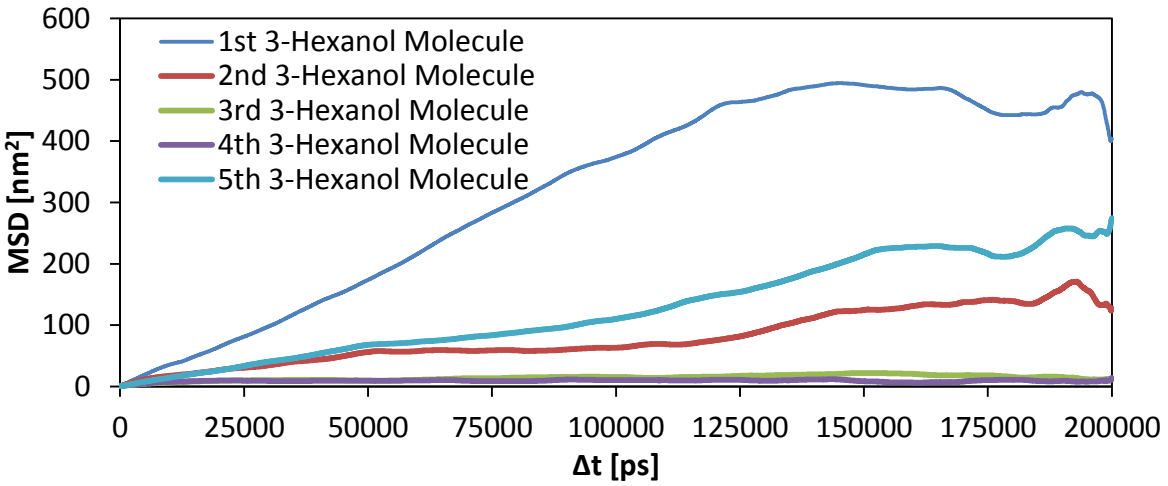

Figure 5.19: Mean square displacement (MSD) with respect to the center of mass for all five 3-hexanol molecules for the simulation of CTAB and low 3-hexanol concentration.

In order to now obtain information about possible changes in the micelle structure and form, the moments of inertia about the three principal micelle axes, I1 to I3, as well as the total moment of inertia, Itot, were also calculated for the five systems as shown in Chapter

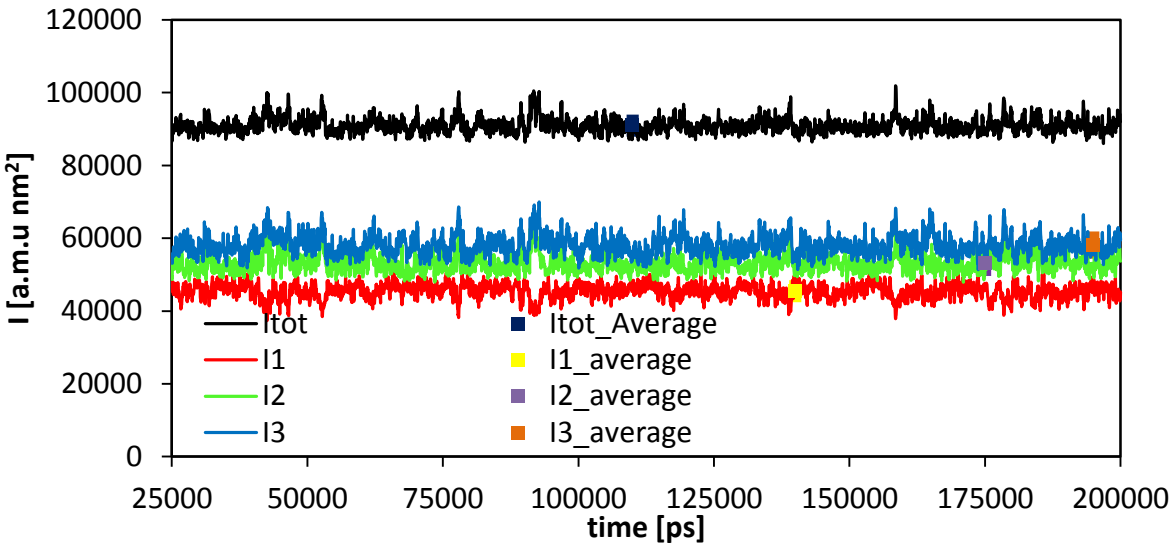

Figure 5.20: Time development of the moments of inertia for all three principal micelle axes and total moment of inertia for pure CTAB micelle containing 80 surfactant molecules in aqueous solution. The average is calculated over period 25-200 ns and the error bar is calculated as the standard deviation.

4.3 (see Equations 4.1 to 4.5). The moments of inertia for the pure CTAB micelle containing 80 surfactant molecules and for the aqueous solutions of a CTAB micelle (105 and 80 molecules) in the presence of 1-hexanol and 3-hexanol in low and high concentration are plotted over the simulation time (omitting first 25 ns as equilibration time) in Figure 5.23 and in the figures Figure 8.8 to Figure 8.11 in the Appendix. Furthermore, the average values of the moments of inertia with their standard deviations for the five simulations are depicted in Table 2 and visualized in Figure 5.5. The corresponding radii of gyration (see Chapter 4.3) are shown in the Figures Figure 8.12 to Figure 8.16 in the Appendix. From all these diagrams the slightly oblate micelle form can be derived again, due to the fact that the moment of inertia and the radius of gyration for the principal micelle axis 1 lie below the other two ones. Furthermore the plots show that the micelle containing either 5 1-hexanol

Table 2: Average values and standard deviations of the moments of inertia for the simulations of the aqueous systems of a pure CTAB micelle containing 80 surfactant micelles, a CTAB micelle (105 molecules) with both low and high 1-hexanol concentration and a CTAB micelle (80 molecules) with both low and high 3-hexanol concentration.

[a.m.u nm^2]	CTAB (80 molecules)	CTAB + 30 1-hexanol molecules	CTAB + 30 3-hexanol molecules
Itot	91000 ± 2000	98300 ± 2400	97900 ± 2600
I1	45500 ± 2100	48300 ± 2300	47800 ± 2400
I2	53000 ± 2400	57300 ± 2900	57300 ± 3100
I3	58100 ± 2800	63500 ± 3000	63200 ± 3200
[a.m.u nm^2]	CTAB + 5 1-hexanol molecules	CTAB + 5 3-hexanol molecules	
Itot	148000 ± 4200	148100 ± 4300	
I1	69100 ± 3800	69500 ± 3900	
I2	87100 ± 5400	86700 ± 5300	
I3	97400 ± 4700	97600 ± 5000	

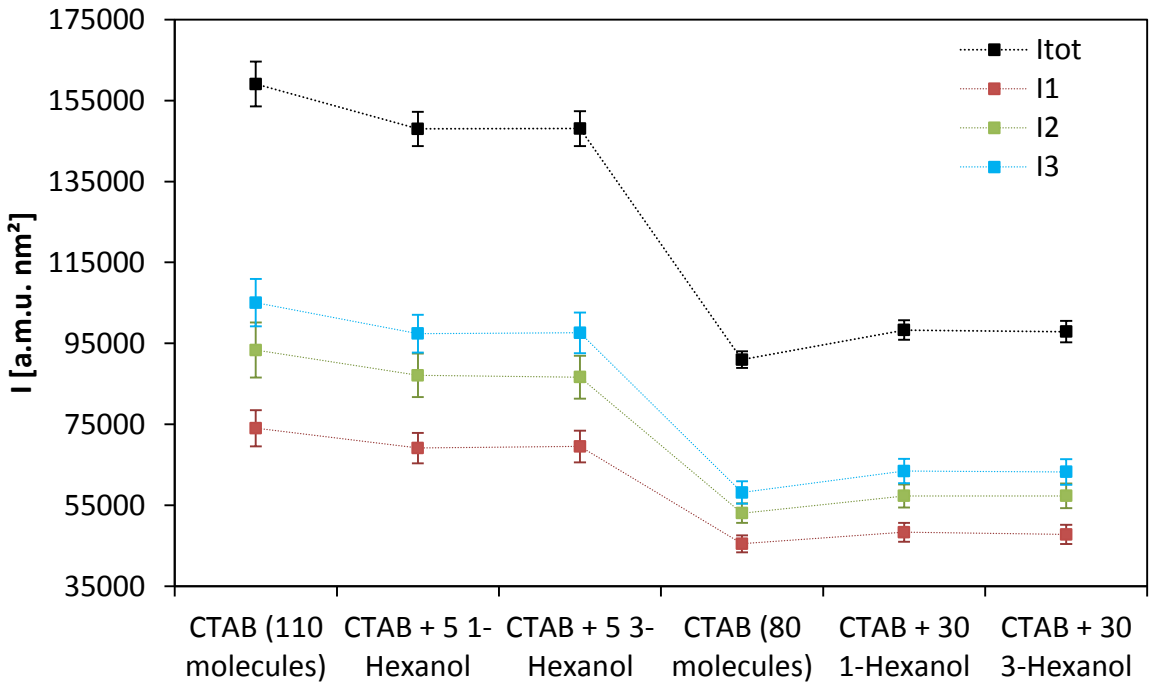

Figure 5.21: Mean values and standard deviations of the moments of inertia for the simulations of two pure CTAB micelles (110 and 80 molecules), a CTAB micelle (105 molecules) with either five 1-hexanol or five 3-hexanol molecules and a CTAB micelle (80 molecules) with either 30 1-hexanol or 30 3-hexanol molecules.

or 3-hexanol molecules stays stable for the whole simulation time by looking at each of the curves in the diagrams. The only differences, which are the lower values for all data points compared to the micelle containing 110 surfactant molecules and no added alcohol, arises from the fact that the micelle only contains 105 surfactant molecules. This trend can also be observed from the moment of inertia plot of the micelle containing 80 surfactant molecules and no added alcohol in Figure 5.20, where the values are yet smaller. Again it is found that the alcohol in small concentration does not affect the micelle structure at all. Since no changes can be noticed, it was not found necessary to simulate a pure micelle with 105 surfactant molecules in aqueous solution. From the simulations with the higher alcohol concentrations (Table 2 and Figure 5.21) it can be noticed that the mean values and standard deviations for the moments of inertia show distinct higher values than those of the pure micelle containing 80 surfactant molecules and that the fluctuations are slightly increased. However, all values of the moments of inertia about the three principal micelle axes are

raised by almost the same amount. This means that there is no change in the form, since all micelle dimensions are just increased in the same way. Consequently, it is obvious that, despite the number of surfactant molecules in the micelle is kept constant, the 30 1-hexanol and 3-hexanol molecules do influence the micelle structure in the same way. Even if the values do not reach those of the micelle containing 110 surfactant molecules (compare Table 2), the values of the moments of inertia are raised by approximately five to nine percent for the simulations with high 1-hexanol and 3-hexanol concentration. Consequently, it can be assumed, that the CTAB surfactant molecules and the longer chain alcohols 1-hexanol and 3-hexanol form comicelles, which was already detected experimentally by Dubey.[24] Medium to long chain alcohols are known to lower the cmc and to raise the aggregation number of CTAB at the same time. With more molecules forming the micelle, the ionization degree is increased, which in turn leads to stronger repulsions of the headgroups.[18] This could explain the higher fluctuations of the micelles containing 30 alcohol molecules compared to the pure micelle consisting of 80 molecules. The presence of comicelles can be confirmed by the mean square displacement plots of CTAB for the simulations of the CTAB micelle with either 1- or 3-hexanol and the CTAB micelles containing both 110 and 80 surfactant molecules and no added alcohol in Figure 5.22 and Figure 5.23.

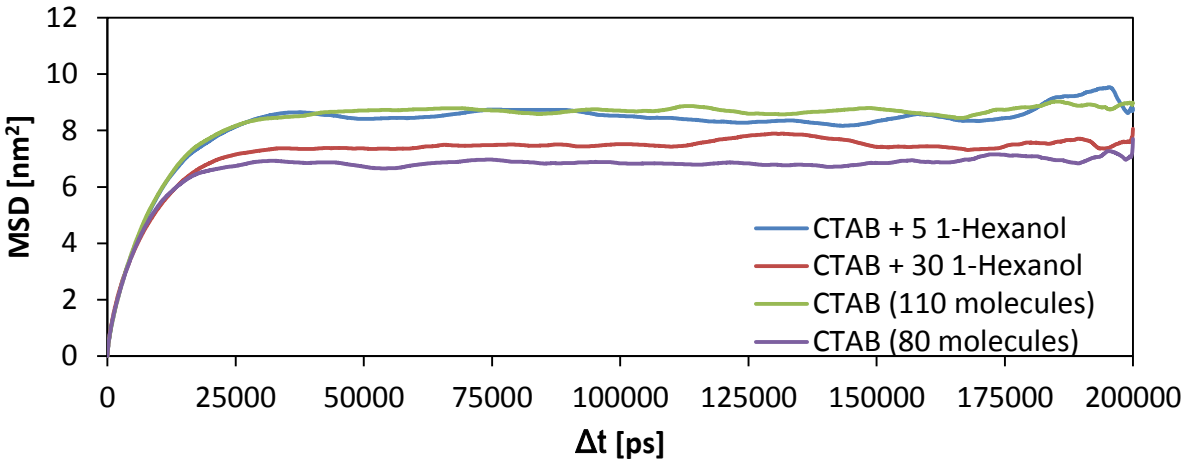

Figure 5.22: Mean square displacement with respect to the center of mass of CTAB for the simulations of both micelles consisting of 110 and 80 molecules with no added alcohol and for the CTAB micelles with low and high 1-hexanol concentration.

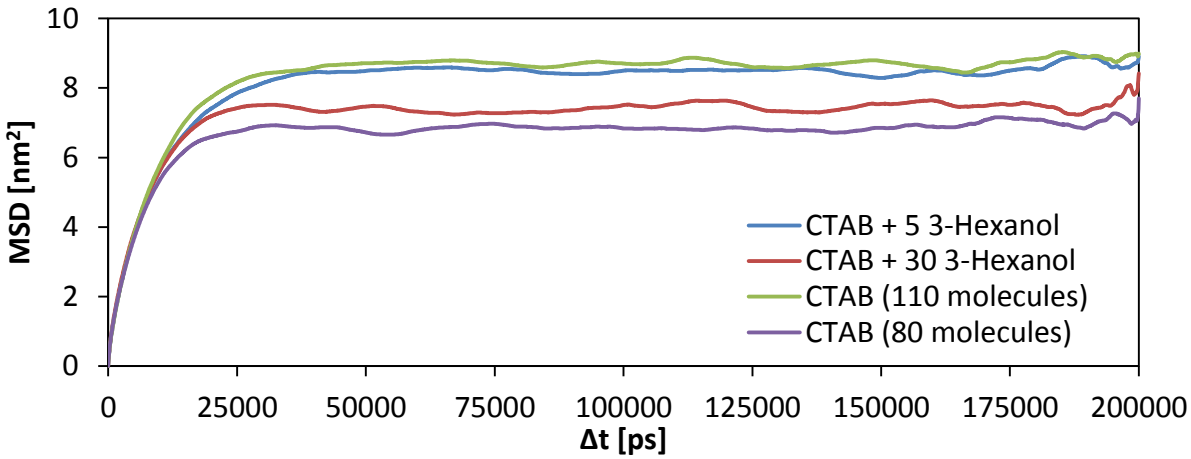

Figure 5.23: Mean square displacement with respect to the center of mass of CTAB for the simulations of both micelles consisting of 110 and 80 molecules with no added alcohol and for the CTAB micelles with low and high 3-hexanol concentration.

The slight difference between the curve of the CTAB micelle containing 110 molecules and no added alcohol and the CTAB micelle with either low 1- or 3-hexanol simply arises from the fact that the latter simulations were carried out with a micelle of just 105 surfactant molecules and therefore exhibit lower values. However, from both Figure 5.22 and Figure 5.23 the shift from the curve of the micelle containing 80 surfactant molecules towards the curve of the micelle containing 110 surfactant molecules for both simulations containing high 1- and 3-hexanol concentration can be noticed. This again is explained by the fact that more molecules are present in the micelle or that comicelles are present, respectively.

In order to gain more information about these comicelles and especially where the alcohol molecules like to be located between the surfactant molecules, the radial distribution functions between the micelle center of mass, the surfactant tail atoms and surfactant headgroup atoms as well as between the alcohol OH-groups, the micelle center of mass and headgroup atoms were computed according to Equation 4.6. The values for the 1-hexanol and 3-hexanol-RDFs, which are normalized by the number of present alcohol molecules, are partly multiplied by a factor of five and 30, respectively, in order to make the curves visible in the plot. First the RDFs for the CTAB micelle simulation with low and high 1-hexanol concentration are discussed, which are presented in Figure 5.24 and Figure 5.25.

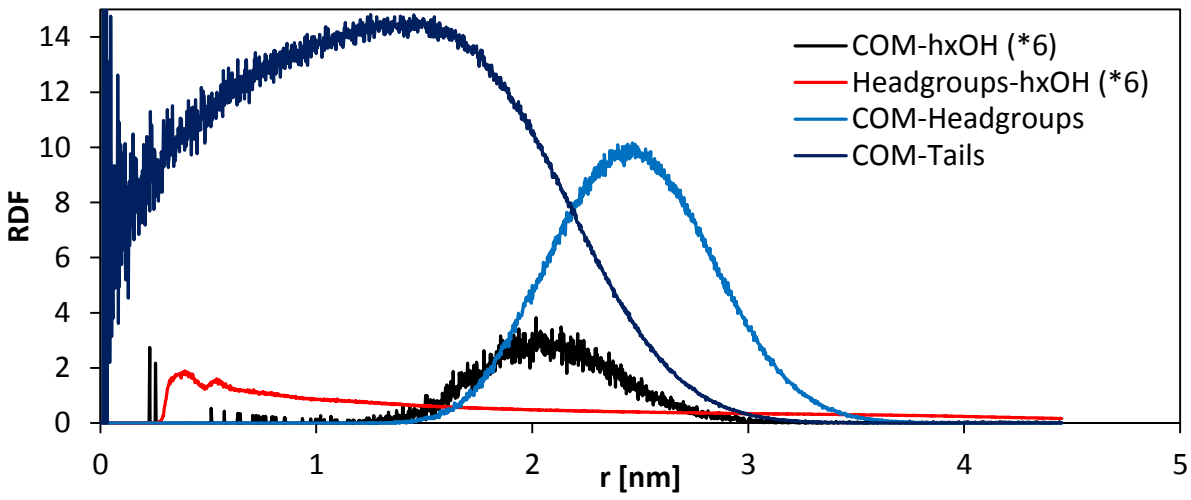

Figure 5.24: Radial distribution functions (RDFs) for the CTAB micelle simulation containing 5 1-hexanol molecules. The RDFs between the micelle center of mass (COM), headgroup atoms, tail atoms and the 1-hexanol OH-groups as well as between the 1-hexanol OH-groups and the surfactant headgroup atoms are shown.

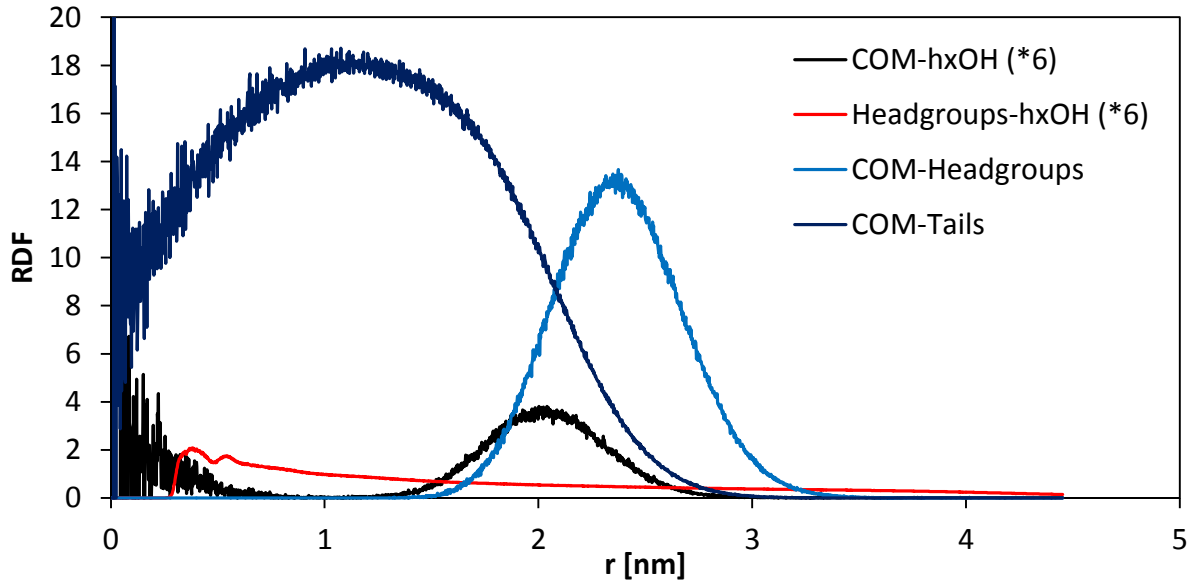

Figure 5.25: Radial distribution functions (RDFs) for the CTAB micelle simulation containing 30 1-hexanol molecules. The RDFs between the micelle center of mass (COM), headgroup atoms, tail atoms and the 1-hexanol OH-groups as well as between the 1-hexanol OH-groups and the surfactant headgroup atoms are shown.

From the RDFs between the micelle center of mass and the 1-hexanol OH-group for low and high alcohol concentration and the RDFs between the micelle center of mass and the headgroup atoms for both 1-hexanol concentrations, the locations of 1-hexanol or the OH-groups, respectively, can be obtained by picking the highest value of the peaks. The alcohol groups hence lie approximately 0.4 nm (low concentration) and 0.3 nm (high concentration) below the headgroups next to the first or second carbon atoms below the nitrogen atom. Other than for the ethanol molecules, these peaks become zero for greater distances. This means that the alcohols preferably stay within the micelle (see Figure 5.14). The same can be derived from the RDFs between the surfactant headgroup atoms and the 1-hexanol OH-groups. However, here two peaks occur at a distance of approximately 0.35 nm (0.4 nm) and 0.50 nm (0.55 nm) in both diagrams, which show two preferential whereabouts of the 1-hexanol molecules. This was already found for ethanol above (see Figure 5.6 and Figure 5.7). Again this finding agrees with experimental results of for example Zana et al.[18] or Patra et al.,[63] who reported that alcohols molecules favor a position within the palisade layer. Furthermore, the RDFs between the micelle center of mass, the tails atoms and headgroup atoms for the high 1-hexanol concentration in Figure 5.25 and both ethanol concentrations in Figure 5.6 and Figure 5.7 show that the micelle containing only 80 surfactant and 30 1-hexanol molecules tends to be more compact than the one with 110 surfactant molecules. The distance between the micelle center of mass and the headgroup atoms is reduced from approximately 2.4 nm for the micelle consisting of 110 molecules to 2.3 nm for the micelle consisting of only 80 molecules and 30 1-hexanol molecules. The noise at the beginning of the RDFs between the micelle COM and the surfactant tail atoms and between the micelle COM and the 1-hexanol OH-groups (especially for the high alcohol concentrations) is expected due to the RDF calculation method for small distances: since the volume of the slice around the central point, the micelle center of COM, exhibits very small values for short radii (see Figure 4.4) and surfactant tail atoms and some 1-hexanol OH-groups are located in the close vicinity of the micelle COM at some points during the simulation, huge values of the RDF can be generated.

Additionally the RDFs between the micelle center of mass, the surfactant tail atoms and surfactant headgroup atoms as well as between the alcohol OH-groups, the micelle center of mass and headgroup atoms for the simulation of the CTAB micelle containing low and high 3-hexanol content are shown in Figure 5.26 and Figure 5.27.

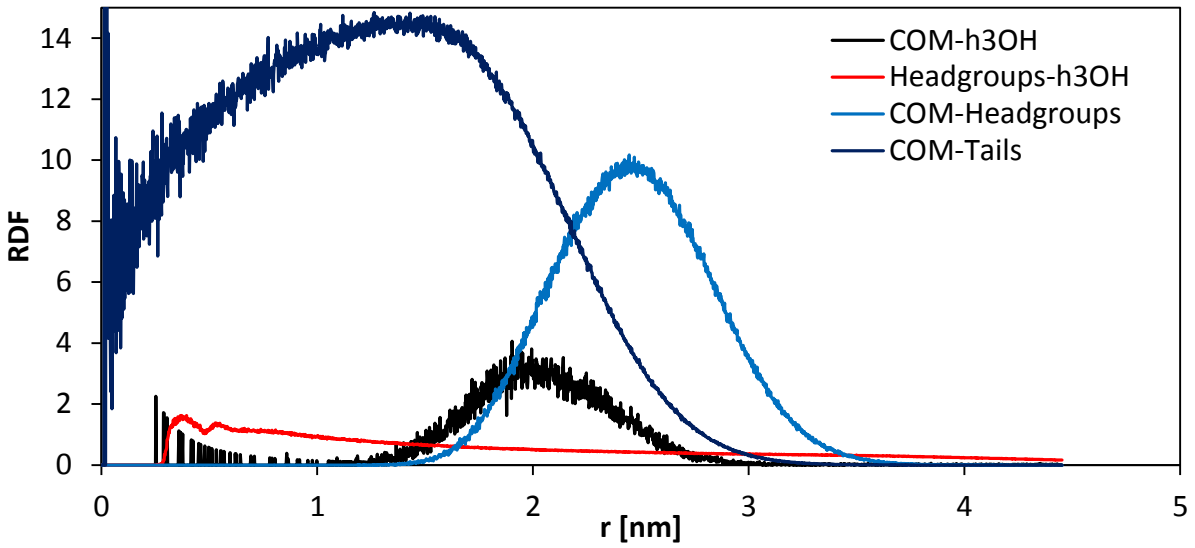

Figure 5.26: Radial distribution functions (RDFs) for the CTAB micelle simulation containing 5 3-hexanol molecules. The RDFs between the micelle center of mass (COM), headgroup atoms, tail atoms and the 3-hexanol OH-groups as well as between the 3-hexanol OH-groups and the surfactant headgroup atoms are shown.

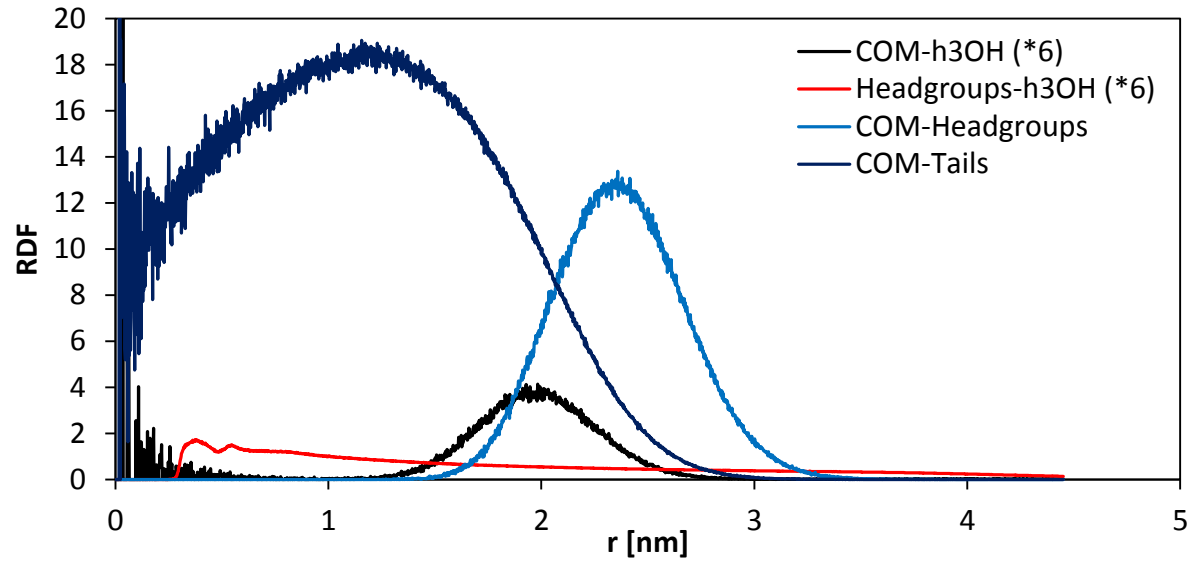

Figure 5.27: Radial distribution functions (RDFs) for the CTAB micelle simulation containing 30 3-hexanol molecules. The RDFs between the micelle center of mass (COM), headgroup atoms, tail atoms and the 3-hexanol OH-groups as well as between the 3-hexanol OH-groups and the surfactant headgroup atoms are shown.

From these two RDF plots of 3-hexanol basically the same finding as for the micelle with 1-hexanol can be derived. Again a distance of 0.3 to 0.4 nm between the OH-group and the headgroups of the surfactant molecules can be obtained from both RDFs between 3-hexanol and the surfactant headgroups. This means that 3-hexanol, just like 1-hexanol, favors a position close to the first or second carbon atom below the N-atom of the headgroup. Additionally the effect of the more compact micelle can also be observed for the 3-hexanol simulations, with the micelle radius being reduced from approximately 2.4 nm to 2.3 nm again.

In order to further investigate this effect, the RDFs between the micelle center of mass and both the surfactant tails and surfactant headgroups were calculated for the simulations of both the pure CTAB micelle containing 110 and 80 surfactant molecules, for the simulations of the CTAB micelle with low and high 1-hexanol concentration and for the simulations of the CTAB micelle with low and high 3-hexanol concentration. The results are plotted in Figure 5.28 and Figure 5.29.

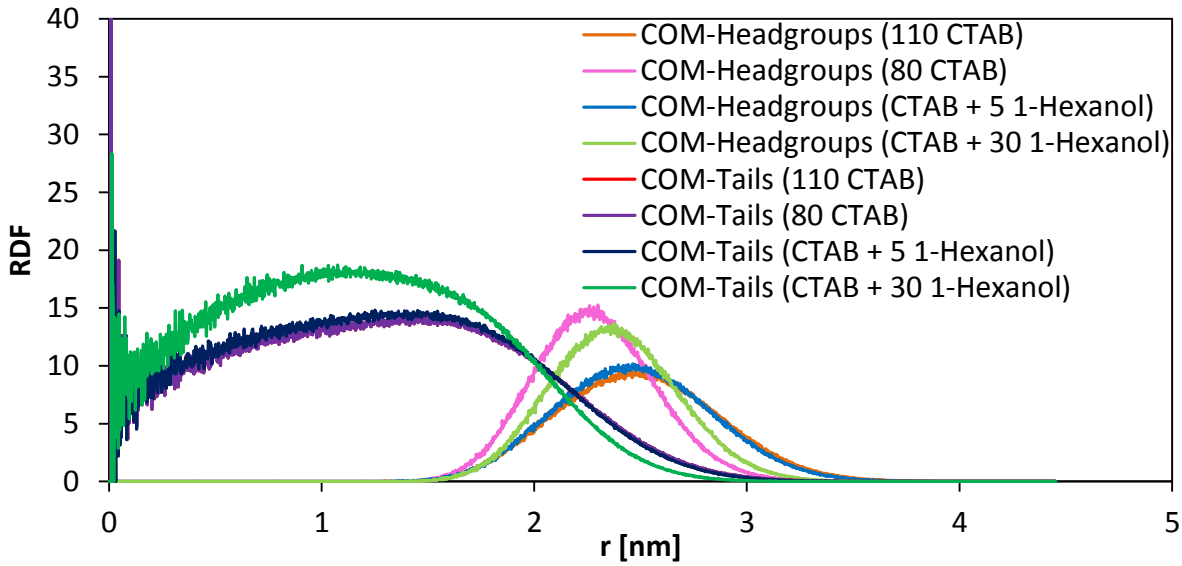

Figure 5.28: Radial distribution functions between the micelle center of mass, the surfactant headgroup atoms and surfactant tail atoms for the simulations of the micelle containing 110 surfactant molecules with no added alcohol, the CTAB simulation with 5 1-hexanol molecules and from the CTAB simulation with 30 1-hexanol molecules.

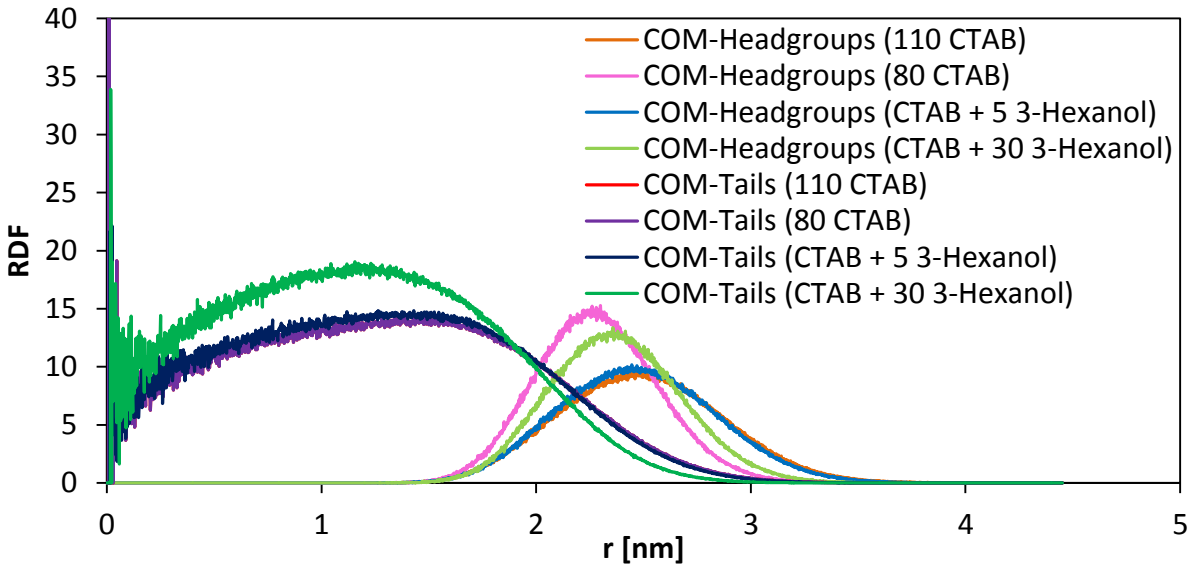

Figure 5.29: Radial distribution functions between the micelle center of mass, the surfactant headgroup atoms and surfactant tail atoms for the simulations of the micelle containing 110 surfactant molecules with no added alcohol, the CTAB simulation with 5 3-hexanol molecules and from the CTAB simulation with 30 3-hexanol molecules.

The RDFs between the micelle center of mass and the surfactant tails for the simulation of both pure CTAB micelles and the CTAB micelle with 1-hexanol and 3-hexanol at low and high concentration in Figure 5.28 and Figure 5.29 show that the tail groups of the surfactant molecules are packed more tightly in the presence of the longer chain alcohols than for the pure micelle with 80 and 110 molecules (compare dark green curve to purple and dark blue one, which cover the red curve). The fact, that the curves for the micelles containing only 80 molecules lie above the ones of the micelles with 110 molecules, simply stems from smaller amount of surfactant molecules present. This again exhibits the more compact micelle with 80 surfactant molecules. The same holds true for the surfactant headgroups, whereas a shift of the distance towards the micelle center of mass is visible. Cata et al.[40] simulated a micelle containing 80 surfactant molecules for 10.5 ns and obtained a micelle radius of 2.46 nm by picking the highest value of the peak for the RDF between the headgroups and the micelle center of mass. For the CTAB micelle with 80 surfactant molecules and no added alcohol a radius of approximately 2.2 nm was achieved. Considering the different conditions for the simulations used in this work, like already discussed in Section 5.1, the finding in this work is

reasonable. The RDFs between the micelle center of mass and the headgroups for the simulations of the micelle with 30 1-hexanol and 3-hexanol molecules additionally show a greater distance and a lower peak in comparison to the RDFs of the micelle with 80 molecules and no added alcohol. This elucidates again that the CTAB molecules form comicelles with 1-hexanol and 3-hexanol. The alcohol molecules hence compensate the vanished surfactant molecules to a certain level.

To further investigate the influence of 1-hexanol and 3-hexanol on the CTAB micelle and its inner structure, the dihedral angle distributions for the CTAB tail groups and hence the gauche defect probabilities were also calculated. The dihedral angle distribution of the surfactant tails for the CTAB simulation (110 molecules) with no added alcohol is presented in Figure 5.30. Together with the dihedral angle distribution of the surfactant tails for the CTAB micelle with 110 surfactant molecules in Figure 5.10 it can be concluded, that the pure micelle containing only 80 surfactant molecules exhibits equal dihedral angle distributions. The higher probability of having a kink for the first dihedral group compared to all dihedrals stems from the influence of the polar headgroup like already discussed in Section 5.1 for ethanol. The dihedral angle distributions for the CTAB micelle (105 and 80 molecules) with low and high 1-hexanol concentration and for the CTAB micelle (105 and 80 molecules) with low and high 3-hexanol concentration, plotted in the Figure 8.17 to Figure 8.20 in the

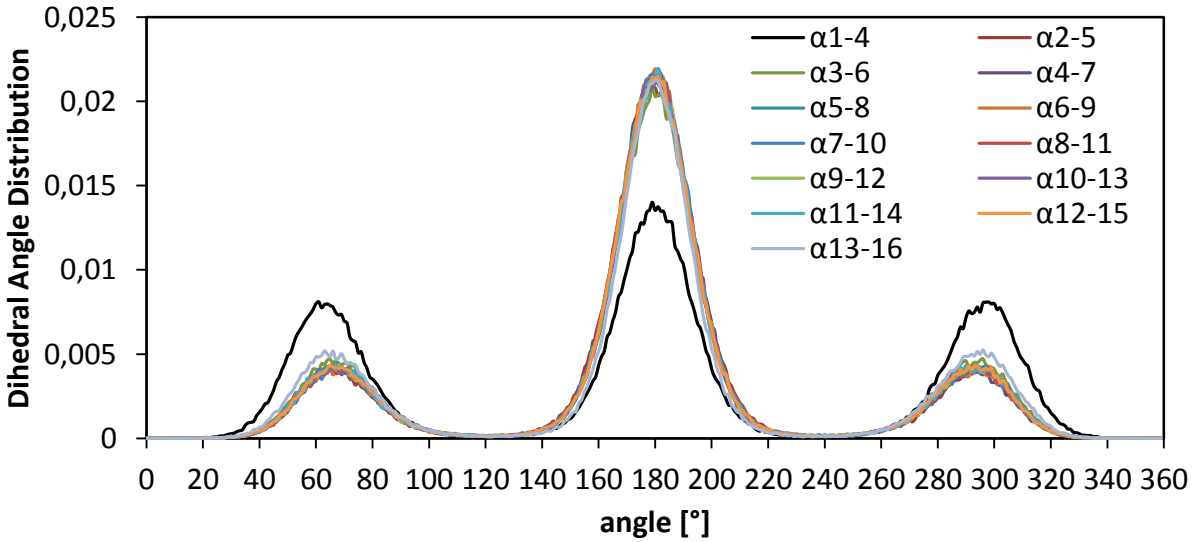

Figure 5.30: Dihedral angle distribution for the CTAB micelle containing 80 surfactant molecules and no added alcohol. Labeling is according to Figure 5.9.

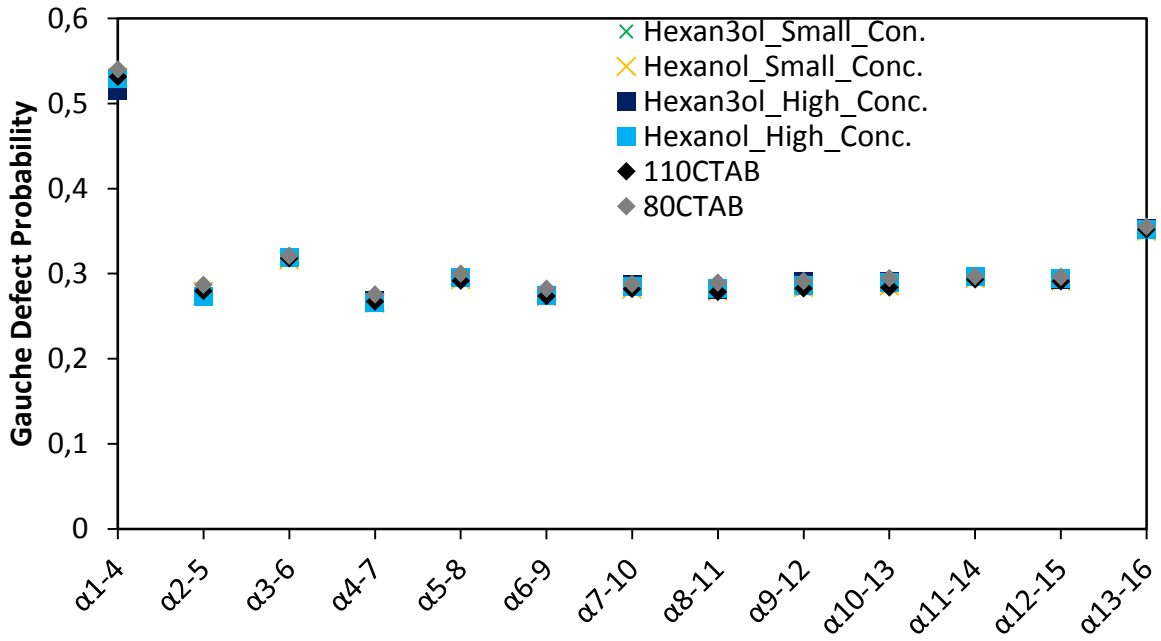

Figure 5.31: Gauche defect probabilities of the surfactant tail group dihedrals for the systems CTAB (110 and 80 surfactant molecules), both CTAB with 5 1-hexanol and 5 3-hexanol molecules and both CTAB with 30 1-hexanol and 30 3-hexanol molecules. Labeling is according to Figure 5.9.

Appendix, show the same dihedral angle distribution. The integration of the areas under the peaks according to Equation 5.1, which yields the gauche defect probabilities and which is shown in Figure 5.31, exhibits the same finding for the five systems. Obviously 1-hexanol and 3-hexanol also do not influence the CTAB molecules with respect to their stability.

Additionally to the CTAB molecules, the dihedral angle distributions were also computed for the 1-hexanol and 3-hexanol molecules. The dihedral labeling for both alcohols is displayed in Figure 5.32. At first the dihedral angle distributions for 1-hexanol molecules and the corresponding gauche defect probabilities for the simulation of the micelle with low and high 1-hexanol concentration are depicted in Figure 5.33 and Figure 5.34.

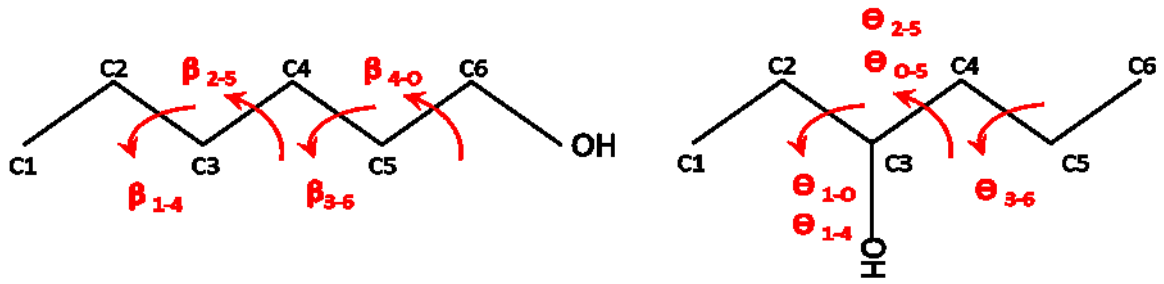

Figure 5.32: 1-hexanol (left) and 3-hexanol (right) with dihedrals β_{i-j} and Θ_{i-j}, respectively, used in this work. The subscript O refers to the oxygen-atom.

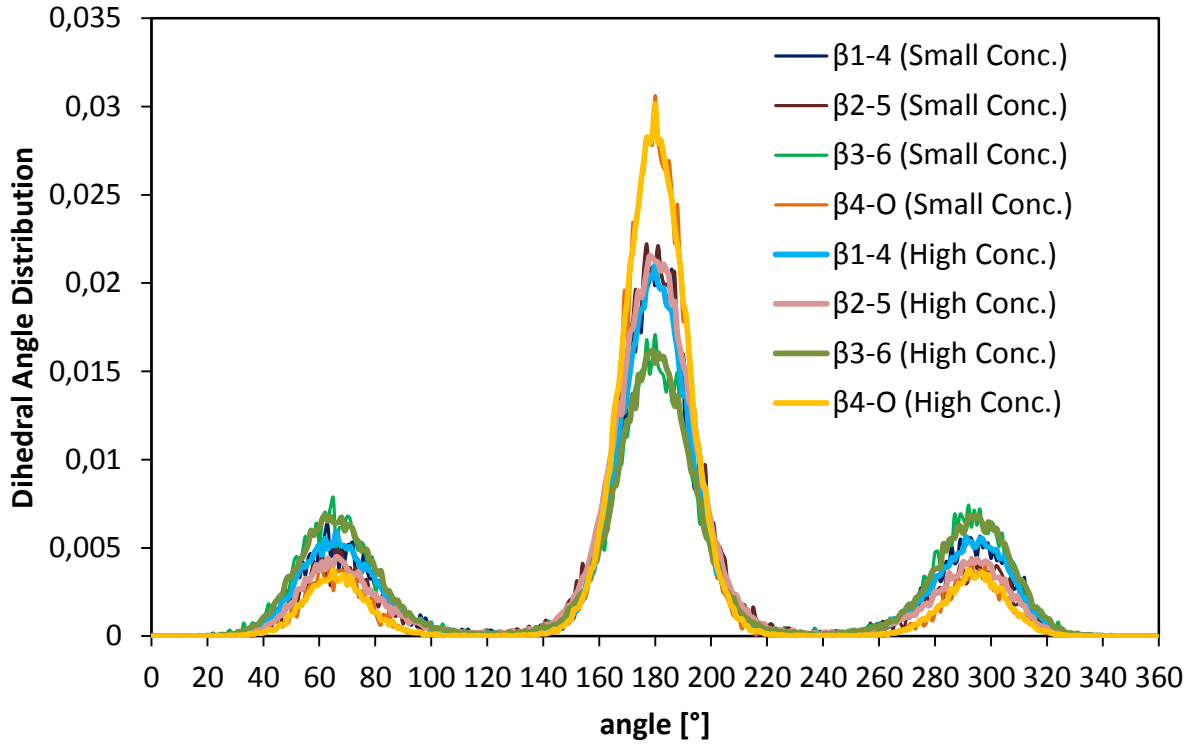

Figure 5.33: Dihedral angle distributions of the 1-hexanol dihedrals for the simulations of the CTAB micelle with both low and high 1-hexanol concentration. Labelling is according to Figure 5.32.

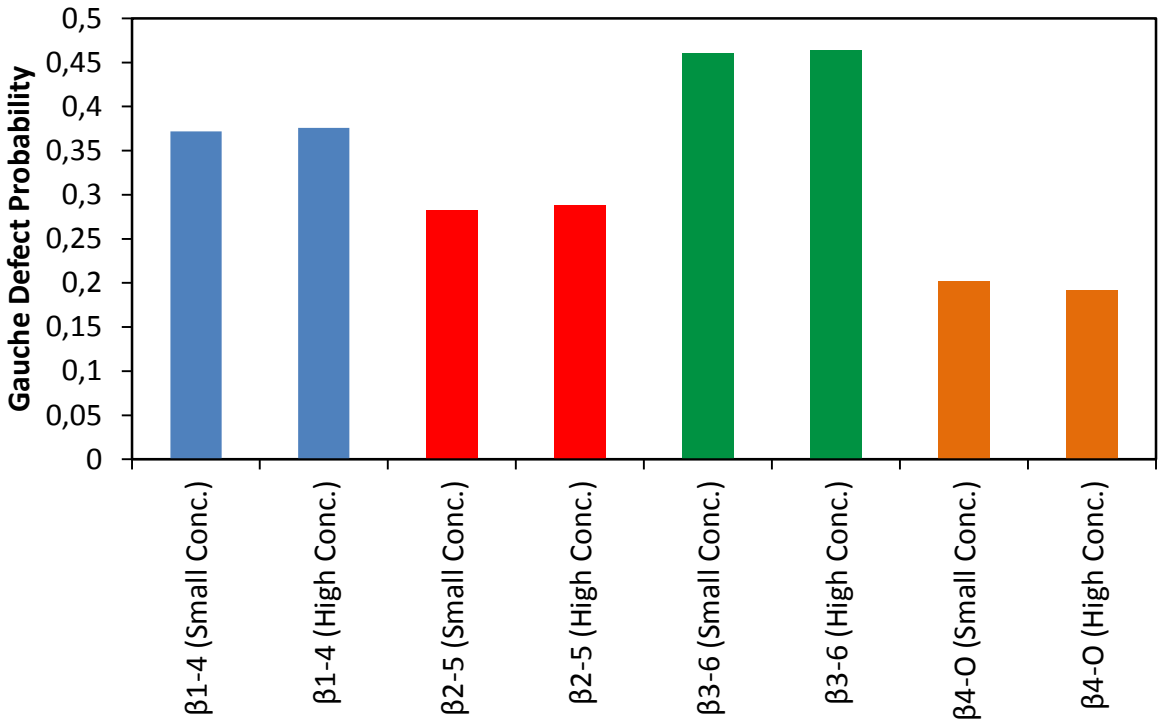

Figure 5.34: Gauche defect probabilities of 1-hexanol dihedrals for the simulations of the CTAB micelle with both low and high 1-hexanol concentration. Labelling is according to Figure 5.32.

First Figure 5.33 reveals that all the dihedral distribution curves for the low concentration simulation match their corresponding curves for the high concentration simulations. However, the low concentration curves fluctuate more, which can be explained by the smaller number of data points available for the simulations containing only five alcohols. Furthermore, Figure 5.34 shows the following descending order of the dihedrals with the highest gauche defect probability: the dihedral, which contains all the C-atoms above the alcohol group (β_{3-6}) and the first and the second dihedral starting from the terminal C-atom (β_{1-4} and β_{2-5}). On the contrary the dihedral angle distributions and gauche defect probabilities for 3-hexanol, shown in Figure 5.35 and Figure 5.36, demonstrate a different behavior. Not only are the gauche defect probabilities strikingly higher than those for the 1-hexanol molecules, the dihedrals additionally are distributed differently with the curves of the low and high alcohol concentrations distinguishing more from each other. The 3-hexanol molecules therefore seem to fluctuate more in form and according to Figure 5.35 the two C-atom chains of the 3-hexanol molecule are favorably bent.

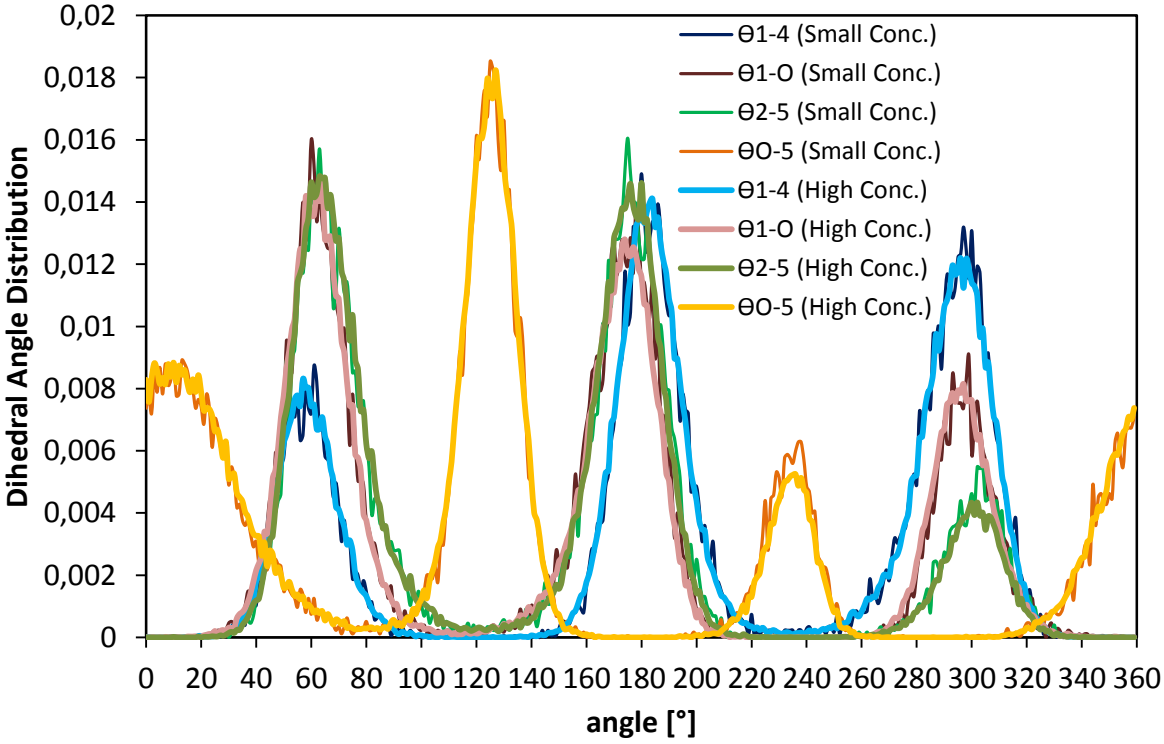

Figure 5.35: Dihedral angle distributions of the 3-hexanol dihedrals for the simulations of the CTAB micelle with both low and high 3-hexanol concentration. Labelling is according to Figure 5.32.

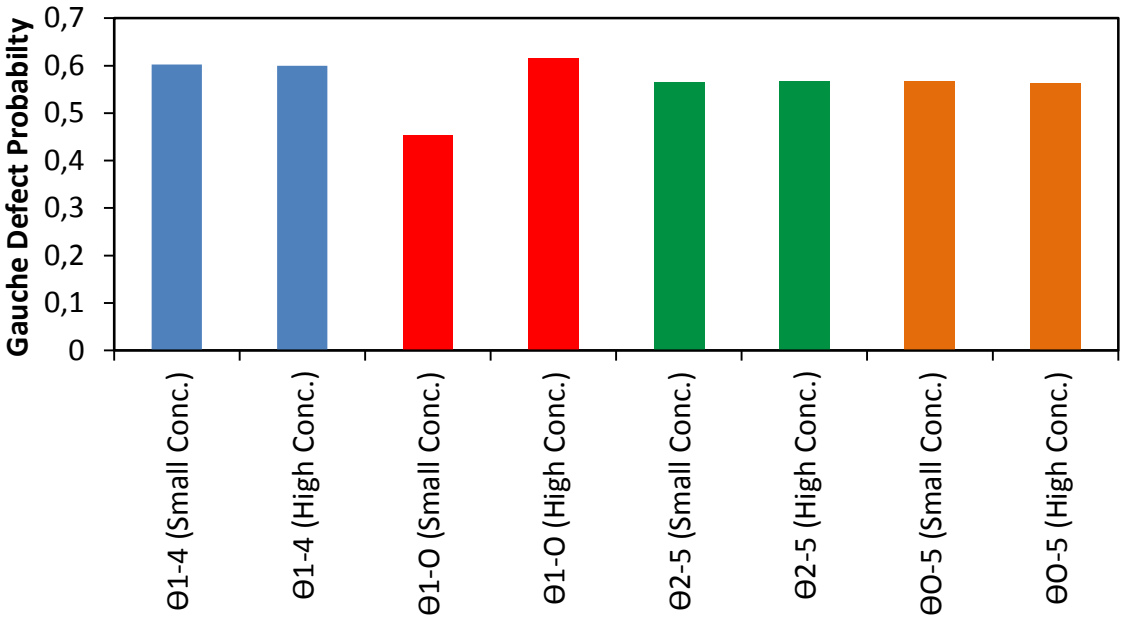

Figure 5.36: Gauche defect probabilities of 3-hexanol dihedrals for the simulations of the CTAB micelle with both low and high 3-hexanol concentration. Labelling is according to Figure 5.32.

This means that 3-hexanol molecules, other than 1-hexanol molecules, do not favor an elongated, unbowed structure. This can be explained by the position of the OH-group within the molecule. Whereas 1-hexanol has its OH-group located at one end of the molecule, just like the CTAB molecules have their polar groups at one end, the OH-group of 3-hexanol is bonded to the third C-atom along the chain. In this case the charge is differently distributed than for 1-hexanol, which influences the two carbon chains of 3-hexanol. Comparing the dihedral angle distributions for CTAB, 1-hexanol and 3-hexanol (see Figure 5.10, Figure 5.33 and Figure 5.35), the plots for the first two compounds basically look alike, whereas the one of 3-hexanol differs noticeably.

5.3. Comparison of the Systems

In this chapter, the influences of the three different alcohols on the CTAB micelle and the behavior of the alcohol itself are compared. While the ethanol molecules were randomly placed in the simulation box, surfactant molecules were replaced by the corresponding number of 1- and 3-hexanol molecules of the micelle.

First thing to say is that ethanol, 1-hexanol and 3-hexanol in their low concentration do not affect the structure and form of the CTAB micelle. This can be observed from the moments of inertia for CTAB for the pure CTAB micelle containing 110 surfactant molecules for CTAB with five ethanol molecules, for CTAB with five 1-hexanol molecules and for CTAB with five 3-hexanol molecules (see Table 1, Table 2, Figure 5.5 and Figure 5.21). While the pure CTAB micelle reveals a value for the total moment of inertia Itot of 159100 a.m.u · nm ± 5500 a.m.u.·nm² (Table 1), the simulation of CTAB and low ethanol concentration differs only by 0.04% (Table 1), which is only a tiny difference. The smaller values of 148000 a.m.u.·nm² ± 4200 a.m.u.·nm² and 148100 a.m.u.·nm² ± 4300 a.m.u.·nm² (Table 2) for the simulations of CTAB with low 1-hexanol and 3-hexanol concentration only arise from

the fact that five surfactant molecules are replaced by five alcohol molecules. So the micelle only consists of 105 surfactant molecules.

The results look different for all simulations with higher alcohol concentrations. The higher ethanol concentration obviously brings a small but noticeable fluctuation in the micelle structure, which is confirmed by the Itot value of 161500 a.m.u.·nm² ± 6400 a.m.u.·nm² with its higher standard deviation compared to the pure CTAB micelle. Due to both similarly strong polar and nonpolar parts of the ethanol molecules, they do not only flow through the water phase (see mean square displacement plot of ethanol in Figure 5.3), but also enter the micelles up to the palisade layer at the first carbon atoms below the nitrogen-atom of the headgroup, which is in turn confirmed by the radial distribution function plot of the micelle and ethanol molecules in Figure 5.6 to Figure 5.8. A clear peak below the surfactant headgroups with a distance of approximately 2.1 nm of the OH-group of ethanol to the micelle center of mass for both low and high ethanol concentration can be seen. Consequently ethanol acts as cosolvent, enhancing the solubility of CTAB in water.

With values that are 5% and 9% higher for the total moments of inertia for the simulations of CTAB with both high 1-hexanol and 3-hexanol concentration, the pure micelle containing 80 surfactant molecules (Table 2), a distinct micelle swelling can be observed. This can be explained by the greater number of molecules forming the micelle and that comicelles for both longer chain alcohols exist.[24] In fact, the OH-groups of both 1- and 3-hexanol favor a position of approximately 0.3 to 0.5 nm below the headgroups of the surfactant molecules (see RDF plots in Figure 5.24 to Figure 5.29), although some alcohol molecules for both CTAB simulations with 1- and 3-hexanol in both concentrations moved out of the micelle for some time. This can be observed in Figure 5.14 and Figure 5.15. Consequently both 1- and 3-hexanol act as cosurfactant, forming a micelle together with the CTAB molecules.

Furthermore, to gain information about the changes of the inner structure of the micelles, in essence, if the gauche probabilities are affected, the dihedral angle distributions were calculated along the surfactant carbon chain. The results clearly show that all three alcohols in both low and high concentrations do not have any influence on the gauche probabilities of the surfactant chain dihedrals, which can be seen from Figure 5.11 and Figure 5.31.

Finally the structure of 1- and 3-hexanol itself was investigated by calculating the dihedral angle distributions for atoms along these molecules. The results indicate that 1-hexanol behaves quite similarly to the CTAB molecules, with the first dihedral below the OH-group

consisting of only C atoms having the highest gauche probability just as for the CTAB molecules (see Figure 5.10, Figure 5.33 and Figure 5.34). In contrast to this, the 3-hexanol reveals a different behavior. Not only are the dihedral angles shifted to different values, but also have the 3-hexanol molecules higher gauche probabilities than 1-hexanol and CTAB (see Figure 5.35 and Figure 5.36). This can be explained by the position of the polar group (OH-group), which is, unlike for 1-hexanol and CTAB, localized within the molecule and not at one end. This structure leads to positions of the dihedrals, where huge repulsions can occur.

5.4. CTAB Micelle solvated in Ethanol

Since only small differences of the micelle structure were caused by ethanol molecules in this work (see Chapter 5.1), it was found necessary to examine the validity of the model used in this work. Therefore the ethanol content is raised to a maximum, in order to verify, if changes occur at all. The system of the CTAB micelle and ethanol was composed and the simulation was carried out according to Section 4.2. The starting conformation of the CTAB micelle, the state after the NVT simulation and the final structure of the micelle are depicted

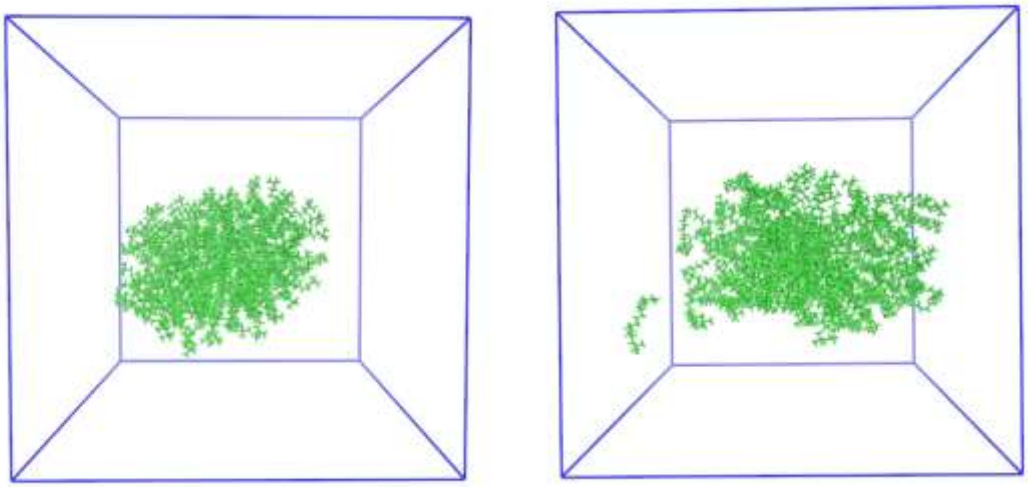

Figure 5.37: CTAB micelle before the simulation (left) and CTAB micelle after 200 ps simulation in the NVT-ensemble (right) (ethanol is omitted due to visibility reasons).

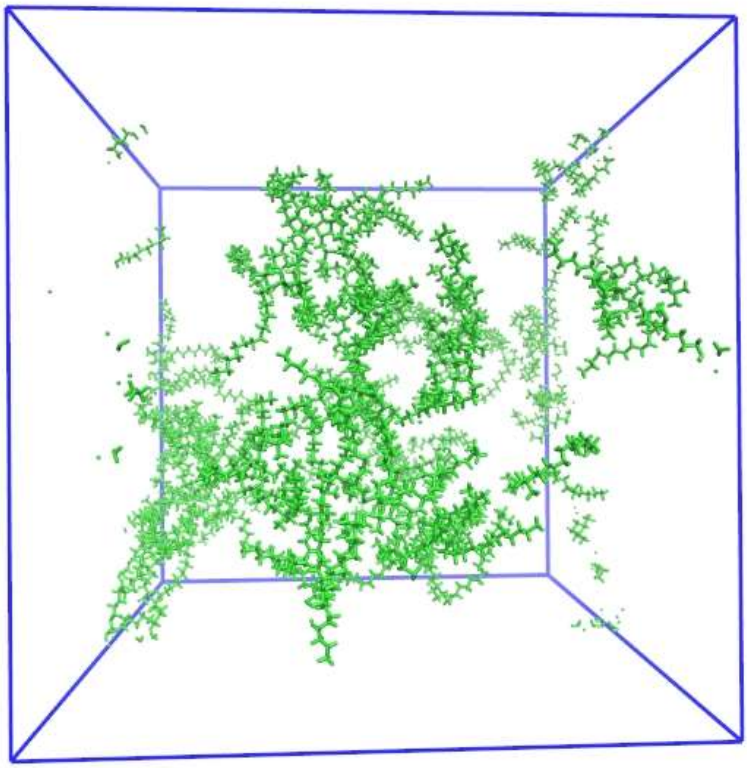

Figure 5.38: CTAB micelle after 20 ns simulation in the NPT-ensemble. Single atoms and molecule parts at the edges of the box occur due to periodic boundary conditions (ethanol is omitted due to visibility reasons).

in Figure 5.37 and Figure 5.38. From those figures, a slow decomposition of the CTAB micelle after the short NVT simulation (200 ps) can already be noticed. The micelle becomes broader and some surfactant molecules have already left the micelle and flow in the ethanol bulk phase. After 20 ns NPT simulation a clear breakdown of the micelle can be observed. A micelle structure can no longer be seen. Instead some small surfactant clusters and free surfactant molecules exist. Hydrophobic effects among the surfactant tail groups, which are the driving forces for the micellization process, are weakened, as they now interact strongly with the ethanol molecules. That is why micelles now can hardly form.[31]

This simulation was carried out to examine the validity of the computer model used in this work. Since similar simulations of CTAB micelles in pure ethanol, carried out by Li et al.[31] and Meng et al.[60], also show a micelle breakdown and the presence of small clusters already at 90% ethanol content in the solution,[31] the qualitive reliability of the computer model used in this work can be inferred at least in the sense of inducing the micelle to break down in pure

ethanol. This also means that the obtained results for influences of ethanol on the CTAB micelle are reasonable and that greater effect could be seen, if the concentrations were raised from the studied concentration.

6. Conclusion

In this work, the aqueous systems of a CTAB micelle (consisting of 110 and 80 surfactant molecules) with the three alcohols ethanol, 1-hexanol and 3-hexanol in both low and high concentration (5 and 30 molecules) were investigated by means of molecular dynamics simulations with respect to the influence of the alcohols on the micelles, meaning its structure and form, and the behavior of the alcohols itself. The software used for the simulations was the GROMACS package.[45] Whereas the ethanol molecules were randomly distributed in the simulation box, a corresponding number of surfactant molecules of the micelle were replaced by 1- and 3-hexanol molecules, respectively, since the medium chain alcohols tend to favor a position inside the micelle due to their more hydrophobic nature. First it was shown that for all three alcohols in their small concentration no changes in any way could be observed at all, meaning the micelle behaves like the pure micelle solvated in pure water. Obviously the small amount of alcohols was not sufficient to bring about influences on the micelle structure. However, raising the ethanol concentration exhibited a minor micelle swelling and greater fluctuations in its structure (trend can be seen), which could be shown by means of higher moments of inertia along with standard deviations. This can be explained by ethanol molecules constantly moving into the micelle up to the palisade layer, which could be noticed from both simulations snapshots and radial distribution functions plots. Furthermore, it is known from experiments that ethanol raises the cmc and reduces the aggregation number of CTAB, due to a decrease of the dielectric constant of water.[18, 21, 29, 31] This intensifies the repulsions of the headgroups. Additionally ethanol molecules break the water structure, which causes a weakening of the hydrophobic interactions between the surfactant tails.[18, 21-22, 31] As a result, the micelle fluctuates more in form and is more unstable. Therefore the tendency shown by the computational results for ethanol being a cosolvent in this work agree well with experimental data.

An even higher increase in the moments of inertia could be detected for the micelles with 1- and 3-hexanol in their high concentrations to a similar extent, compared to the pure micelle consisting of 80 surfactant molecules. The reason for that is the presence of more molecules inside the micelles or that the CTAB molecules form comicelles with both medium chain alcohols (1-hexanol and 3-hexanol act as cosurfactants), respectively, although some 1- and 3-hexanol molecules flow out of the micelle at some point for a certain time. The existence of comicelles formed by CTAB and medium to longer chain alcohols was experimentally already reported by for example Dubey.[24] Additionally, it can be stated that all three alcohols in both low and high concentrations do not affect the inner structure of the micelle (CTAB molecules), meaning changing the probabilities for the dihedrals along the surfactant carbon chains of having a kink. This could be seen from the dihedral angle distribution and the gauche probability plots.

However, it was found that ethanol, 1-hexanol and 3-hexanol favor a position below the surfactant headgroups (0.3 to 0.5 nm below). The preferential position for alcohols within the palisade layer was already reported by Zana et al. [18] or Patra et al.[63]

Finally the dihedrals of 1- and 3-hexanol were compared. The results reveal that 1-hexanol behaves like the CTAB molecules almost in the same way. By contrast, the 3-hexanol molecules preferably show a bent structure, as they exhibit a different distribution of the dihedral angles compared to CTAB and 1-hexanol. This can be explained by the different position of the polar group (OH-group), which is not located at one end, but in the middle of the molecule.

Furthermore, a simulation with a CTAB micelle solvated in pure ethanol was also carried out to validate the validity of the computer model used in this work, since only small changes were obtained for the CTAB micelle in the presence of ethanol. Already after 200 ps in the NVT-ensemble, a micelle broadening as well as some loose CTAB molecules could be noticed. After 20 ns in the NPT-ensemble, the micelle completely broke down. This is in good agreement with similar simulations carried out by Li et al.[31] and Meng et al.[62], with experimental results, like the increasing of the cmc etc. [18, 21-22, 29, 31] and with the structural changes induced by ethanol shown in this work.

Generally, it can be noted that the alcohols in their higher concentration start to affect the micelle and its structure. To obtain even stronger visible changes, the concentrations should

be raised further in the simulation. This can also be seen from the RDF between the surfactant headgroups and the bromide counterions, which was additionally calculated for both pure CTAB simulations (80 and 110 molecules) and for the simulations of a CTAB micelle with all three alcohols in the higher concentration. These RDF between the headgroups and the bromide ions, which are presented in Figure 8.21 in the Appendix, show no differences of the curves (distances of bromide ions from headgroups are approximately 0.4 and 0.6 nm), meaning that the alcohols in the higher concentrations still do not affect the counterion binding and the ionization degree, α, which could in turn lead to more distinct changes of the micelle structure.

Another thing to change is the simulation time, since 200 ns in the micelle equilibration timescale is rather short.[61] Therefore the simulations should be continued until equilibrium can be ascertained. Additionally, the potential mean forces of the alcohol molecules should be calculated, using other programs than GROMACS (e.g. COSMO-RS[39]). From this, inferences about the alcohol partitioning could be drawn, which could further validate the computational model. Unfortunately it was impossible to obtain significant changes during this work due to the small sizes of the alcohols compared to the CTAB micelle using GROMACS. Furthermore also other primary and secondary alcohols like for example methanol, 1-butanon or 2-butanon should be analyzed in conjunction with the CTAB micelle, in order to systematically complete a series of alcohols together with their influences on the micelle. This is useful for both validating the computational model and gaining knowledge about tuning the micelle to desired features for certain applications (e.g. for the synthesis of nanoparticles). Finally the CTAB micelle should be solvated in different ethanol/water mixtures, in order to detect the systematic ethanol response and to analyse the involved structural and dynamics changes.

7. Literature

(1) Wang, Z. *Applied Microbiology and Biotechnology* 2007, *75*, 1–10.

(2) Hinze, W. L.; Pramauro, E. *Critical Reviews in Analytical Chemistry* 1993, *24*, 133–177.

(3) Sun, C.; Xie, Y.; Tian, Q.; Liu, H. *Separation Science and Technology* 2007, *42*, 3259–3270.

(4) Schramm, L. L.; Stasiuk, E. N.; Marangoni, D. G. *Annual Reports on the Progress of Chemistry, Section C: Physical Chemistry* 2003, *99*, 3–48.

(5) Rosen, M. *Surfactants and Interfacial Phenomena;* Wiley, 2004.

(6) Holmberg, K.; Jonsson, B.; Kronberg, B.; Lindman, B. *Surfactants and polymers in aqueous solution,* 2nd ed.; J. Wiley, Chichester, New York, 2002.

(7) Mishra, M.; Muthuprasanna, P.; Surya Prabha, K.; Sobhita Rani, P. *International Journal of PharmTech Research* 2009, 1354–1365.

(8) Bibette, J.; Calderon, F.; Poulin, P. *Reports on Progress in Physics* 1999, *62*, 969.

(9) Sprunger, L. M.; Gibbs, J.; Acree, W. E.; Abraham, M. H. *QSAR and Combinatorial Science* 2009, *28*, 72–88.

(10) Torchilin, V. P. *Advanced Drug Delivery Reviews* 2006, *58*, 1532–1555.

(11) Peetla, C.; Vijayaraghavalu, S.; Labhasetwar, V. *Nanotechnology and drug resistance* 2013, *65*, 1686–1698.

(12) Vega Moreno, D.; Sosa Ferrera, Z.; Santana Rodriguez, J. J. *Journal of Chromatography A* 2006, *1104*, 11–17.

(13) Hillmyer, M. A. *Science* 2007, *317*, 604–605.

(14) Yue, J.; Jiang, X.; Zeng, Q.; Yu, A. *Solid State Sciences* 2010, *12*, 1152–1159.

(15) Tel-zur, N.; Abbo, S.; Myslabodski, D.; Mizrahi, Y. *Plant Molecular Biology Reporter* 1999, *17*, 249-254.

(16) Tang, J.; Huang, J.; Man, S.-Q. *Spectrochimica Acta A: Molecular and Biomolecular Spectroscopy* 2013, *103*, 349–355.

(17) Liu, K.; Ahmed, A.; Chung, S.; Sugikawa, K.; Wu, G.; Nie, Z.; Gordon, R.; Kumacheva, E. *ACS Nano* 2013, *7*, 5901–5910.

(18) Zana, R. *Advances in Colloid and Interface Science* 1995, *57*, 1–64.

(19) Muñoz, M.; del Mar Graciani, M.; Rodríguez, A.; Moyá, M. L. *International Journal of Chemical Kinetics* 2004, *36*, 634–641.

(20) Wall, J. F.; Zukoski, C. F. *Langmuir* 1999, *15*, 7432–7437.

(21) Li, W.; Han, Y.-C.; Zhang, J.-L.; Wang, B.-G. *Colloid Journal* 2005, *67*, 159-163.

(22) Li, W.; Han, Y.-C.; Zhang, J.-L.; Wang, L.-X.; Song, J. *Colloid Journal* 2006, *68*, 304-310.

(23) Larsen, J. W.; Tepley, L. B. *Journal of Colloid and Interface Science* 1974, *49*, 113–118.

(24) Dubey, N. *Journal of Molecular Liquids* 2013, *184*, 60–67.

(25) Bahri, M. A.; Hoebeke, M.; Grammenos, A.; Delanaye, L.; Vandewalle, N.; Seret, A. *Colloids and Surfaces A: Physicochemical and Engineering Aspects* 2006, *290*, 206–212.

(26) Oelschlaeger, C.; Willenbacher, N. *Colloids and Surfaces A: Physicochemical and Engineering Aspects* 2012, *406*, 31–37.

(27) Francisco, K. R.; da Silva, M. A.; Sabadini, E.; Karlsson, G.; Dreiss, C. A. *Journal of Colloid and Interface Science* 2010, *345*, 351–359.

(28) Zdziennicka, A.; Szymczyk, K.; Krawczyk, J.; Jańczuk, B. *Fluid Phase Equilibria* 2012, *322–323*, 126–134.

(29) Bielawska, M.; Chodzińska, A.; Jańczuk, B.; Zdziennicka, A. *Colloids and Surfaces A: Physicochemical and Engineering Aspects* 2013, *424*, 81–88.

(30) Anachkov, S. E.; Danov, K. D.; Basheva, E. S.; Kralchevsky, P. A.; Ananthapadmanabhan, K. P. *Advances in Colloid and Interface Science* 2012, *183-184*, 55–67.

(31) Li, W.; Zhang, M.; Zhang, J.; Han, Y. *Frontiers of Chemistry in China* 2006, *1*, 438-442.

(32) Sharma, V. K.; Mitra, S.; Garcia Sakai, V.; Hassan, P. A.; Peter Embs, J.; Mukhopadhyay, R. *Soft Matter* 2012, *8*, 7151–7160.

(33) Sharma, V. K.; Mitra, S.; Garcia Sakai, V.; Mukhopadhyay, R. *The Journal of Physical Chemistry B* 2012, *116*, 9007–9015.

(34) Yuan, S.; Ma, L.; Zhang, X.; Zheng, L. *Colloids and Surfaces A: Physicochemical and Engineering Aspects* 2006, *289*, 1–9.

(35) Phan, C. M.; Le, T. N.; Nguyen, C. V.; Yusa, S.-i. *Langmuir* 2013, *29*, 4743–4749.

(36) Perez-Sanchez, G.; Gomes, J. R. B.; Jorge, M. *Langmuir* 2013, *29*, 2387–2396.

(37) Wang, Z.; Larson, R. G. *The Journal of Physical Chemistry B* 2009, *113*, 13697–13710.

(38) Stephenson, B. C.; Beers, K.; Blankschtein, D. *Langmuir* 2006, *22*, 1500–1513.

(39) Ingram, T.; Storm, S.; Kloss, L.; Mehling, T.; Jakobtorweihen, S.; Smirnova, I. *Langmuir* 2013, *29*, 3527–3537.

(40) Cata, G. F.; Rojas, H. C.; Gramatges, A. P.; Zicovich-Wilson, C. M.; Alvarez, L. J.; Searle, C. *Soft Matter* 2011, *7*, 8508–8515.

(41) Meller, J. Molecular Dynamics. Encyclopedia of Life Sciences; John Wiley & Sons, Ltd, 2001.

(42) Hockney, R. W. *Methods in Computational Physics* 1970, 136–211.

(43) Leach, A. *Molecular Modelling: Principles and Applications (2nd Edition);* Prentice Hall, 2001.

(44) Verlet, L. *Physical Review* 1967, *159*, 98–103.

(45) van der Spoel, D.; Lindahl, E.; Hess, B. a. t. G. d. t. GROMACS User Manual version 4.6.3. ftp://ftp.gromacs.org/pub/manual/manual-4.6.3.pdf (accessed Nov 19, 2013).

(46) Klauda, J. B.; Venable, R. M.; Freites, J. A.; O'Connor, J. W.; Tobias, D. J.; Mondragon-Ramirez, C.; Vorobyov, I.; MacKerell, A. D.; Pastor, R. W. *The Journal of Physical Chemistry B* 2010, *114*, 7830–7843.

(47) Piggot, T. J.; Piñeiro, Á.; Khalid, S. *Journal of Chemical Theory and Computation* 2012, *8*, 4593–4609.

(48) Parrinello, M.; Rahman, A. *Journal of Applied Physics* 1981, *52*, 7182–7190.

(49) Nosé, S. *The Journal of Chemical Physics* 1984, *81*, 511–519.

(50) Hoover, W. G. *Physical Review A* 1985, *31*, 1695–1697.

(51) Hess, B.; Bekker, H.; Berendsen, H. J. C.; Fraaije, J. G. E. M. *Journal of Computational Chemistry* 1997, *18*, 1463–1472.

(52) Darden, T.; York, D.; Pedersen, L. *The Journal of Chemical Physics* 1993, *98*, 10089–10092.

(53) William Humphrey; Andrew Dalke; Klaus Schulten. *Journal of Molecular Graphics* 1996, *14*, 33–38.

(54) Storm, S.; Jakobtorweihen, S.; Smirnova, I.; Panagiotopoulos, A. Z. *Langmuir* 2013, *29*, 11582–11592.

(55) Sangster, J. *Journal of Physical and Chemical Reference Data* 1989, *18*, 1111–1229.

(56) Cussler, E. L. *Diffusion*: Mass transfer in fluid systems, 3rd ed.; Cambridge University Press, Cambridge, 2009.

(57) Sammalkorpi, M.; Karttunen, M.; Haataja, M. *The Journal of Physical Chemistry B* 2007, *111*, 11722–11733.

(58) Horinek, D.; Mamatkulov, S. I.; Netz, R. R. *The Journal of Chemical Physics* 2009, *130*, 124507.

(59) Paiva, A.; Petronetto, F.; Lewiner, T.; Tavares, G. In *Computer Graphics and Image Processing, 2006. SIBGRAPI '06. 19th Brazilian Symposium on: Computer Graphics and Image Processing.*

(60) Meng, S.; Zhang, J.; Wu, C.; Zhang, Y.; Xiao, Q.; Lu, G. *Molecular Simulation* 2014, 1–7.

(61) Sammalkorpi, M.; Sanders, S.; Panagiotopoulos, A. Z.; Karttunen, M.; Haataja, M. *The Journal of Physical Chemistry B* 2011, *115*, 1403–1410.

(62) http://stattrek.com/regression/slope-confidence-interval.aspx (accessed Feb 13, 2014).

(63) Patra, M.; Salonen, E.; Terama, E.; Vattulainen, I.; Faller, R.; Lee, B. W.; Holopainen, J.; Karttunen, M. *Biophysical Journal* 2006, *90*, 1121–1135.

8. Appendix

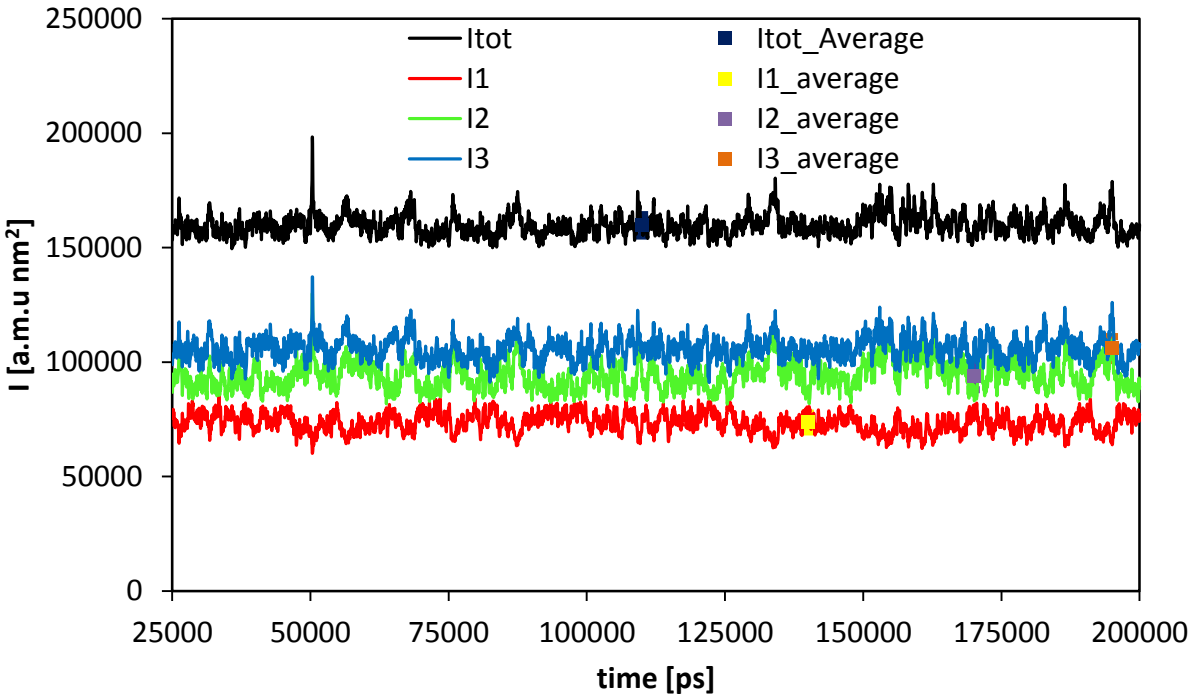

Figure 8.1: Time development of the moments of inertia for all three principal micelle axes and the total moment of inertia for a CTAB micelle and 5 ethanol molecules in aqueous solution. The average is calculated over period 25-200 ns and the error bar is calculated as the standard deviation.

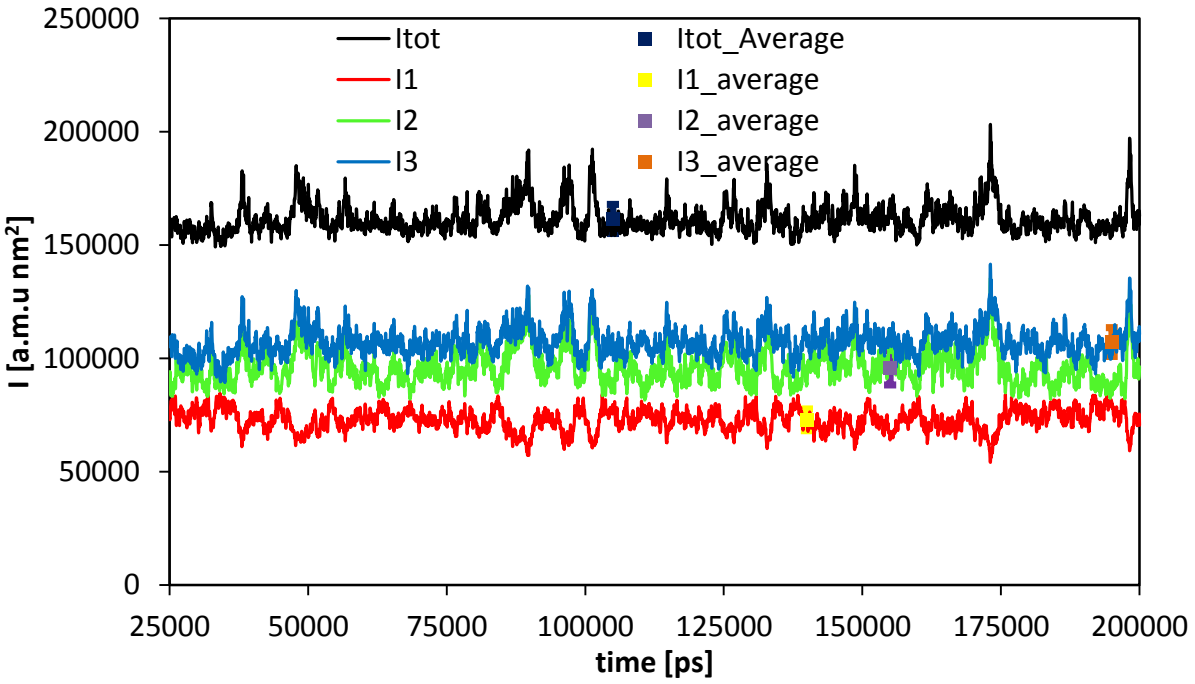

Figure 8.2: Time development of the moments of inertia for all three principal micelle axes and the total moment of inertia for a CTAB micelle and 30 ethanol molecules in aqueous solution. The average is calculated over period 25-200 ns and the error bar is calculated as the standard deviation.

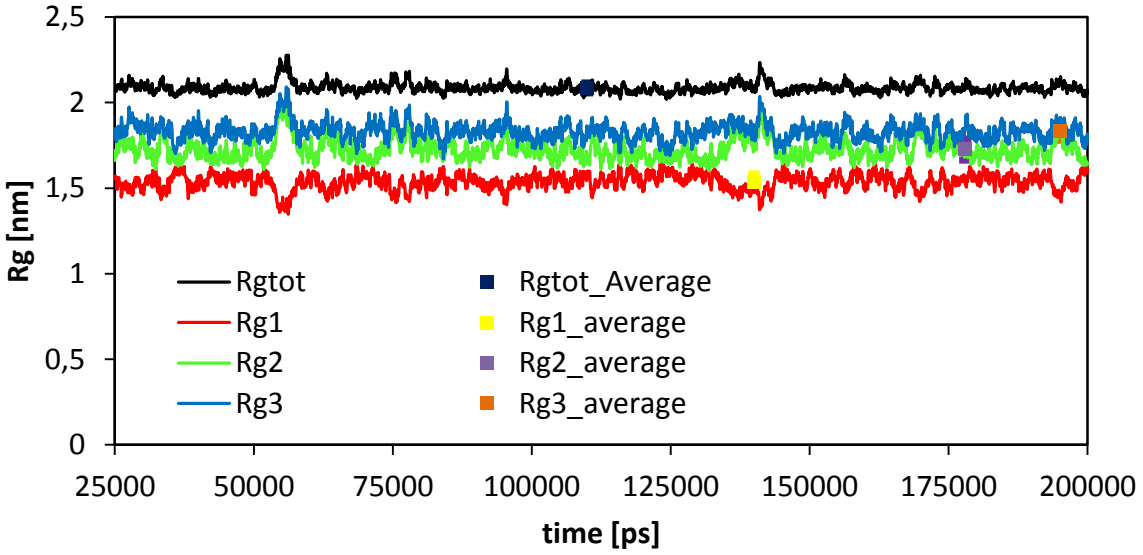

Figure 8.3: Time development of the radius of gyration for all three principal micelle axes and the total radius of gyration pure CTAB micelle containing 110 surfactant molecules in aqueous solution. The average is calculated over period 25-200 ns and the error bar is calculated as the standard deviation.

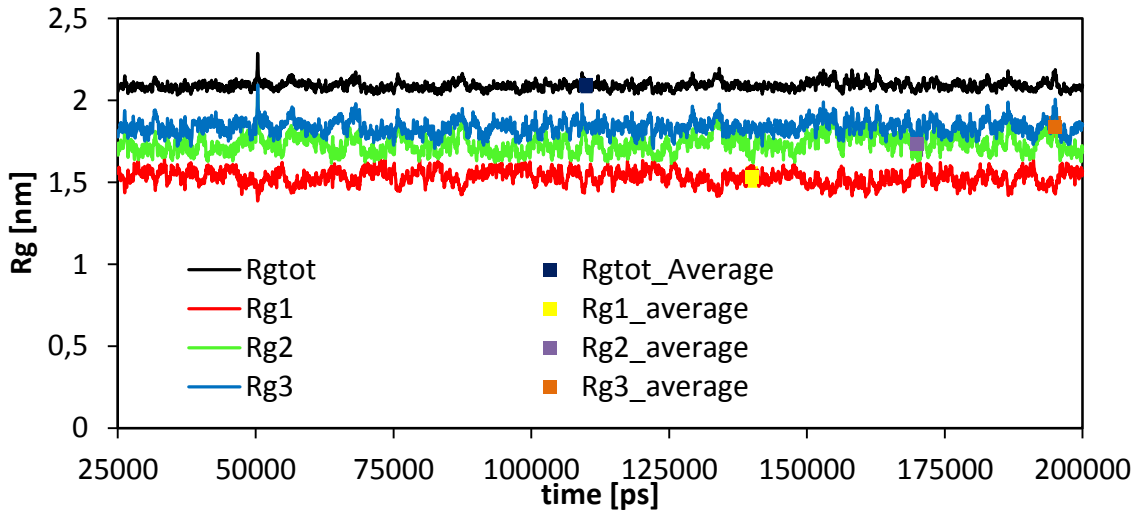

Figure 8.4: Time development of the radius of gyration for all three principal micelle axes and the total radius of gyration for a CTAB micelle and 5 ethanol molecules in aqueous solution. The average is calculated over period 25-200 ns and the error bar is calculated as the standard deviation.

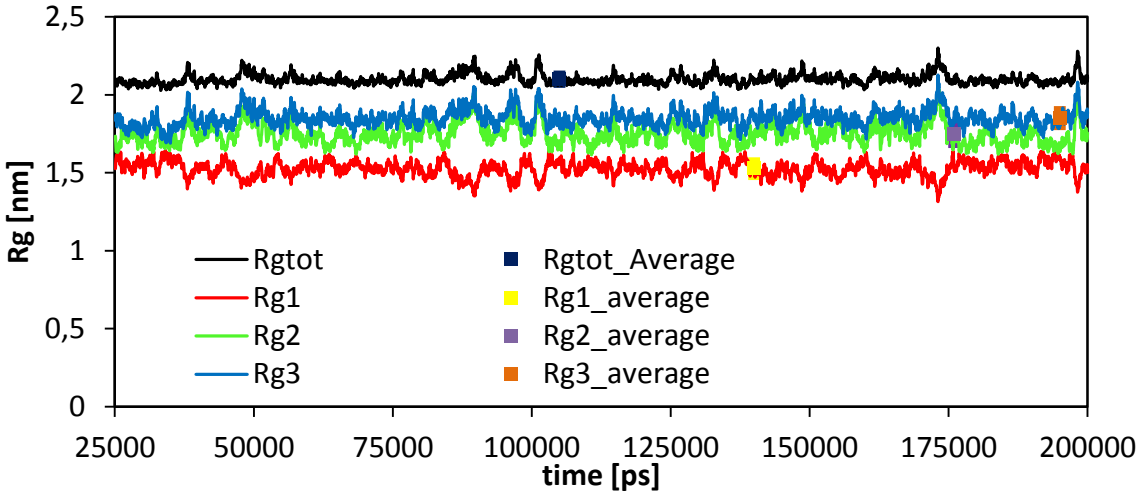

Figure 8.5: Time development of the radius of gyration for all three principal micelle axes and the radius of gyration for a CTAB micelle and 30 ethanol molecules in aqueous solution. The average is calculated over period 25-200 ns and the error bar is calculated as the standard deviation.

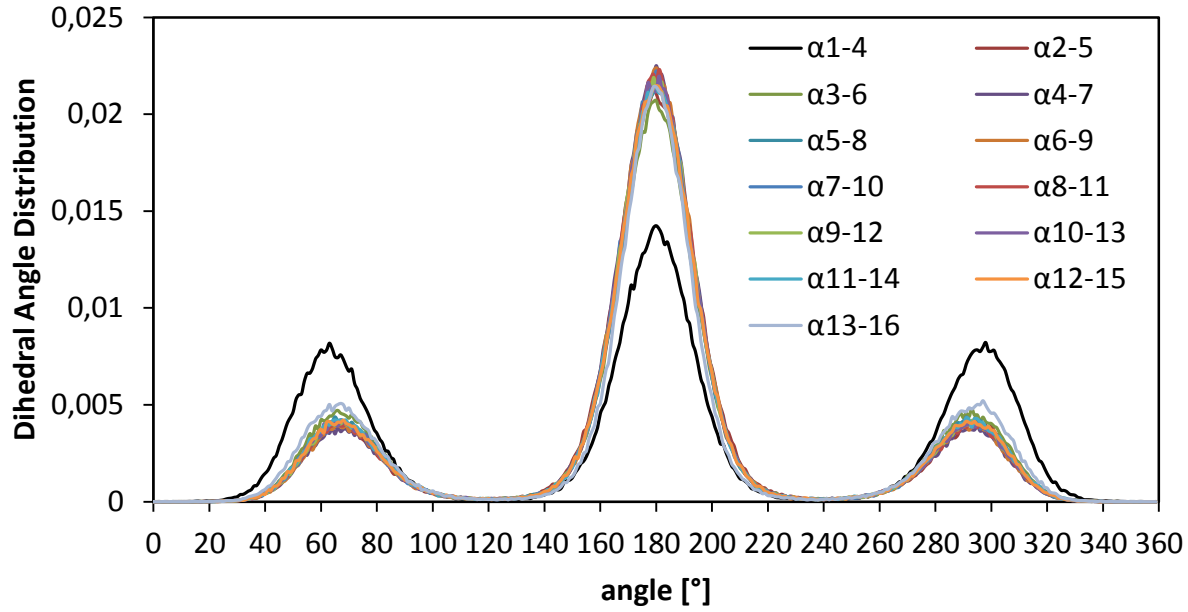

Figure 8.6: Dihedral angle distribution for the CTAB micelle containing 110 surfactant molecules with low ethanol concentration. Labeling is according to Figure 5.9.

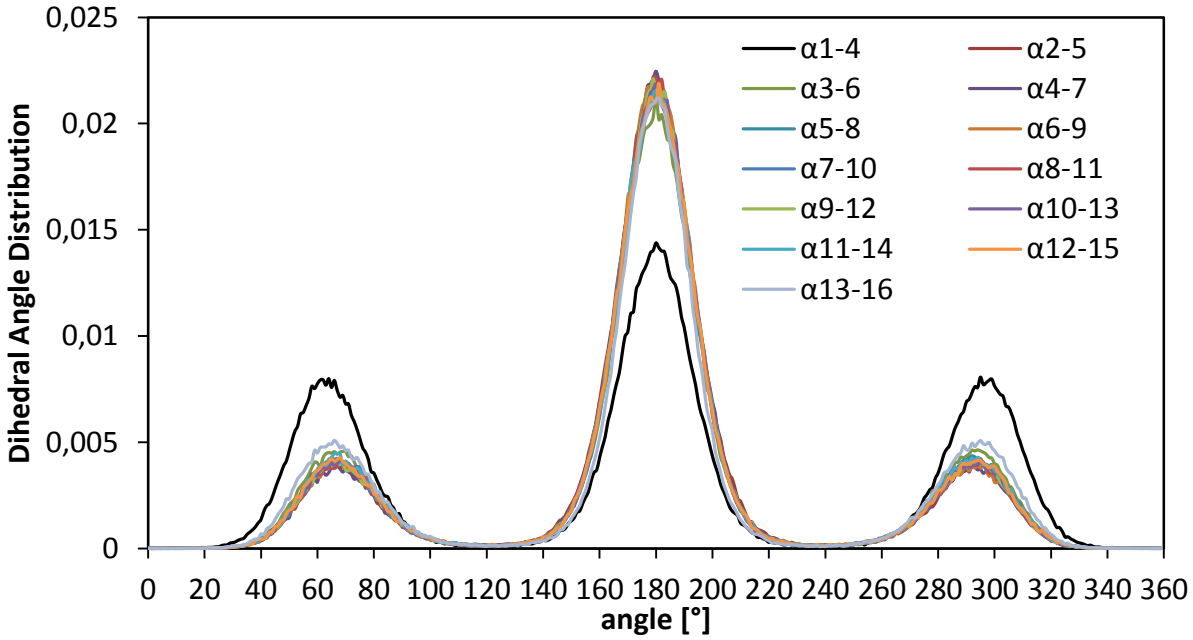

Figure 8.7: Dihedral angle distribution for the CTAB micelle containing 110 surfactant molecules with high ethanol concentration. Labeling is according to Figure 5.9.

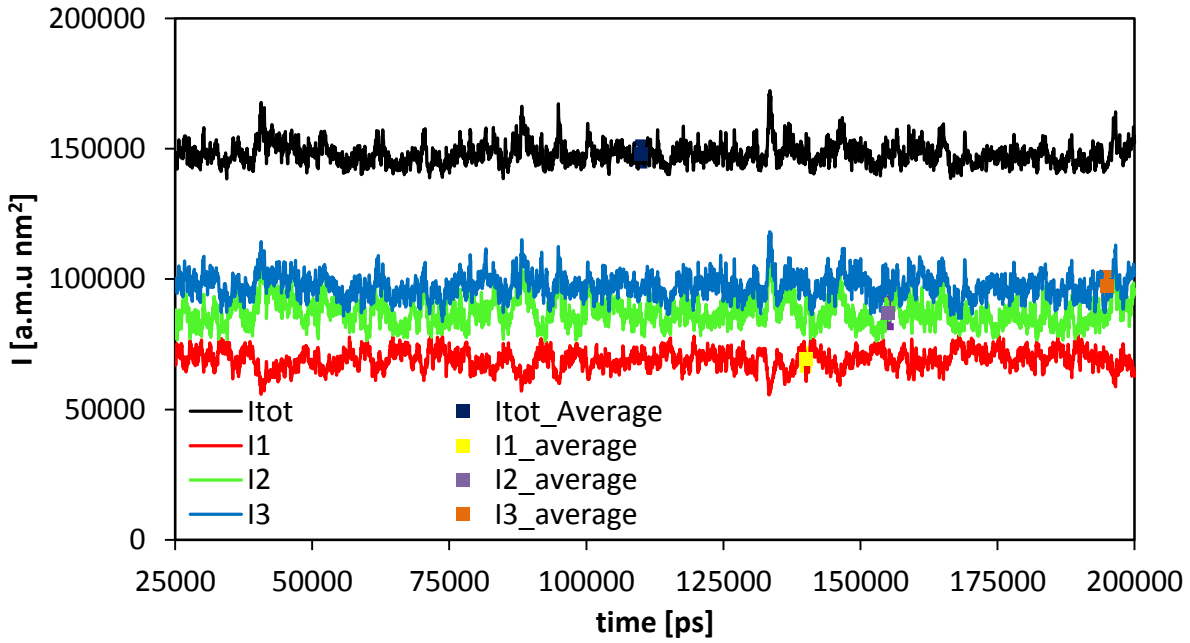

Figure 8.8: Time development of the moments of inertia for all three principal micelle axes and the total moment of inertia for a CTAB micelle and 5 1-hexanol molecules in aqueous solution. The average is calculated over period 25-200 ns and the error bar is calculated as the standard deviation.

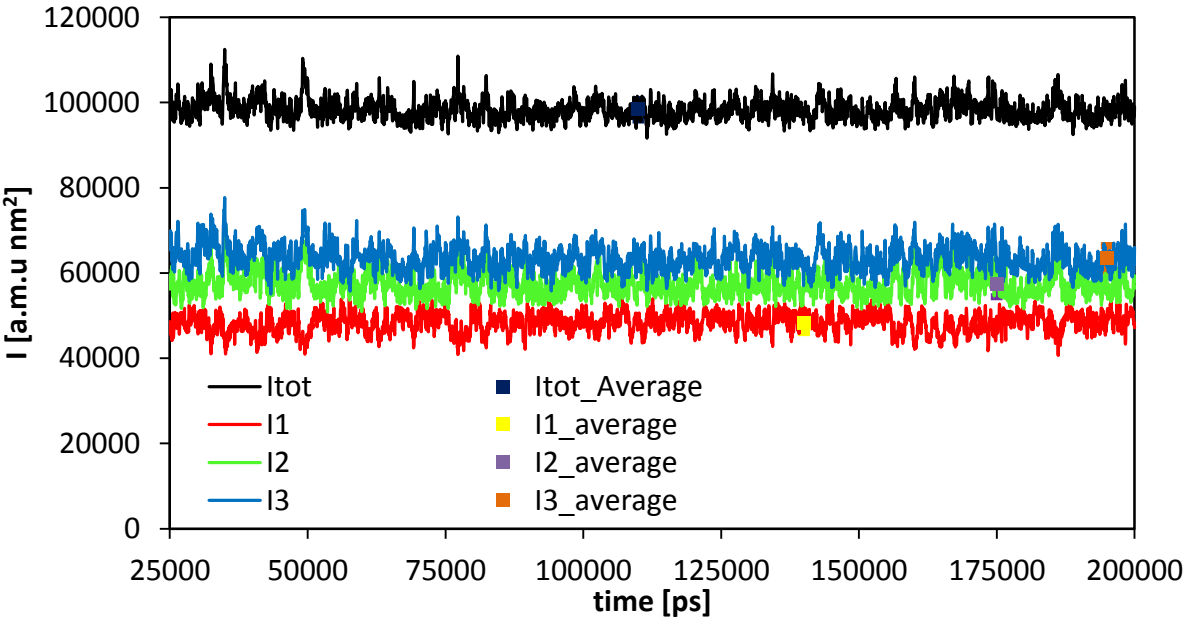

Figure 8.9: Time development of the moments of inertia for all three principal micelle axes and the total moment of inertia for a CTAB micelle and 30 1-hexanol molecules in aqueous solution. The average is calculated over period 25-200 ns and the error bar is calculated as the standard deviation.

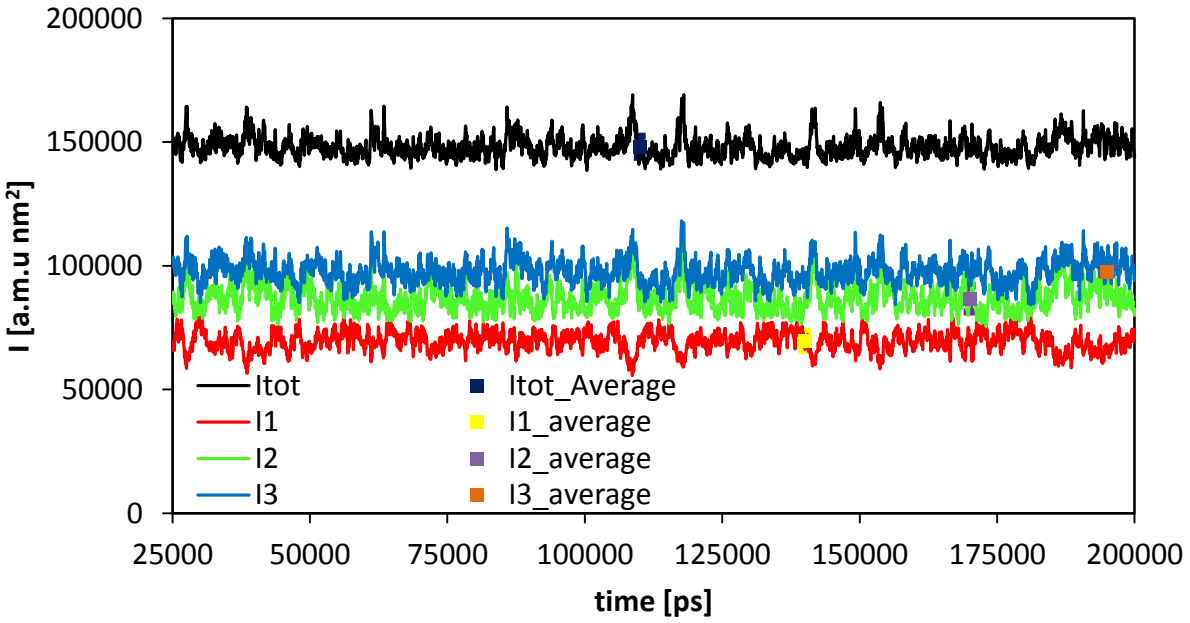

Figure 8.10: Time development of the moments of inertia for all three principal micelle axes and the total moment of inertia for a CTAB micelle and 5 3-hexanol molecules in aqueous solution. The average is calculated over period 25-200 ns and the error bar is calculated as the standard deviation.

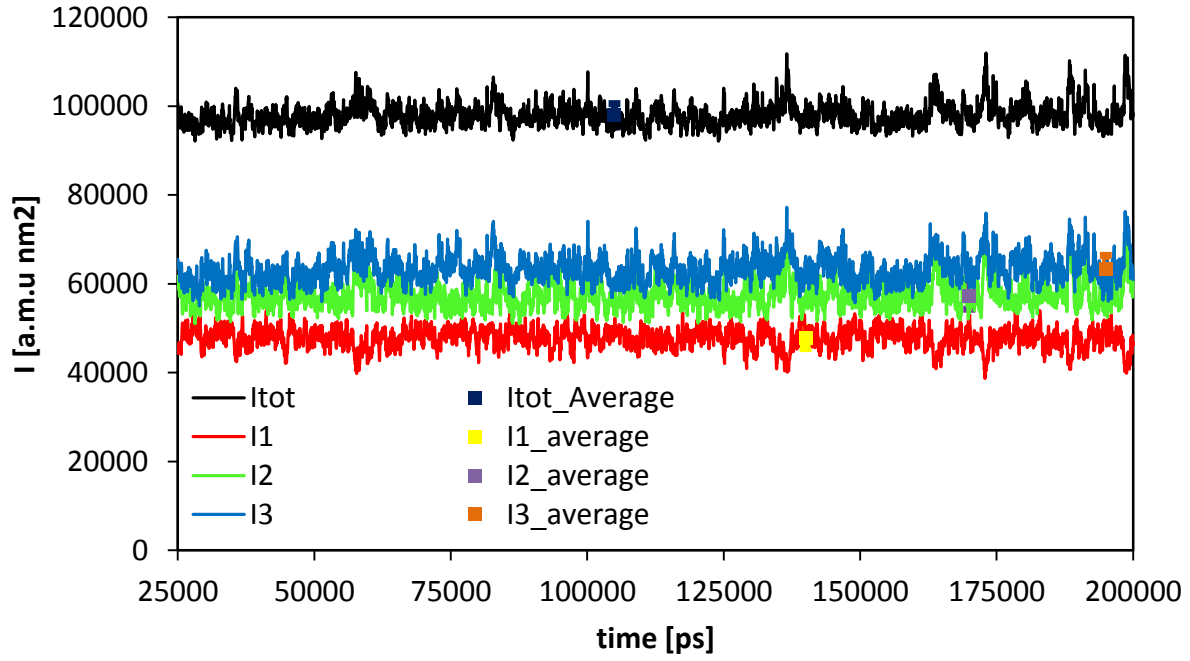

Figure 8.11: Time development of the moments of inertia for all three principal micelle axes and the total moment of inertia for a CTAB micelle and 30 3-hexanol molecules in aqueous solution. The average is calculated over period 25-200 ns and the error bar is calculated as the standard deviation.

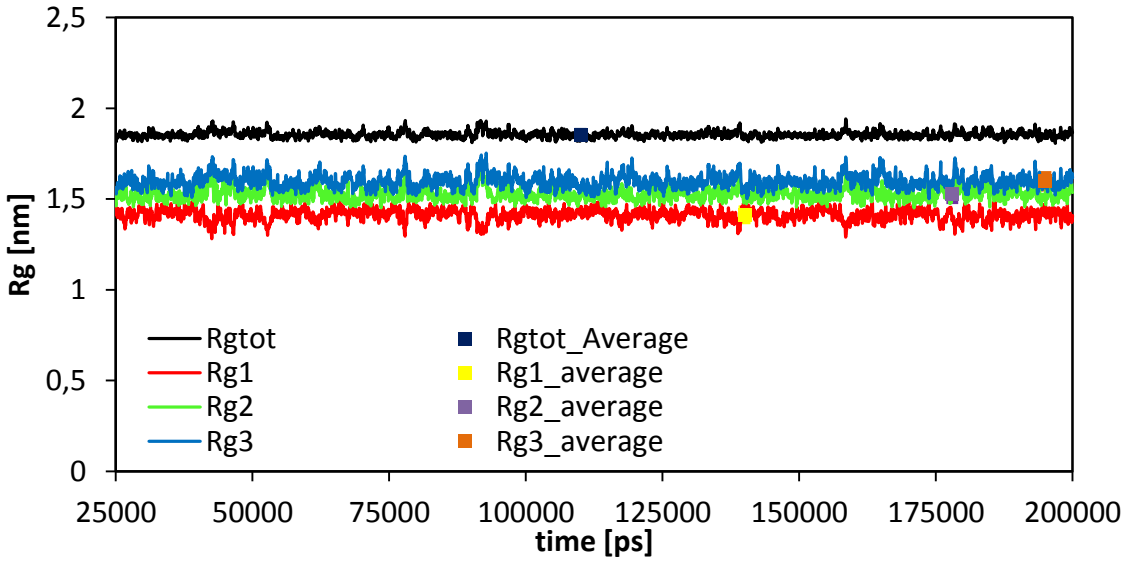

Figure 8.12: Time development of the radius of gyration for all three principal micelle axes and the total moment of inertia for pure CTAB micelle containing 80 surfactant molecules in aqueous solution. The average is calculated over period 25-200 ns and the error bar is calculated as the standard deviation.

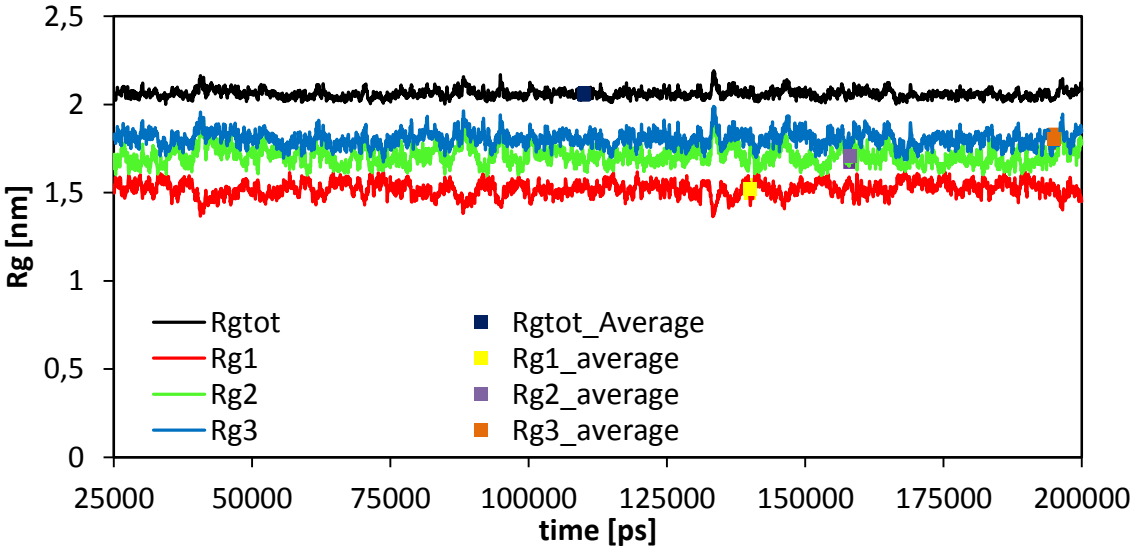

Figure 8.13: Time development of the radius of gyration for all three principal micelle axes and the total radius of gyration for a CTAB micelle and 5 1-hexanol molecules in aqueous solution. The average is calculated over period 25-200 ns and the error bar is calculated as the standard deviation.

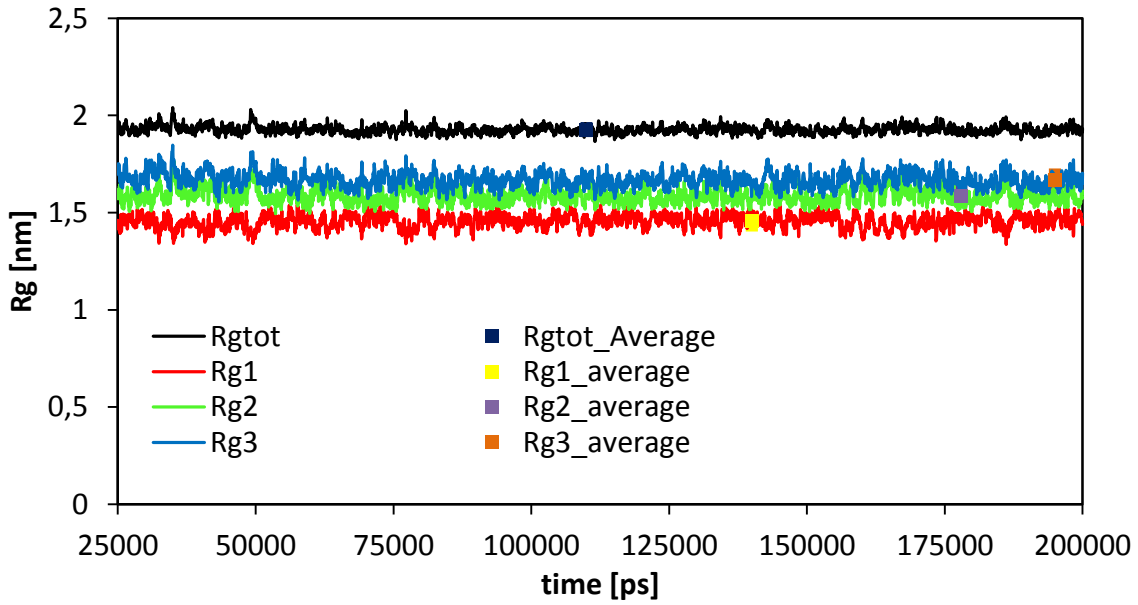

Figure 8.14: Time development of the radii of gyration for all three principal micelle axes and the total moment of inertia for a CTAB micelle and 30 1-hexanol molecules in aqueous solution. The average is calculated over period 25-200 ns and the error bar is calculated as the standard deviation.

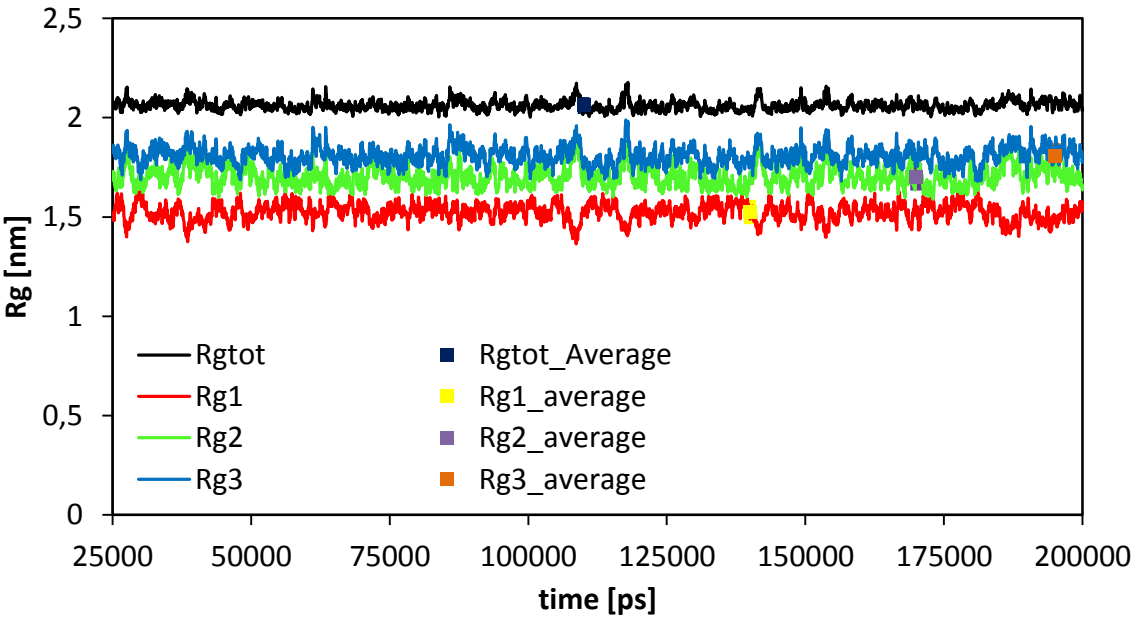

Figure 8.15: Time development of the radius of gyration for all three principal micelle axes and the total radius of gyration for a CTAB micelle and 5 3-hexanol molecules in aqueous solution. The average is calculated over period 25-200 ns and the error bar is calculated as the standard deviation.

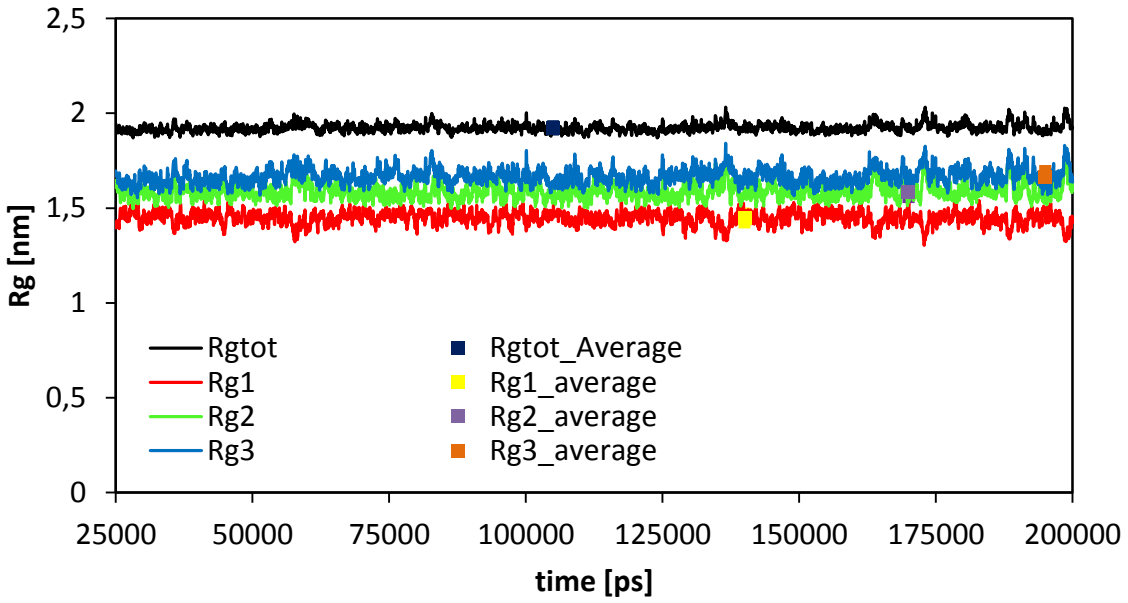

Figure 8.16: Time development of the radii of gyration for all three principal micelle axes and the total moment of inertia for a CTAB micelle and 30 3-hexanol molecules in aqueous solution. The average is calculated over period 25-200 ns and the error bar is calculated as the standard deviation.

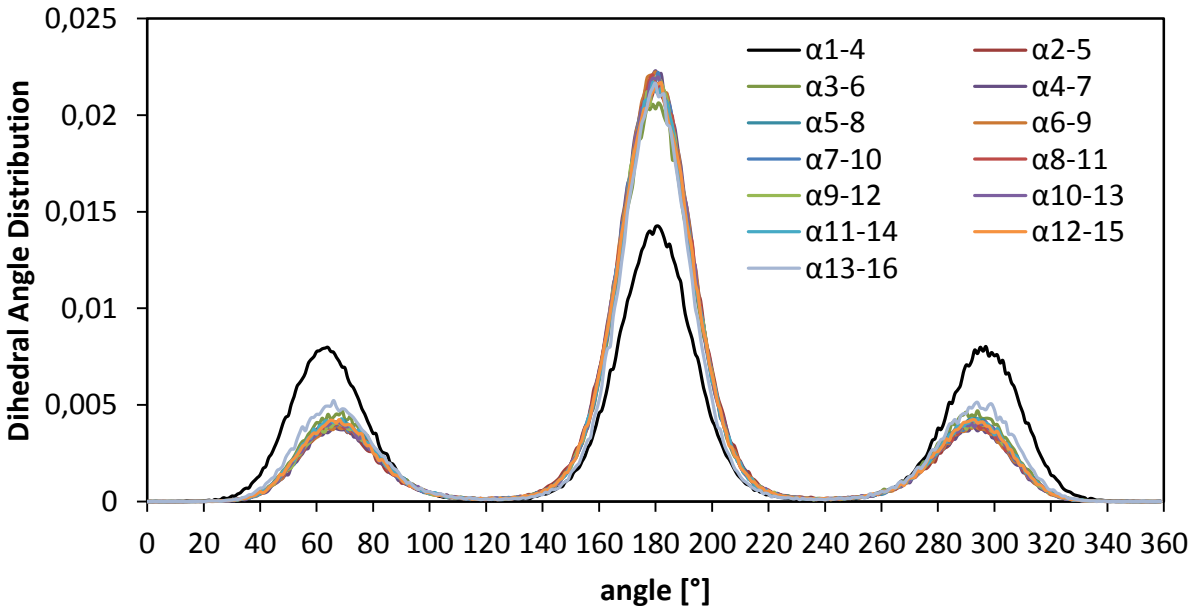

Figure 8.17: Dihedral angle distribution for the CTAB micelle containing 80 surfactant molecules with low 1-hexanol concentration. Labeling is according to Figure 5.9.

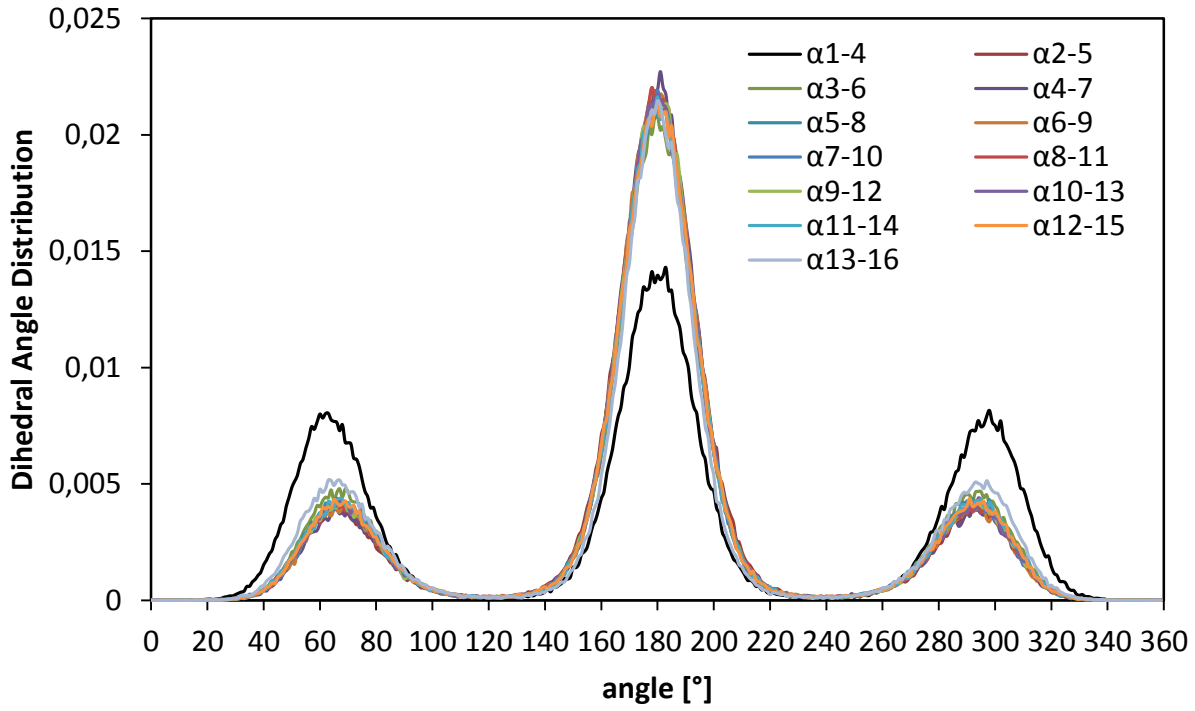

Figure 8.18: Dihedral angle distribution for the CTAB micelle containing 80 surfactant molecules with high 1-hexanol concentration. Labeling is according to Figure 5.9.

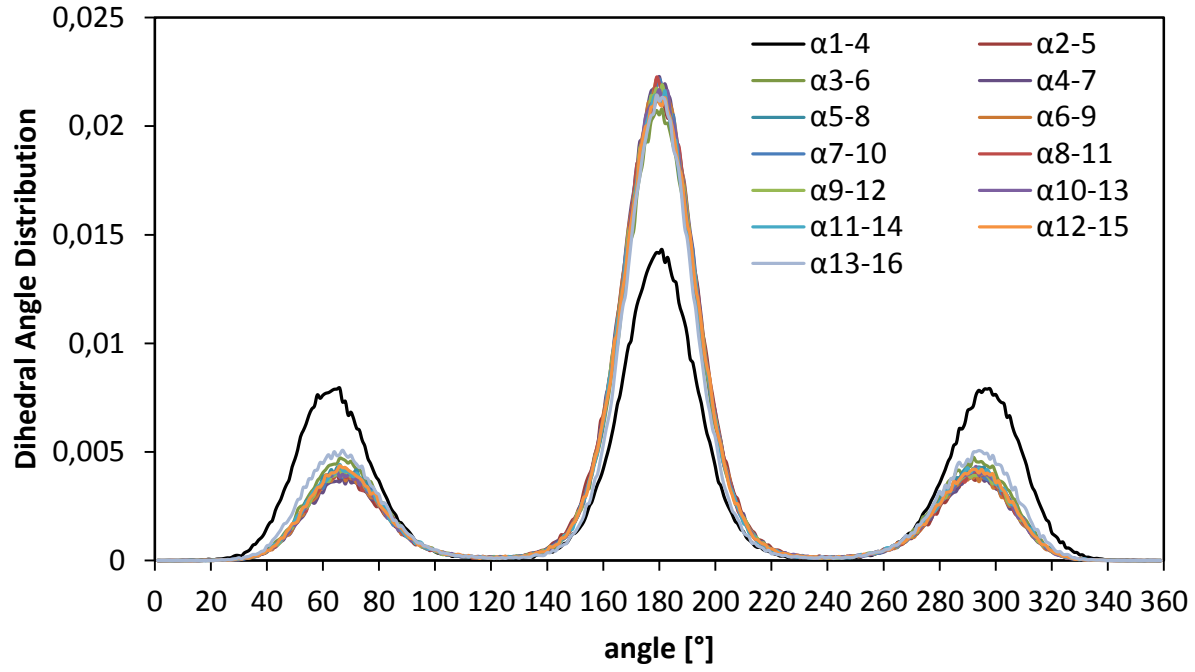

Figure 8.19: Dihedral angle distribution for the CTAB micelle containing 80 surfactant molecules with low 3-hexanol concentration. Labeling is according to Figure 5.9.

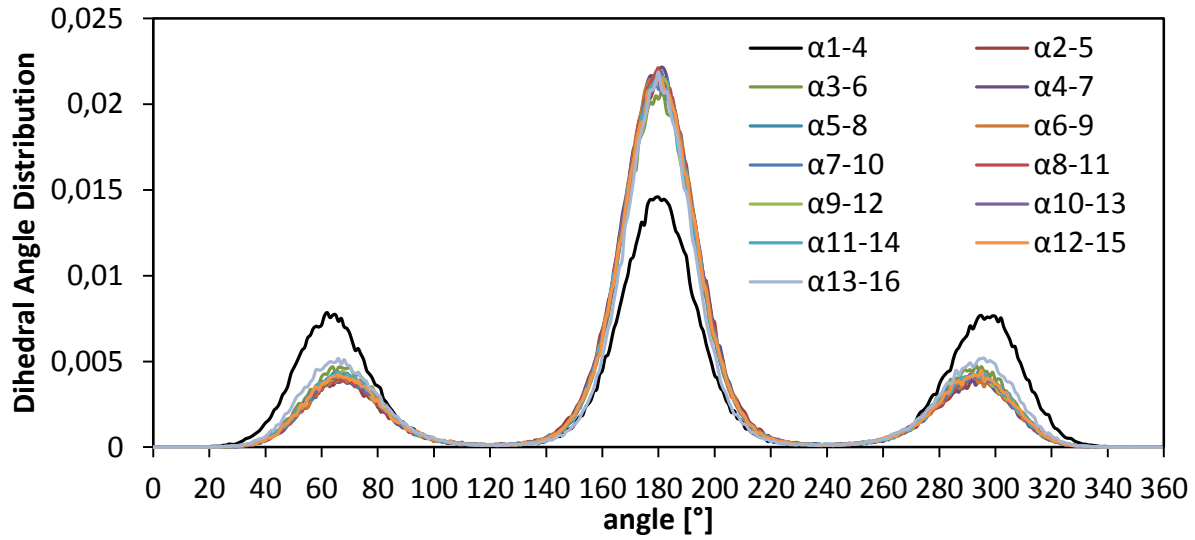

Figure 8.20: Dihedral angle distribution for the CTAB micelle containing 80 surfactant molecules with high 3-hexanol concentration. Labeling is according to Figure 5.9.

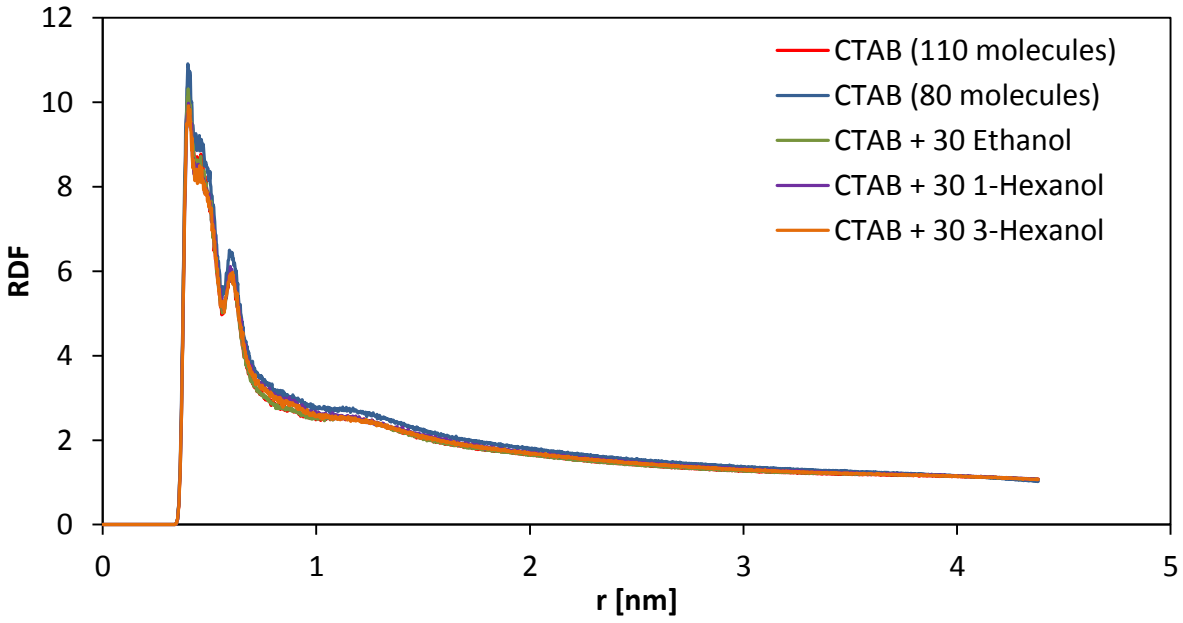

Figure 8.21: Radial distribution functions between the surfactant headgroups and the bromide counterions for the simulations of the pure CTAB micelle simulations (110 and 80 molecules), for the simulation of the CTAB micelle (110 molecules) with 30 ethanol molecules and for the simulations of the CTAB micelle (80 molecules) with 30 1-hexanol and 30 3-hexanol molecules.